University of Southern Queensland
Faculty of Engineering and Surveying

TDR Probes for the Measurement of Root Zone Soil Moisture

A Dissertation submitted by

Gary David Bolitho

In partial fulfillment of the requirements of

Course ENG4111 –Research Project Part 1
Course ENG4112 – Research Project Part 2

Thesis for BEngBBus: Batchelor of Engineering – Electrical/Electronic
Batchelor of Business - Leadership

Submitted 1st November 2007

Abstract

There can be no doubt that the efficient management of water resources is a topic that is highly relevant today. A decline in traditional levels of seasonal rain is impacting on rural and urban areas alike as public attention is directed towards recycling programs and public campaigns of efficient use of water. In agriculture, crop yields are directly related to soil moisture, levels that are most important at the root zone area of the plant.

There have been many technical approaches to the monitoring and control of soil moisture levels. One of the most convenient and accurate in-situ methods that has established itself as a recognised standard around the world uses Time Domain Reflectometry (TDR) to determine volumetric water content of the soil.

TDR is most popularly used with soil probes (typically 30 - 60 cm in length) that are inserted directly into the soil and produce a soil moisture measurement that is averaged over the length of the probes. More specific information such as the soil moisture in the root zone is not easily determined with such probes.

This project investigates an alternative TDR probe design that provides more information about the root zone area of interest. The launch of the TDR incident wave is from a point along the length of the probe, rather than from the start of the probe. Transmission line theory is used to determine the expected behaviour of the incident and subsequent reflection waves. 3D electro-magnetic design and simulation software is used as an aid to the design process. A prototype probe has been designed and constructed, and laboratory tested for performance.

Disclaimer

University of Southern Queensland

Faculty of Engineering and Surveying

ENG4111 Research Project Part 1 &
ENG4112 Research Project Part 2

Limitations of Use

The Council of the University of Southern Queensland, its Faculty of Engineering and Surveying, and the staff of the University of Southern Queensland, do not accept any responsibility for the truth, accuracy or completeness of material contained within or associated with this dissertation.

Persons using all or any part of this material do so at their own risk, and not at the risk of the Council of the University of Southern Queensland, its Faculty of Engineering and Surveying or the staff of the University of Southern Queensland.

This dissertation reports an educational exercise and has no purpose or validity beyond this exercise. The sole purpose of the course "Project and Dissertation" is to contribute to the overall education within the student's chosen degree programme. This document, the associated hardware, software, drawings, and other material set out in the associated appendices should not be used for any other purpose: if they are so used, it is entirely at the risk of the user.

Professor Frank Bullen
Dean
Faculty of Engineering and Surveying

Certification

I certify that the ideas, designs and experimental work, results, analyses, and conclusions set out in this dissertation are entirely my own effort, except where otherwise indicated and acknowledged.

I further certify that the work is original and has not been previously submitted for assessment in any other course or institution, except where specifically stated.

Gary David Bolitho

Student Number: 0019921385

Signature

Date

Acknowledgements

The successful completion of this thesis was brought about with the assistance of many people to whom I am most appreciative.

To my supervisor Dr. Jim Ball for his guidance, supervision and valuable advice. In particular for his understanding and patience with the unexpected interruptions that forced a twelve month delay mid-term.

To my friend Mr. Ian Santinella of San-Tech Machining (14 Rockla Ct. Toowoomba) for his interest and assistance in the construction of probes, supply of materials and use of workshop tools and equipment.

And to my family for their support throughout the entire course of my studies

Table of Contents

List of Figures

Page

List of Tables

Chapter 1 Introduction

1.1 Introduction and Background

There have been several approaches to the monitoring and control of soil moisture in recent years. Industries that cover aspects of hydrology, agriculture, engineering and forestry have looked for fast, economical, and accurate methods that promote economical and good management practice of water as a limited resource.

Traditionally, soil water content was obtained through gravimetric testing procedures that required soil samples from the field to be weighed and then oven-dried. The change in mass is then used to accurately calculate the volumetric water content of the soil. This of course is a time-consuming and expensive procedure that not only has environmental implications associated with the removal of soil from the environment, but also represents significant tendency for error. Errors can be experienced due to poor sampling procedures including deficient selection of soil samples that may not be representative of the area of interest. In-situ testing has become the favored approach.

Early in-situ testing was accomplished through the use of the neutron probe and the dual gamma ray techniques (Greacen 1981). Both of these methods overcame the destructive nature of previous laboratory sampling and provided a quick and accurate method of soil moisture measurements. Disadvantages however are the dangerous radioactive nature of the technology. Also the neutron probe responds to the hydrogen content of the soil itself and not just that of the water present in the soil. This means that calibration of the instrument is difficult as it must first account for the type of soil present. Use of these technologies is also restricted by government laws. To overcome these limitations, work in the nineteen-eighties by researchers focused on the dielectric properties of the soil as a means of calculating water content.

The premise of this approach relied on the fact that at frequencies below 1GHz, the dielectric permittivity of water is much higher than that of the dry soil. This meant that the dielectric permittivity is more closely related to the water present in the soil rather than the soil itself. Hence permittivity readings once measured could be directly equated

to soil moisture content. One early technique developed relied on the capacitive effect of the water present in the soil (Dean, Bell & Batty, 1987).

Testing bulk soil dielectric permittivity with capacitance probes inserted into the soil is a quick and convenient method. The equipment necessary is inexpensive and has none of the dangerous radioactive components of the earlier technologies. Results from capacitance techniques (Selig & Mansukhani, 1975; McKim. et al., 1980) however are greatly dependant on specific electrode configurations and detailed calibration in the field. Limitations arise with the variation in permittivity readings due to the presence of any air gaps between the probe and the soil. The method of installing the probes requires that a suitable tunnel be formed in the ground into which the probes can be inserted. This procedure inherently introduces air gaps. It was also found that the soil type significantly influenced the consistency of results, in particular the conductive properties of the soil. These limitations were largely overcome with research into TDR as an alternative method.

TDR was found to possess all of the advantages of the capacitance probes, but produced more consistent and reliable results (Topp, Davis & Annan, 1980). The technology works by applying an electric pulse to probes inserted into the earth. The probes act as a 'waveguide' for this electromagnetic wave as it travels through the soil. The soil is the dielectric material contained by the waveguides. Soil moisture is determined by first measuring the propagation velocity of this electromagnetic wave as it travels along the probes and is reflected off the open end and back to the start of the probes.

The speed of the reflected pulse depends on soil conductivity, which in turn is highly correlated with the soil's moisture content (Robinson et al. 2003). This is due to the fact that the propagation velocity of an electromagnetic wave is inversely proportional to the square root of the apparent dielectric permittivity (Ka) of the material surrounding the transmission line. It is also known that the permittivity of the dielectric is most strongly affected by the water content, rather than the air, mineral and organic particles that

constitute the soil. This can be seen with comparison of the typical dielectric constants of these materials:

Table 1.1 *Dielectric constants of soil constituents and major textures of soils*

Material	Dielectric Constant
Air	1
Water	81 @ 20°C
Ice	3 @□5°C
Basalt	12
Granite	7 - 9
Sandstone	9 - 11
Dry Loam	3.5
Dry Sand	2.5

(Source: Noborio2001, p. 217)

Therefore, TDR makes use of the propagation velocity to calculate the apparent permittivity of the soil. Extensive empirical studies (Topp, Davis & Annan, 1980) enabled a direct correlation of the apparent dielectric permittivity to the soil moisture content (θ_v). A universal curve that describes this relationship for a particular soil type has been dubbed the Topp Curve. The accuracy of TDR has gained recognition as a world-wide standard to which all other methods are compared.

1.2 Project Aims and Specific Objectives

Conventional TDR probes measure the average soil water content over the length of the probes. This presents a limitation to their usefulness when more accurate information of water content throughout the soil profile is required. For example a farmer may only be interested in soil moisture at the root zone area of the crop, rather than the condition of the soil including the immediate surface soil. This thesis is then concerned with the design, construction and testing of an alternative probe design that attempts to capture more soil profile information.

Laboratory experimentation with soil samples and the university's TDR equipment is first carried out using the conventional probes provided. A thorough literature review of relevant theory and history of TDR for the use of soil moisture monitoring is also undertaken. This is done to gain an understanding of the current theory and application of TDR in the soil moisture measurement context.

The USQ owns a TDR instrument that is available for the purpose of this project. Familiarisation with the TDR equipment and the theory of TDR is essential for the successful completion of this project. Also is an understanding of the physical properties of soil, the combination of soil and water, soil type and mineral content, all in the presence of a traveling electromagnetic wave.

Specific objectives are then to:

- Design and construct a soil probe that yields soil profile information rather than averaged information.
- Gain familiararity with simulation software; used to aid in the design and testing of potential probe configurations.
- Assess the new probe for accuracy and functionality.

The full project specification can be found in Appendix A

1.3 Conclusions: Chapter 1

This chapter has introduced the TDR approach to the in-situ measurement of soil moisture content. Some background to alternative methods has shown TDR to be a reliable and accurate method. An investigation of current practice of TDR has highlighted the need of more specific measurements such as in the root zone area. The project aims and specific objectives have been outlined; namely the design, construction and testing of an alternative probe that will interrogate selected soil profiles. The next chapter will look at the historical development of TDR for soil moisture applications in more detail.

Chapter 2 Literature Review

2.1 Introduction

This chapter will review literature related to the history of soil moisture measurement methods using TDR. This will establish an understanding of the theory of TDR, applications and limitations of its use for soil moisture measurement and developments to date that assist the design of a probe suitable for soil profile determination.

2.2 Theory of TDR for Soil Moisture Measurement

Some of the early work of the application of TDR to determine the dielectric properties of soil was done by Hoekstra & Delaney (1974). They were able to identify that over a range of frequencies the relationship between volumetric water content and the complex dielectric constant is relatively independent of soil type. Leading on from there, much of the work to realise the practical potential of TDR for accurate measurement of soil water content was pioneered by Topp, Davis & Annan, (1980). It was their finding that in the frequency range 1MHz to 1GHz, that the real part of the complex dielectric permittivity of soils (ε') was sensitive to the volumetric water content of the soil. They determined that the relationship was not strong with other physical properties such as soil density and type. In particular, they determined that ε' was not strongly dependant on frequency as had been the focus of all previous research of TDR for soil moisture measurements.

The focus for Topp, Davis and Annan (1980) was therefore to measure the propagation velocity of a fast rise time pulse through the soil, use this information to first calculate the apparent permittivity (K_a) of the soil, and from there to determine an accurate transfer of K_a to the volumetric water content (θ_v). Some TDR theory is necessary at this point to understand the process used by them to derive this relationship.

In any given dielectric material, the propagation velocity of an electromagnetic wave (V_p) is less than that of its propagation in free space ($c = 3\times10^8\ m/s$) according to:

$$V_p = \frac{c}{\sqrt{\varepsilon_r \mu_r}} \qquad \text{..... (2.1)}$$

where μ_r is the dielectric permeability of the soil, and

ε_r is the complex permittivity of the soil given by:

$$\varepsilon_r = \varepsilon' - j\left\{\varepsilon'' + \frac{\sigma_{dc}}{\omega\varepsilon_0}\right\} \qquad \text{..... (2.2)}$$

and σ_{dc} is the DC conductivity of the dielectric

ε_0 is the permittivity of free space ($8.854\times10^{-12}\ F/m$)

ω is the radian frequency

The magnetic property of nearly all soils does not vary significantly from that of free space so it can be assumed that $\mu_r = 1$

The velocity equation is now reduced to:

$$V_p = \frac{c}{\sqrt{\varepsilon_r}} \qquad \text{..... (2.3)}$$

Substituting for ε_r we get:

$$V_p = \frac{c}{\frac{\varepsilon'}{2}\left(1+\left(1+\tan^2\delta\right)^{\frac{1}{2}}\right)^{\frac{1}{2}}} \quad \text{..... (2.4)}$$

where $\tan\delta = \frac{\varepsilon'' + \left(\frac{\sigma_{dc}}{\omega\varepsilon_o}\right)}{\varepsilon'}$ ..... (2.5)

Since the propagation velocity is not entirely independent of ε'' the measured dielectric permittivity is generally termed the apparent dielectric permittivity and is given the symbol K_a. Hence the propagation velocity is related to the apparent dielectric permittivity by the simplified equation:

$$V_p = \frac{c}{\sqrt{K_a}} \quad \text{..... (2.6)}$$

For the soil probes of length L and transit time (Δt) for the pulse to travel the length of the probes from the start to the end and back to the start:

$$V_p = \frac{2L}{\Delta t} \quad \text{..... (2.7)}$$

By substitution and rearrangement of (2.6) and (2.7) the apparent dielectric permittivity is related to the propagation velocity by:

$$K_a = \left(\frac{\Delta t \times c}{2L}\right)^2 \quad \text{..... (2.8)}$$

2.3 Application of TDR for Soil Moisture Measurement

Having been able to calculate the apparent dielectric permittivity from the transit time, Topp, Davis and Annan (1980) then embarked on exhaustive laboratory testing of soil samples in a coaxial cell. They were able to use a standard TDR instrument whose primary use was to find faults in cables. The equipment they used is represented in Figure 2.1.

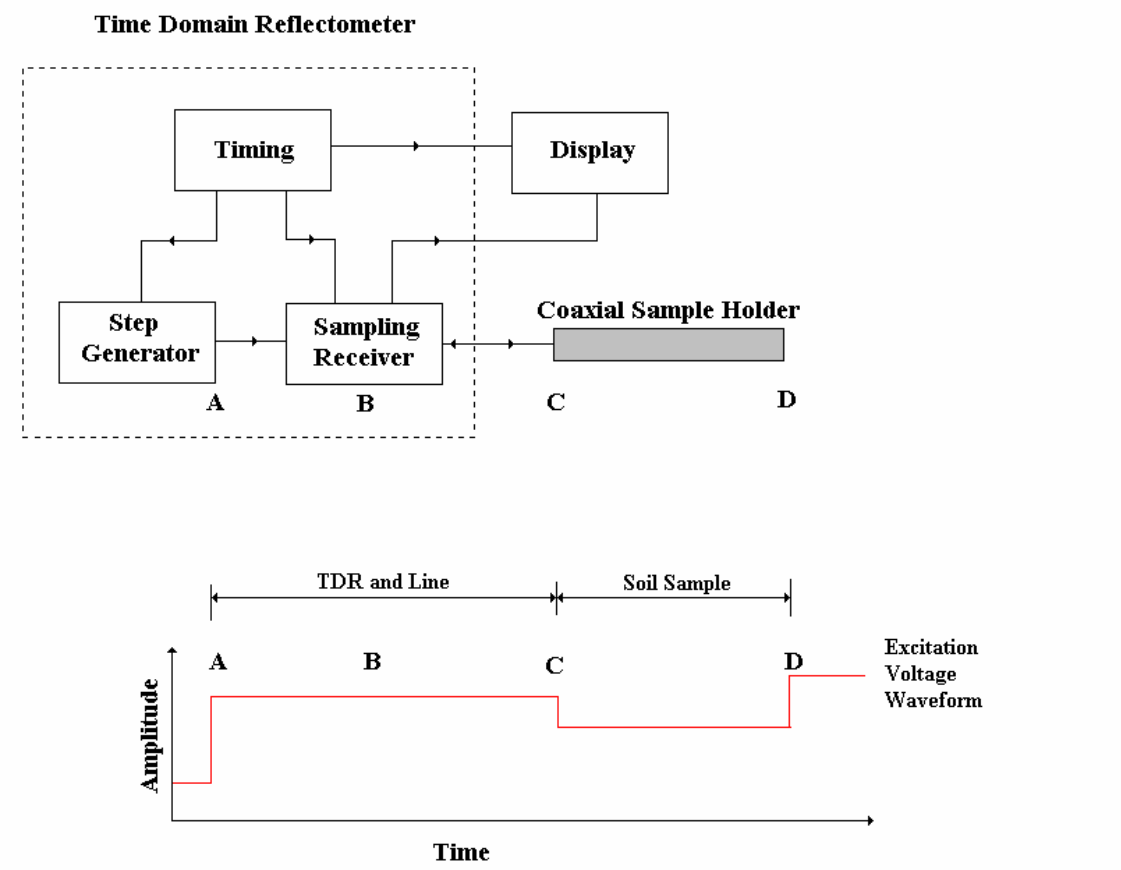

Figure 2.1 *Topp System for TDR Measurement of Coaxial Soil Sample*

The TDR source generates a fast rise time step function, as shown at position A. The step propagates down a standard coaxial transmission line through the sampling receiver at B to the transmission line under test at C. At this point the step encounters an impedance mismatch and some of the incident pulse is reflected back up the transmission line whilst

the remainder is transmitted through the soil sample to the end point D. An open circuit at the end causes the entire signal to be reflected back through the soil sample.

Using the coaxial transmission line cell system, Topp, Davis and Annan (1980a) were able to test different soil types with varying water contents for their transit time and subsequently calculate apparent dielectric permittivity. Through this empirical analysis they were able to derive a 3rd order polynomial that provided accurate representation across the range of soil water contents of general interest. This relationship has since been recognised as a global standard by which all soil water content measurements using TDR methods are now compared. The polynomial was dubbed the 'Topp Curve' is shown in Figure 2.2, and is mathematically expressed as:

$$K_a = 3.03 + 9.3\theta_v + 146.0\theta_v^2 - 76.7\theta_v^3 \quad \text{..... (2.9)}$$

where θ_v is the volumetric water content of the soil.

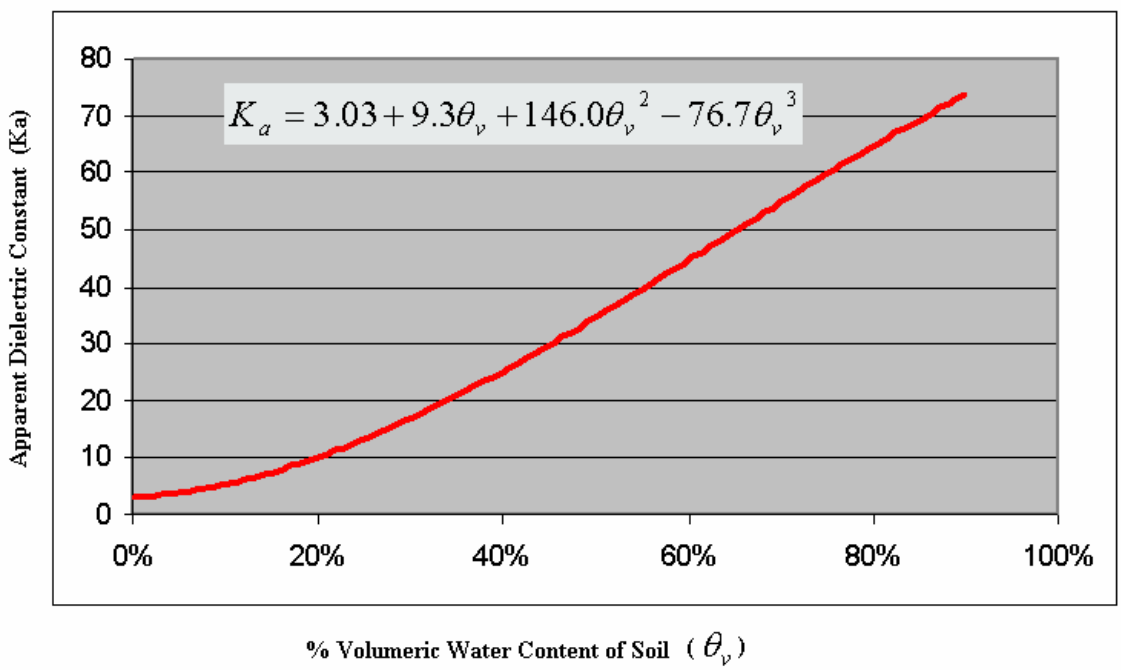

Figure 2.2 *Universal Topp Curve*

The Topp Curve when plotted with square root of K_a against volumetric water content reveals an almost linear relationship as shown if Figure 2.3.

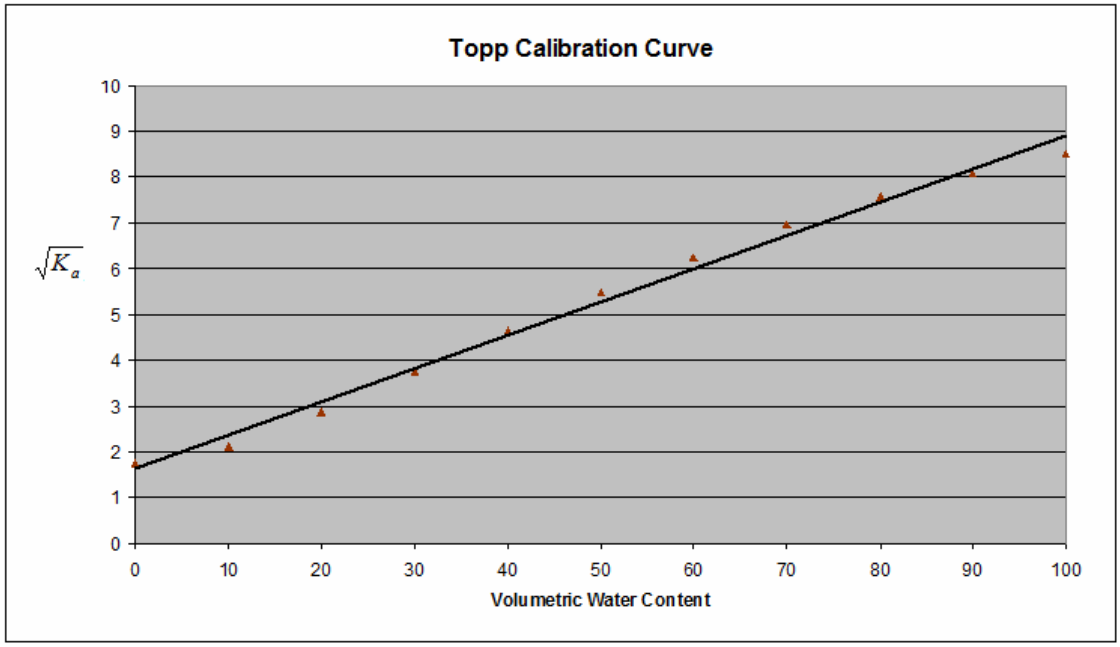

Figure 2.3 *Universal Topp Curve (Linear Relationship between Volumetric Water Content and Apparent Dielectric Constant)*

The apparent linear relationship shown in Figure 2.3 is useful for establishing whether the TDR response does in fact provide an average soil moisture reading over the length of the probe. This will now be investigated.

Let the distance from the start of the probe to the end be a measure of distance z. Making use of equation (2.3) it can be said that the time delay taken for the TDR signal to travel the length of the probe (L) is:

$$\tau_d = 2\int_0^L \frac{dz}{V_p} = 2\int_0^L \frac{\sqrt{\varepsilon_r}}{c} dz \qquad \text{..... (2.10)}$$

Using the relationship of equation (2.6), the time delay can also be written as:

$$\tau_d = \frac{2L}{V_p} = \frac{2L\sqrt{K_a}}{c} \quad \text{..... (2.11)}$$

Equating (2.10) and (2.11) gives:

$$\frac{2L}{c}\sqrt{K_a} = \frac{2}{c}\int_0^L \sqrt{\varepsilon_r}\,dz$$
$$\sqrt{K_a} = \frac{1}{L}\int_0^L \sqrt{\varepsilon_r}\,dz \quad \text{..... (2.12)}$$

Using the linear relationship of Figure 2.3, and adopting the constant *C* for the slope of the graph, and *Y* intercept =2, it can be said that:

$$\sqrt{K_a} = 2 + C\theta_v \quad \text{..... (2.13)}$$

Equating (2.12) and (2.13) and allowing $K_a = \varepsilon_r$:

$$2 + C\theta_v = \frac{1}{L}\int_0^L [2 + C\theta_v(z)]dz$$
$$2 + C\theta_v = 2 + \frac{C}{L}\int_0^L \theta_v(z)dz \quad \text{..... (2.14)}$$
$$\theta_v = \frac{1}{L}\int_0^L \theta_v(z)dz$$

Therefore it can be seen that volumetric water content is indeed found as an average over the length of the probes.

2.4 Development of TDR Practices

The use of TDR was then firmly established and refined as the preferred method for measuring average soil water content rapidly, reliably and routinely. Topp, Davis and Annan (1982b) carried out further TDR research into soil profile testing. They found that

TDR could be used to accurately identify wetting fronts within the soil, but this often required intuitive and expert interpretation of the measured reflection signals. Also, it did not necessarily equate to information about a particular profile of interest.

A number of different designs of probes have emerged. Figure 2.4 shows some two and three-wire probes and a coaxial probe.

Figure 2.4 *Examples of TDR Probes in Use*

(*Source*: Laurent 1998, p.3)

The probes in Figure 2.4 have different characteristics and will be described separately. From left to right, they are:

- A twin-wire probe: wires of varying lengths can be connected to the head section, this is the 'connector' probe developed by *Soil Moisture Equipment Corp*™, and is the probe that will be used as a standard during laboratory testing for this thesis.
- Twin-wire probe: developed by *Imko Gmbh*™. Twin wire probes are most commonly used in the field because of ease of insertion into the soil.
- Three-wire 'buriable' probe: developed by *Soil Moisture Equipment Corp*™ with sealed connections such that the probe can be buried underground.
- Coaxial probe by LTHE (*Laboratoire d'étude des Transferts en Hydrologie et Environnement*).

Guided by the probes, the TDR signal used to interrogate the soil will have various field effect patterns, which implies each probe will test a volume of soil peculiar to the design of the probe. This becomes an important factor in the determination of accuracy of TDR measurements. Figure 2.5 shows various soil testing volumes for four probe types.

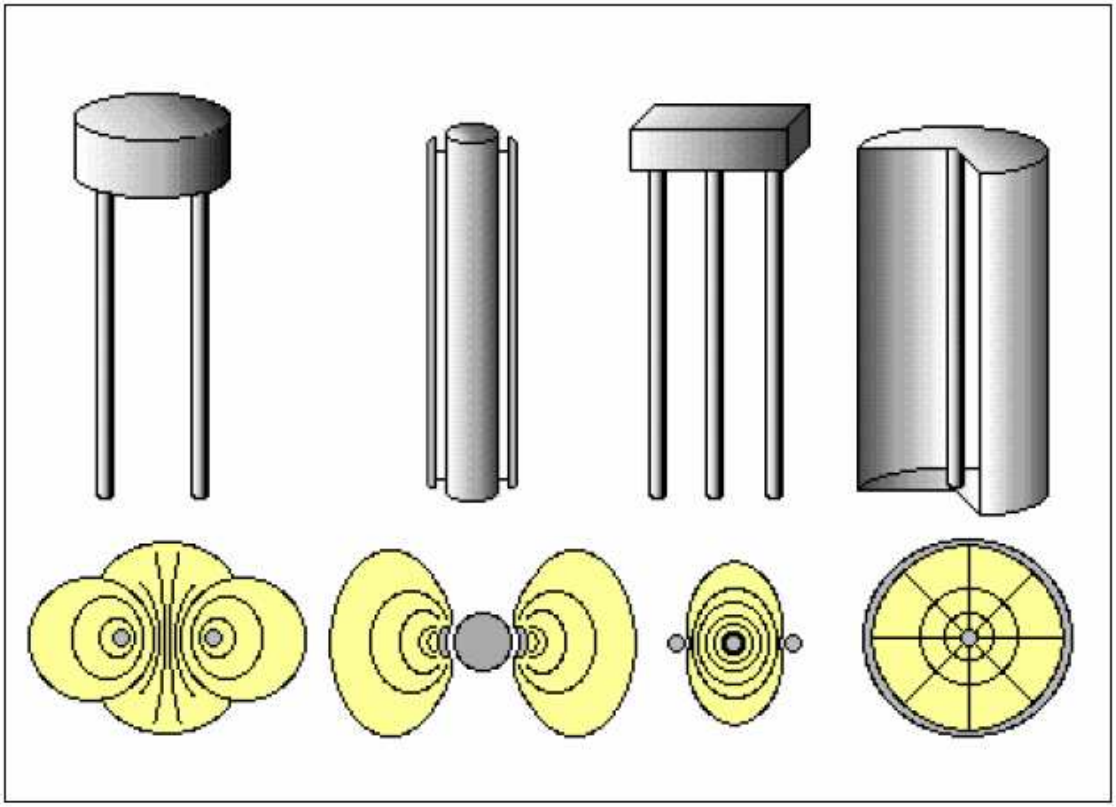

Figure 2.5 *The Shape of Interrogated Soil by TDR Probes*

(*Source*: Laurent 1998, p.4)

The second probe in Figure 2.5 is that of a particular type of twin-wire probe that can be placed at different depths in an access tube, recently developed by Imko Gmbh™ (Laurent 1998). The fourth is that of the coaxial cell by LTHE which are preferred for experiments in the laboratory of for calibration (Laurent 1998). With such probes, the measured volume is perfectly defined: this is the whole inner space of the wave-guide. Also compared to the two-wire probes, it can be seen that the three-wire probe provides better definition of the soil volume under investigation. This will be seen to be significant in design considerations that follow.

Twin-wire probes designed for in-situ testing approximated Topp's laboratory coaxial cell. There is however a geometry mismatch between the unbalanced coaxial cable feeding the balanced twin wire probe. The mismatch was found to introduce problems of

undesirable signal and information loss at the interface between the two. This was originally overcome with the introduction of a balancing transformer, or balun.

The balun itself however was found to introduce unwanted noise causing difficulties in the signal analysis (Zegelin, White & Jenkins, 1989). To overcome the need for a balun, they undertook to re-design the existing two-wire probes with 3 and 4 wire models for field use. Figure 2.6 shows the 3-wire probe of Zeglin, White and Jenkins (1989). Their analysis of the electric field distribution around the probes closely emulated the results achieved by Topp's laboratory testing of a coaxial transmission line cell. The new design also minimised the impedance mismatch which occurred with the two-wire probes.

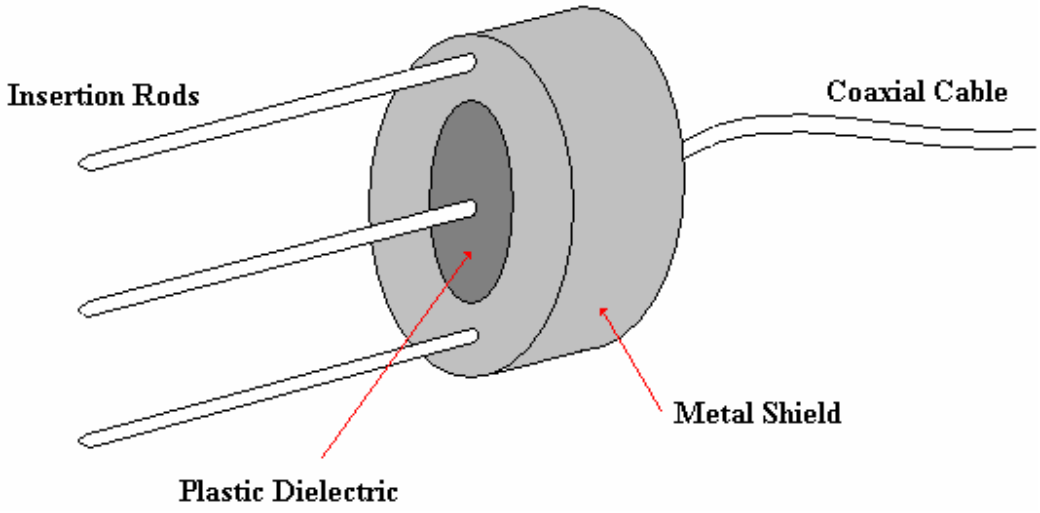

Figure 2.6 *Three-Wire Probe of Zegelin, White & Jenkins (1989)*

Further work by Heimovaara (1993) investigated relationships between lengths of the coaxial lead connecting the test equipment to the probe with various probe lengths. He found accuracy suffered when the probe length is too short in relation to the length of coax. In particular, longer lengths of cable cause the rise-time of the TDR voltage pulse to increase, spreading each reflection across a larger time interval, i.e. the measured transit time becomes skewed.

One modern TDR probe in use makes use of a twin wire transmission line with shorting diodes placed between the wires at different intervals along the probe length (Figure 2.7). With electronic control, different combinations of diodes are switched such that the probe is interrogated over the different segments (Hook et al., 1992). Although this provides profiling information, it is considered that spatial resolution of this system is relatively weak (Laurent, 1998).

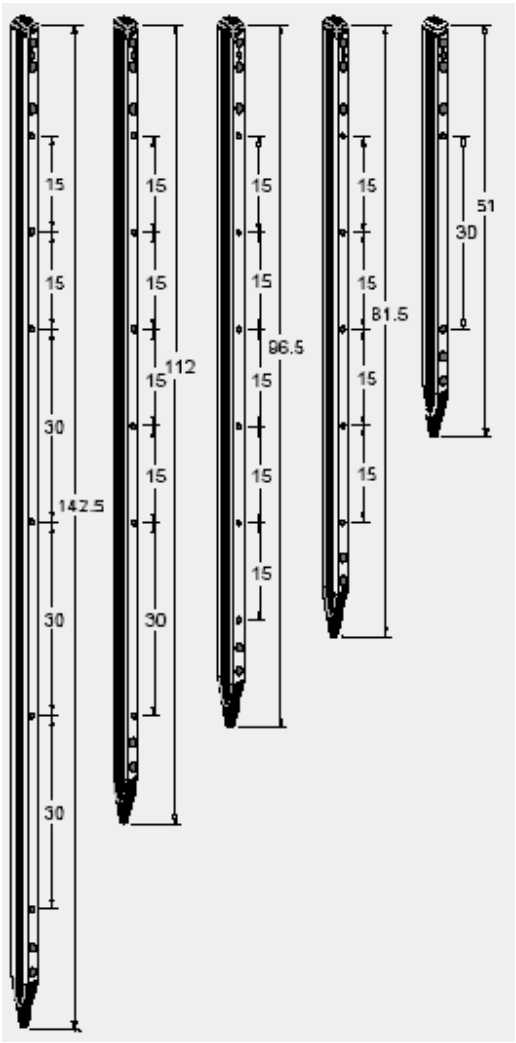

Figure 2.6 *Diode Shorting Probes of Various Lengths*

(*Source:* Moisture Point 2007, p.2)

Laurent's (1998) comments regarding weak spatial resolution of the previous type of probes is supported by the findings of Zegelin, White and Russell (1992). They

investigated the accuracy of TDR in different soil types and found that the response of TDR probes is especially sensitive to the region immediately surrounding the probe wires. Since the area between the probes is filled with the switching diodes and a poured epoxy resin, then the dielectric properties of the soil itself is not the region of greatest interrogation by the TDR induced fields.

Recent studies by Laurent (1998) have sought to extract water-content profile information from the TDR measured waveform, in addition to the traditional overall propagation time and corresponding average water content. A TDR signal inversion method called "TDR_SSI" considers the waveform as a set of elementary reflected signals, not only at the beginning and end of the probe, but also every time an impedance discontinuity is encountered in the soil medium. Any variations in water content throughout the sampled soil will lead to fluctuations of the electrical permittivity, and thus of the impedance. These create reflections that combine as an image of the impedance along the probe. Laurent did however identify several limitations to the method. Practical limitations exist with the insertion of the long plastic tubes or rods into heterogeneous type soils. This long length also introduces unwanted signal attenuation in highly conductive soil types causing inaccuracy in calculations. Also identified was some scattering or variation of K_a with the frequency due to a distribution of relaxation properties throughout the soil.

TDR probe design is still an area of interest today. It is important to note that although Zegelin, White and Jenkins (1989) confirmed the 3 and 4 wire probes as good approximations to the laboratory coaxial cell system, that significant difference between the characteristic impedances of probes couldn't be ignored. Ball (2002) has recently investigated numerical analysis for the calculation of probe air-spaced characteristic impedance, necessary for soil conductivity interpretations. His work has provided a good first approximation of characteristic impedance in the form of a mathematical expression obtained by conformal transformation. Figure 2.8 that follows shows the probe dimensions of interest for which the mathematical equation is related.

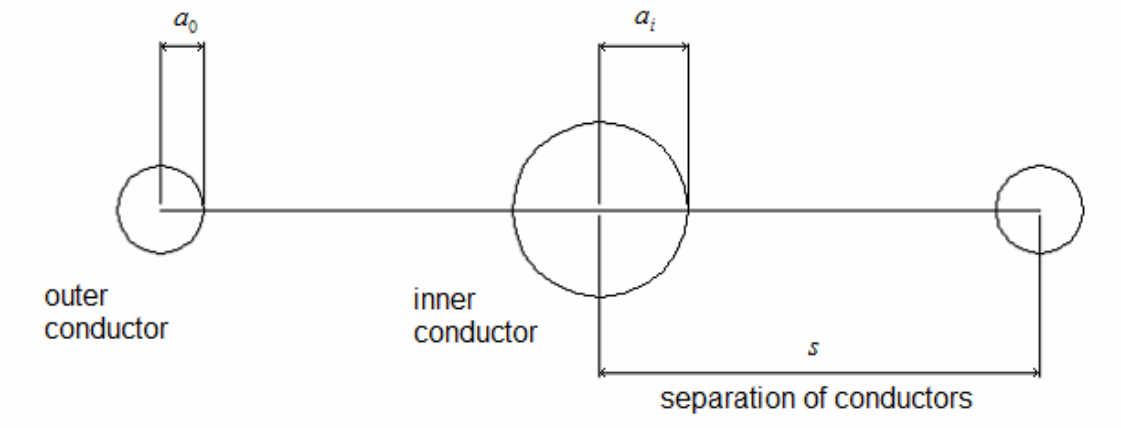

Figure 2.8 *TDR probe cross section, showing inner and outer conductor dimensions*

$$Z_{0\,probe} = \frac{1}{2\pi}\sqrt{\frac{\mu_0}{\varepsilon_0}}\left[\ln\left(\frac{s}{a_i}\right)+\frac{1}{n}\ln\left(\frac{s}{a_0 n}\right)\right] \qquad \text{..... (2.15)}$$

where n = number of outer conductors = 2

Transmission line end effects are of importance to the design and calibration of TDR probes. Pentinellia et al. (2002) comment on TDR signal behaviour at the open-circuited end of the waveguides that is not totally consistent with simple reflections. Rather, there is a combination of radiative and reactive effects at the termination such that some of the electromagnetic strength of the incident wave is partially lost to radiation to the open space and the reflected wave is not necessarily in phase with the incident wave. The radiative effects are considered negligible for most TDR soil measurement applications; however Pentinellia et al. (2002) assert that the reactive end effects are significant. Reactive end effects present as a stored electrical energy relating to the fringing of the electric field at the open-circuit end of the transmission line. The equivalent distributed circuit would be seen as end shunt capacitance, related to frequency. The time-domain effect of the distributed capacitance is to create a delay, the net effect being equivalent to a 'lengthening' of the line. For a two-wire transmission line, Pentinellia et al. (2002) assert as a first approximation, that it is the geometry of the probe (diameter of conductors and separation) and not the filling medium (wet soil) that determines the amount of 'lengthening'.

2.5 Conclusions: Chapter 2

This chapter has conducted a review of literature to investigate TDR principles and applications of TDR to soil moisture measurement. Firstly the theory of TDR in general was established and mathematical equations derived to support that theory. Secondly the application of TDR was examined; facilitated by an investigation of various methods that have been used and the assortment of probes that have been designed.

It is clear that TDR for soil moisture measurement is a mature science, as evidenced by the extent of empirical work done in this area. It has been accepted as an accurate and practical means by which in-situ testing of soils is carried out by those wishing to determine soil properties. Probe design is still an area of interest today as the demand for accurate and precise measurement of soil moisture is needed. The practical aspects of TDR application will be the focus of the next chapter. A TDR instrument will be examined in conjunction with some standard probes in use.

Chapter 3 TDR Equipment and Laboratory Procedures

3.1 Introduction

This chapter will provided an introduction to the TDR test equipment and its use in the laboratory. Details of the TRASE TDR system will be investigated to gain familiarity with its functions and its ability to determine transit time of the signal energy through a soil sample such that apparent dielectric constant can be calculated. It will be shown how the transit time is used to determine volumetric soil moisture content. Soil preparation and laboratory testing procedures will be established, followed by familiarisation testing of soil samples using the TRASE system. Evaluation of the laboratory results provides a benchmark for the rigorous testing that will be required once the prototype probes are designed and constructed.

3.2 TDR Equipment - TRASE

The University of Southern Queensland has a specific TDR measuring instrument developed by *Soilmoisture Equipment Corp*. of California for use in this thesis. It is called a TRASE, an acronym for Time Reflectometry Analysis of Signal Energy. Figure 3.1 shows the TRASE unit with a standard 'connector' type twin-wire soil probe connected.

Figure 3.1 *TRASE Equipment*

The Model 6050X1 TRASE system is designed for use with 15-60cm depth waveguides that can be either portable or permanently installed for periodic moisture measuring in the same location (Soilmoisture 1989). The volumetric moisture content is displayed and the graph of the TDR pulse can be also be displayed. The moisture reading and the graph of the TDR pulse can be tagged and stored within the unit's internal memory for later analysis. In addition, all stored data and graphs can be transferred to an external computer or printer via an RS-232 serial port. Another feature of the TRASE system is the ability to program auto-logging of readings for continuous monitoring. Probe coaxial cables are attached to the unit via a BNC port. Unit settings, measurements and graphs are displayed on the LCD graphical display on the front of the unit. All parameters and controls are easily entered via the 28-key alpha/numeric keypad, also on the front of the unit. More details of the theory of operation will be covered in the next section.

3.3 TDR Equipment – Theory of Operation

General principles of operation of TDR measurement equipment was presented in the literature review chapter (refer to section 2.3: Application of TDR for Soil Moisture Measurement). Figure 3.2 shows how the TRASE TDR system works.

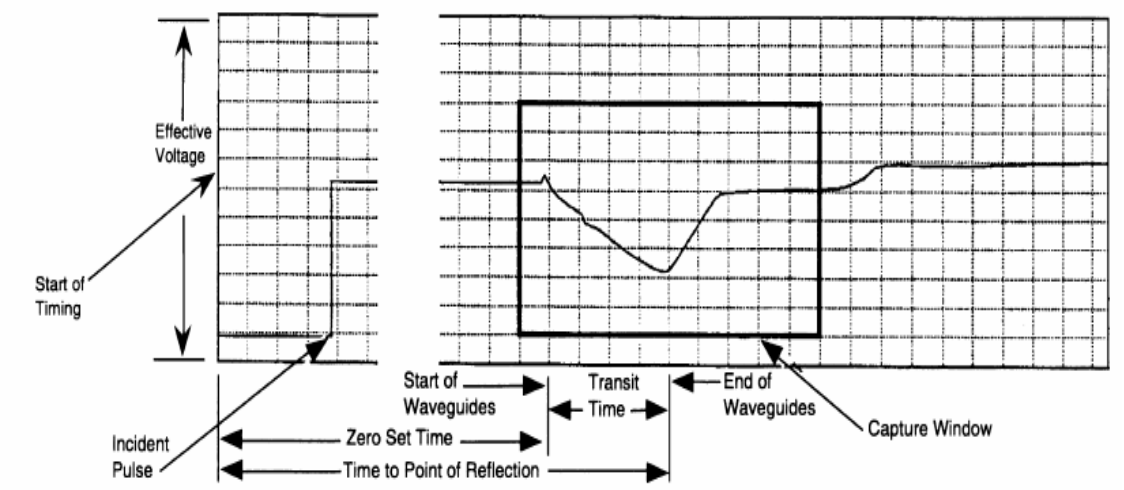

Figure 3.2 *TRASE Measurement System showing Capture Window*

The TDR processor generates a series of fast rise time microwave pulses (rise time < 200ps) which propagate down the transmission line that consists of the coaxial cable and the waveguides that are inserted into the soil. The start of each pulse is referred to as the incident pulse and is the point from which subsequent time measurements are made during the automatic determination of moisture content. It is through a series of pulses and time-shifted measurements that the TRASE system builds up an accurate picture of the TDR response. The iterative process will now be described.

After a single pulse is launched down the transmission line, the effective voltage is measured by the internal sampling receiver unit, at a point in time controlled by a timing unit. With a sampling resolution of 10ps, this first measurement is made 10ps after the launch of the first pulse. Some time later ($40\,\mu s$), a second pulse is launched and the effective voltage measured 20ps later. On the next pulse, the measurement will be made 30ps later. The process is repeated 1000 times with each reading being incremented by

10ps. Each measurement point is stored such that the complete time range of interest is covered. In addition, after the complete time span is covered, the same process is repeated a number of times to provide an 'average' value for each of the 1000 points. Not all of the 1000 points are used for graphical display. How the stored data is processed by the TRASE system software for graphical display will be discussed next.

The TRASE system software detects the point at which the TDR pulse reaches the start of the probe. The time from the start of the pulse measuring process to the time of the start of the probes is called the 'zero-set' time. The time of the first reflection off the end of the probes is also detected. It can be seen from Figure 3.2 that the difference between these two times is determined as the transit time. The TRASE system software will then allocate a portion of the collected waveform that contains these two points to be displayed as the 'capture window'. Figure 3.3 shows detail of a typical waveform displayed in the instrument's capture window after conducting a test in moist soil.

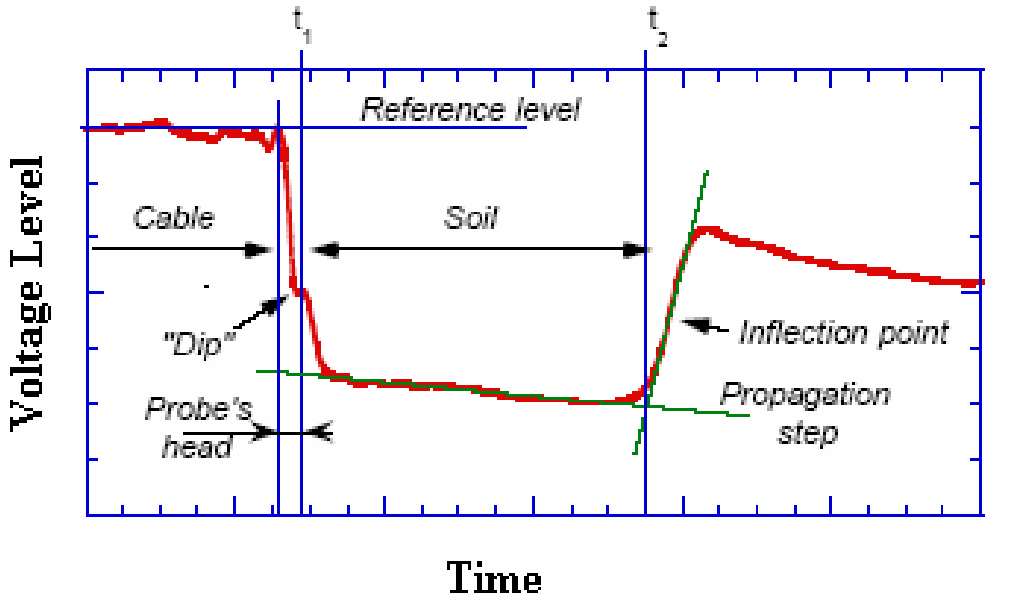

Figure 3.3 *Details of the TRASE Capture Window – Typical Waveform for Uniform Wet Soil*

The capture window starts just before the zero set time. A choice of capture window length can be pre-selected by the user, namely 10, 20 and 40ns. The most significant information the TRASE looks for is the transit time of signal propagation through the soil

($\Delta t = t_2 - t_1$) so that the apparent dielectric permittivity K_a can be calculated. Determination of the point of first reflection is achieved through a process of tangent fitting. In Figure 3.3 it can be seen that the first tangent is fitted to the section of graph as the wave travels along the probe; the second tangent is fitted to the section of graph immediately following the reflection. It is the intersection of these two tangents that is determined as the reflection point.

Having determined apparent dielectric permittivity K_a, the TRASE then converts this to a measure of volumetric water content via an inbuilt look-up table. The user can define certain look-up table parameters or select to use the standard tables calibrated using the universal Topp equation. The Topp equation is only valid for up a range of about 0-40% volumetric water content. The TRASE lookup table however has been extended to cover 0-100% range, based on testing carried out by the manufacturer *SoilMoisture Corp.* For the purpose of this thesis it is still only the range 0-40% that is useful since at about 30% most soils become saturated. The TRASE inbuilt lookup table is displayed in graphical form in Figure 3.4 below. It can be observed from the graph that there is a relatively linear relationship between apparent dielectric constant and volumetric water content over the full range of 0-100%. Taking an example, if a reading of K_a=56 is measured, the corresponding volumetric water content (θ_v) would be read as 78%. For a reading of K_a=18 is measured, the corresponding θ_v would be read as 30%. The variation of K_a is therefore approximately 0.8 for every percent change of water content.

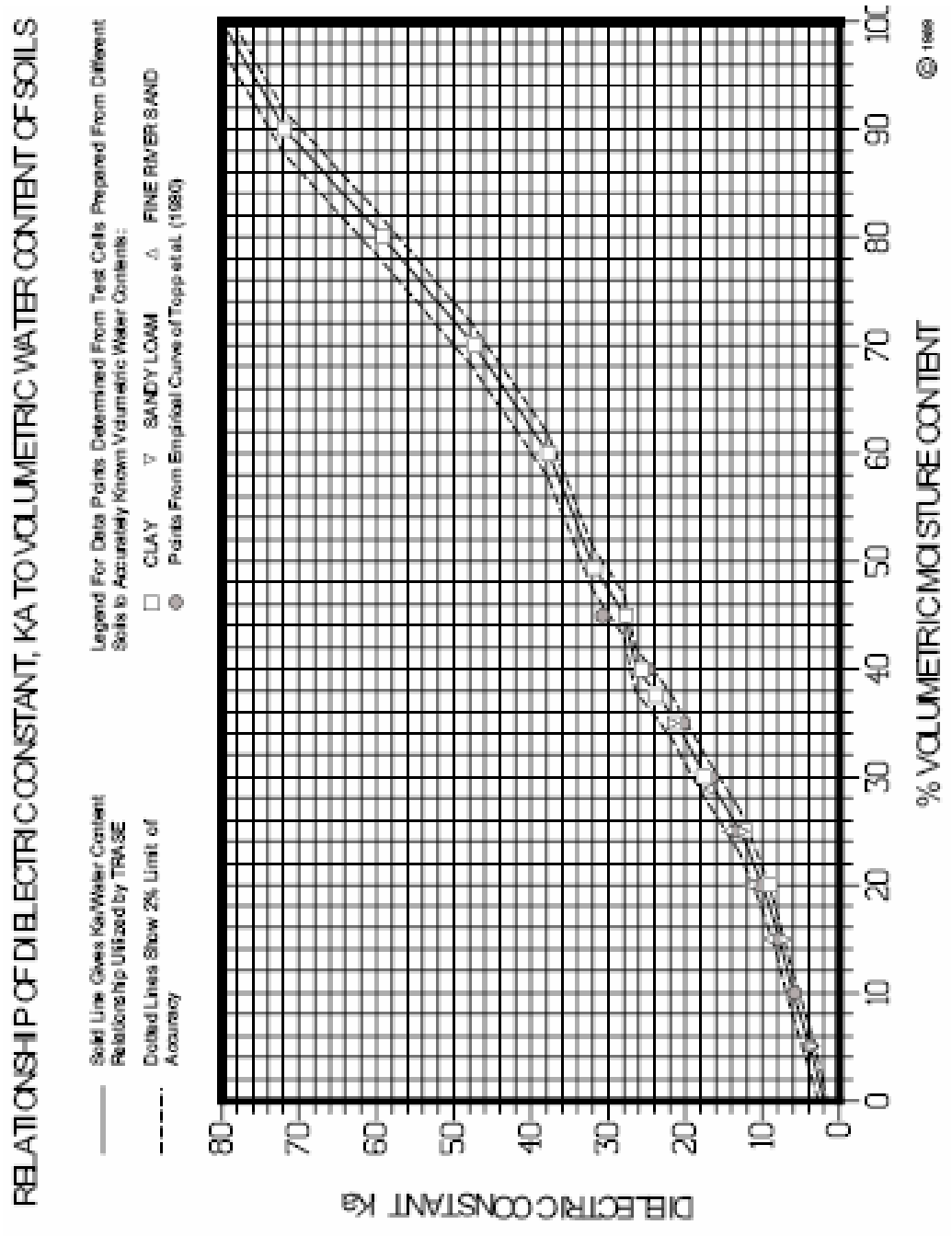

.Figure 3.4 *Graphical Representation of TRASE Inbuilt Lookup Table*

3.4 Soil Preparation

To gain familiarity with the TRASE equipment it was decided to test various soil samples in the laboratory. In alignment with the coaxial cell testing done by Topp, Davis and Annan (1980) and Habash (1994), a sandy loam type soil sample was selected and tested under various water content conditions. Distilled water, rather than town supply or rain water was chosen to also be consistent with established laboratory testing procedures. The process used will now be described.

First the soil sample was sieved to 10mm to remove large stones. The soil was then oven dried for 24 hours at $105^{o}C$ to remove all water content and weighed. The dried soil was placed in a plastic tube of sufficient size to allow at least 5 cm of soil to be present around the outermost dimensions of the probes and beneath the probes. This requirement would ensure adequate containment of the electromagnetic wave through the soil under test, without any of it being exposed to the air outside the bucket or floor underneath. This requirement is also in keeping with proven laboratory procedures used in previous experimentation (Habash, 1994).

3.5 Laboratory Test Procedures

Standard 'connector' type probes of 30cm length were arbitrarily chosen to use in the initial soil testing procedures. The TDR probes were place in the soil up to the full depth of the probes for each test. Five concurrent measurements were made in each of three probe positions in the bucket for every test. Apparent dielectric content and volumetric water content were recorded with an average for the test being calculated.

Next a percentage of distilled water was added to the soil and thoroughly mixed to ensure even distribution throughout the sample. The measurement procedure used above was repeated. This process continued as the water content of the soil was increased, eventually to saturation. Before water was added each time, a small sample container was

filled so that gravimetric testing could be carried out to test against the volumetric data being collected. The test procedure could be summarised in six distinct steps:

1. Oven dry soil sample at $105^{o}C$ for 24 hours.
2. Determine the amount of water required to produce specific water content level.
3. Add and mix measured quantity of water with soil.
4. Leave soil sample to cure for 24 hours
5. Use the TRASE instrument to gather measurements in three different probe positions
6. Take an oven dried soil sample to verify the water content.

Please note that for these initial familiarisation tests, Step 4 was omitted for expediency purposes. This step will however be a part of any formal laboratory testing procedures to verify the operation of the new prototype probe yet to be made.

Figure 3.5 below shows a photo of the TRASE front panel and a typical TDR waveform measured during laboratory experimentation. The first vertical line on the left is the determined zero-set point, and the other two vertical lines are adjustable by the user such that transit time calculations can be made on screen.

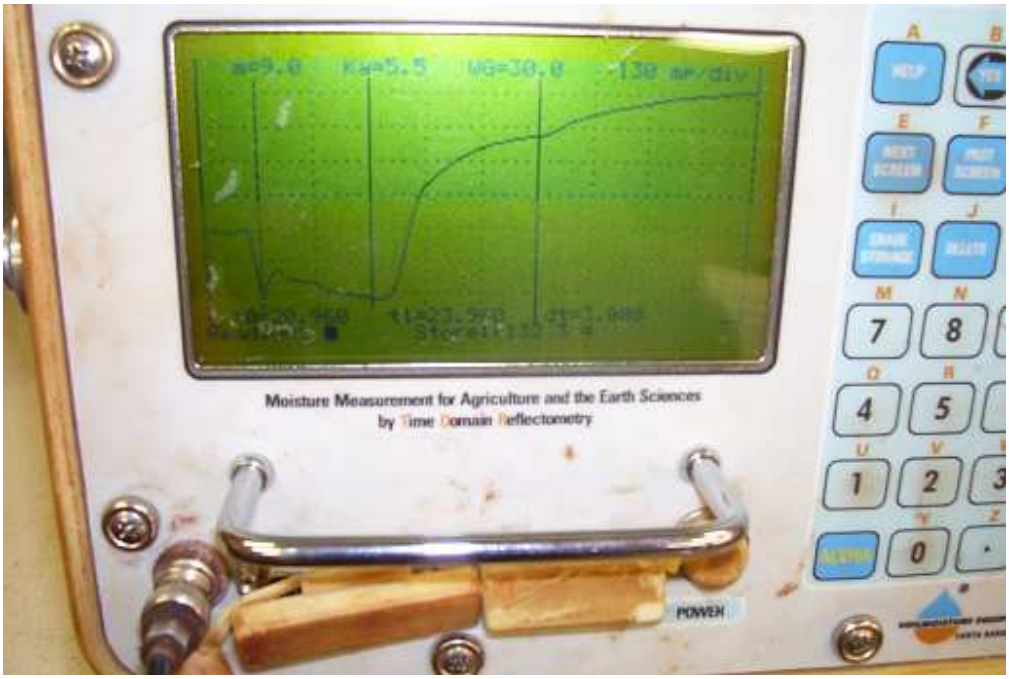

Figure 3.5 *TRASE Capture Window during Laboratory Experimentation*

3.6 Laboratory Familiarisation Test Results

Results of the familiarisation testing showed good alignment with the measurements of others (Habash 1994, Topp, Davis & Annan, 1980) and are shown in Figure 3.6.

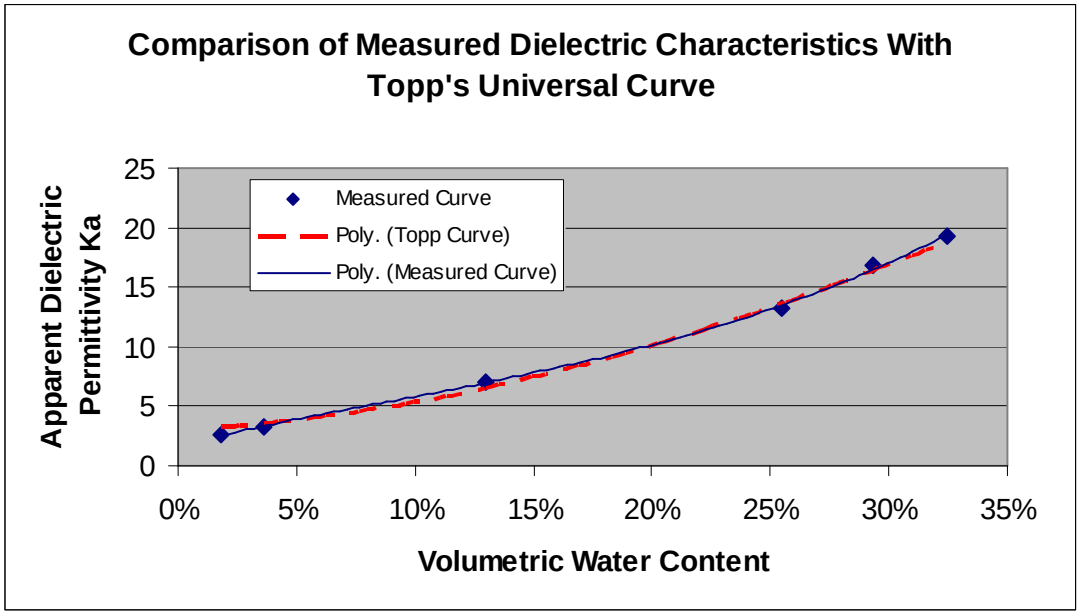

Figure 3.6 *Results of Laboratory Familiarisation Testing with TRASE Instrument*

It can be seen from the chart that the measured results for the sandy loam soil under test were almost identical to the Universal Topp curve. This suggests that the methodology used for this familiarisation was appropriate and would serve as useful experience for later laboratory testing of prototype probes. The familiarisation experiment also unearthed some short-comings in procedure. A look at Figure 3.7 shows a comparison between the actual water content and that measured by the TRASE instrument. It reveals some discrepancies.

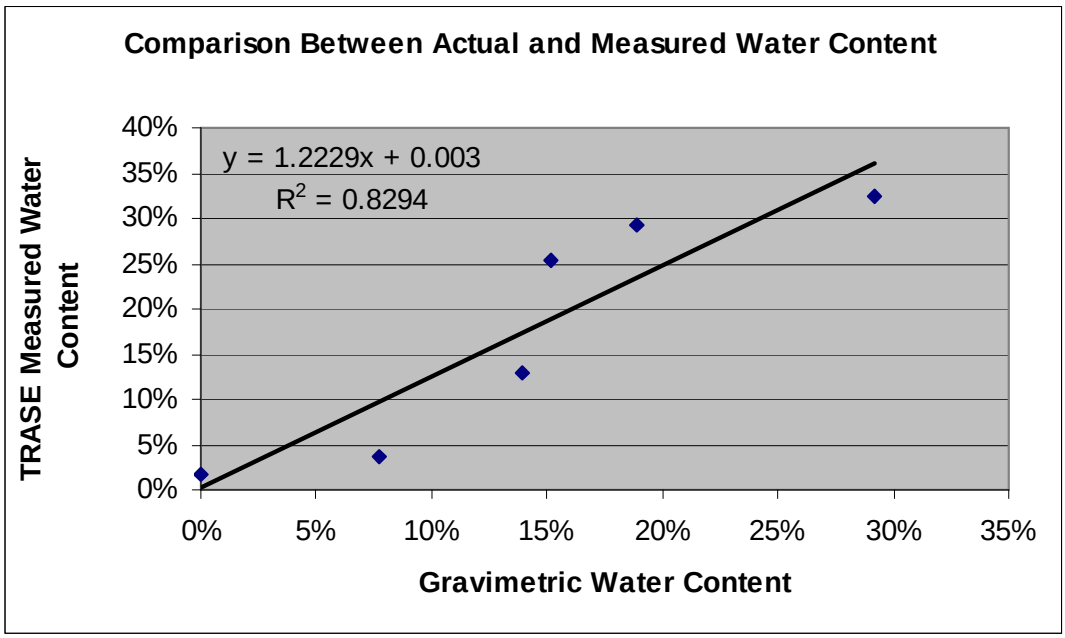

Figure 3.7 *Graph Showing the Difference Between the Actual Water Content and that Measured by the TRASE Instrument for the Sandy Loam Soil*

There is quite a bit of scattering of the data points along a linear line of best fit. There is also some disagreement between measured and actual results. For example, a TRASE measured 25% water content corresponds to a gravimetric result of approximately 22%. This is in some part due to the fact that small sample sizes were used to calculate the actual water content. More care will need to be taken in future experimentation to take accurate volumetric measurements. However, the use of TDR is also recognised as inherently accurate to a limit, the manufacturer's of the TRASE system quote a $\pm 2\%$ measuring accuracy (Soilmoisture 1989). This accuracy is typical of other equipment manufacturers. Certain characteristics of the soil and in particular interaction of the soil and water present lead to variations in accuracy. Discussion of soil moisture characteristics including the properties of 'free' and 'bound' water effects will be discussed later in Chapter 7.

3.7 Conclusions: Chapter 3

This chapter has provided an introduction to the TDR test equipment and its use in the laboratory. Details of the TRASE TDR system were investigated to gain familiarity with its functions and its ability to determine transit time of the signal energy through a soil sample such that apparent dielectric constant can be calculated. It was shown how the transit time could then be used to determine volumetric soil moisture content. Laboratory testing of soil samples using 'standard' waveguides was conducted with results that were matched to expectations of TDR soil moisture measurement accuracy. Design of a prototype probe capable of extraction of soil profile information is based on knowledge of transmission line theory. This is the subject of the next chapter.

Chapter 4 Transmission Line Considerations for TDR

4.1 Introduction

The design of soil probes for use with TDR necessitates an understanding of transmission line characteristics to enable interpretation of the signal produced. This chapter will first develop a transmission line model for a lossless TDR system. Next, an investigation of the waveform as it passes through the system will be facilitated by the use of lattice diagrams. Practical examples of standard probes in air and in water will reveal the effect of probe design and material permittivity on TDR waveforms. In particular it is the effect of the impedance mismatch that the signal encounters at the junction of the coaxial transmission line and the start of the probe that will be investigated. Relative timing and reflection characteristics are examined.

4.2 Transmission Line Modeling

One of the simplest modeling tools available to understand the time domain response of a short transmission line is the lattice diagram. The lattice diagram keeps track of multiple reflections and is usually based on the assumption of lossless line characteristics. On a lossy transmission line it is the high frequency components of a pulse spectrum that define the leading and trailing edges, so that a pulse on a lossy line becomes progressively more rounded as it travels. On a lossless line however, the amplitude and waveshape of the pulse is maintained, so that the line behaves purely as a time delay.

The assumption therefore is that the dielectric permittivity of the soil is constant over all frequencies and any losses due to the dielectric and the system are negligible. Under these conditions, to the TDR pulse the line appears as a resistance equal to the characteristic impedance of the line. This implies that the characteristic impedance of the probe is an important design consideration. The characteristic impedance of the coaxial part of the transmission line can be simply determined from manufacturer's specifications.

The TDR system can now be represented by consideration of the various components and how they relate to transmission line properties. The components of interest are the step generator, the coaxial transmission line of impedance Z_0, and the probe section that represents an open circuit transmission line with impedance Z_{pSoil}. The impedance Z_{pSoil} will vary according to the dielectric properties that the soil and moisture present. Figure 4.1 shows the TDR transmission line circuit with standard 3-wire probe.

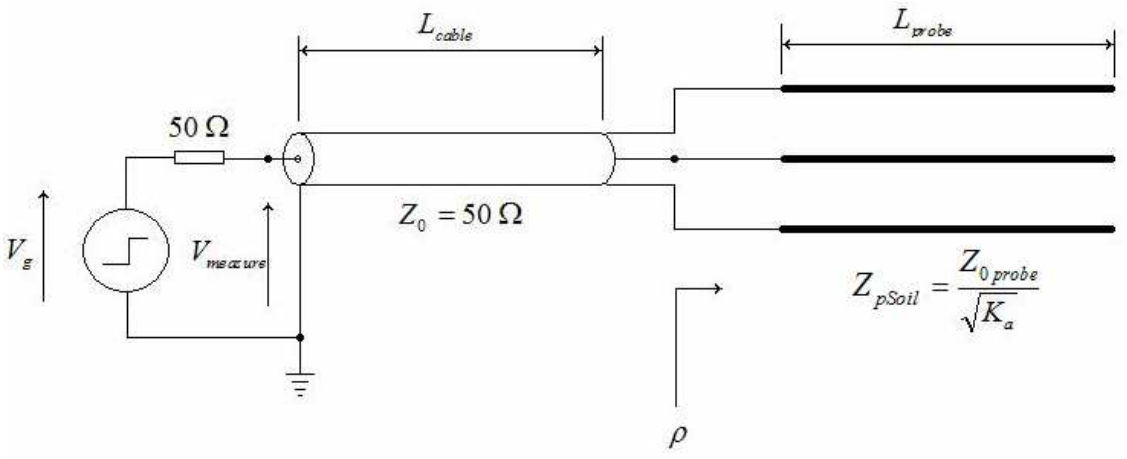

Figure 4.1 *TDR System TX-line Circuit Diagram – 3-Wire Standard Probe*

The step generator will produce a step pulse that is passed into the transmission line system. There will be no affect on the shape of the pulse as it travels along the coaxial line since it is perfectly matched to the internal impedance of the step generator unit, typically $50\,\Omega$. When the pulse arrives at the head of the probe, it will encounter an impedance mismatch. As a result, some of the signal energy of the pulse will be reflected back up the coaxial line to the step generator and will be absorbed, since it is perfectly matched. The rest of the signal energy however will continue to propagate down through the soil, guided by the probe acting as a waveguide. At the end of the probe, the signal energy will be reflected back of the open circuit termination. The returning energy will encounter an impedance mismatch when it arrives at the head of the probe again. Some of the energy will continue to travel up the coaxial cable to the generator and be absorbed;

however some will be reflected and travel back down the probe again. This process will continue until the energy in the reflected pulse decays to zero.

The extent to which the incident energy is reflected off the mismatch will depend on the reflection coefficient of the mismatch and is given the symbol ρ, where:

$$\rho = \frac{Z_{pSoil} - Z_0}{Z_{pSoil} + Z_0} \qquad \text{..... (4.1)}$$

If the step value that first appears is considered to be normalized with a value 1, then the amount that propagates through the mismatch is determined as the transmission coefficient (*t*), such that:

$$t = (1 + \rho)$$
$$= \frac{2Z_{pSoil}}{Z_{pSoil} + Z_0} \qquad \text{.....……...……. (4.2)}$$

With this information, it is now possible to create a simple lattice diagram as shown if Figure 4.2 below:

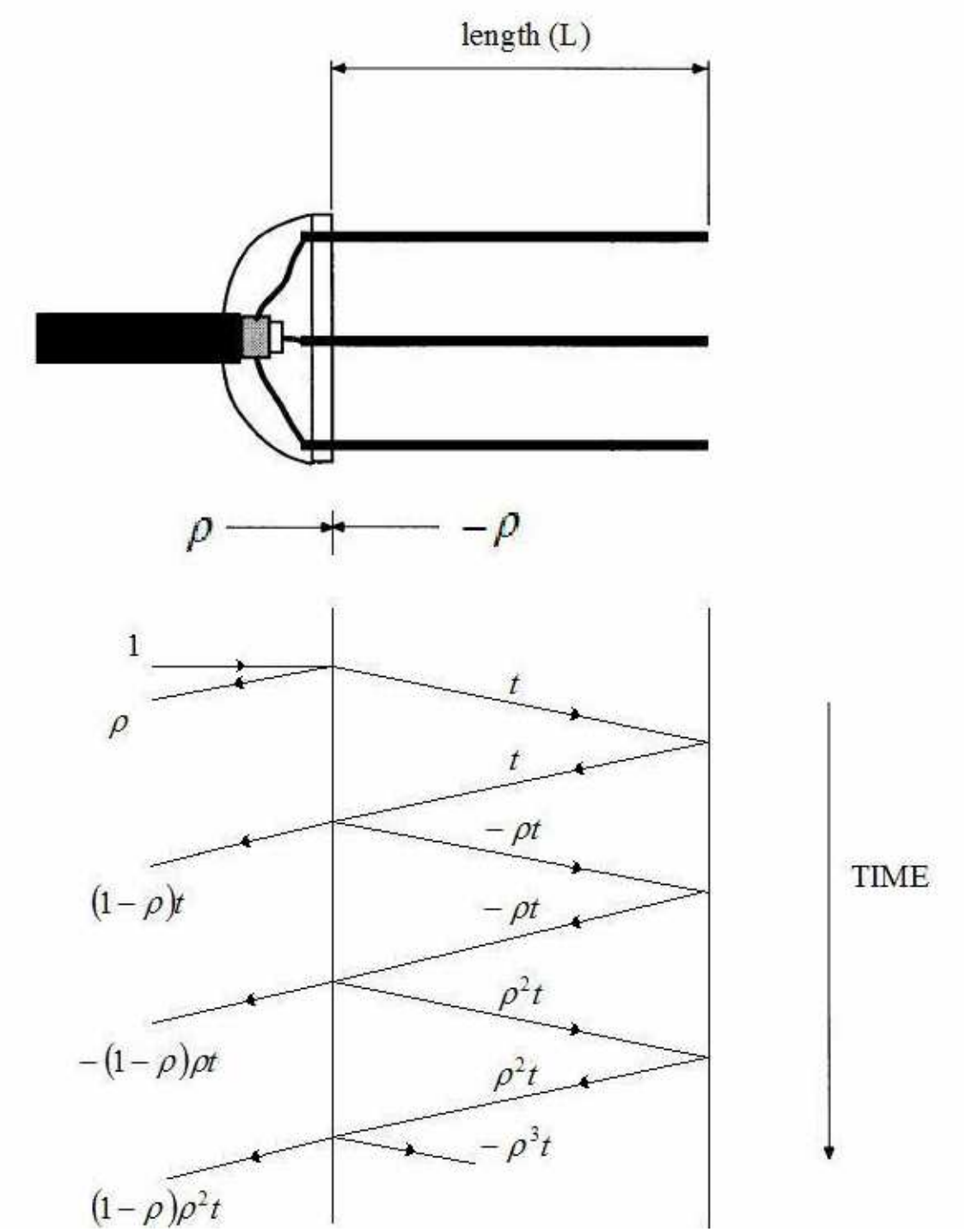

Figure 4.2 *Simple Lattice Diagram for Standard 3-Wire Probe*

The time taken for the pulse to travel from the start of the probe to the end, and reflected back to the start of the probe again is the time delay (T). Making use of equation (2.8) from earlier, we can say:

$$T = \frac{2L\sqrt{K_a}}{c} \qquad \text{…….……..} \quad (4.3)$$

Using the lattice diagram of Figure 4.2 and following the path of the pulse for the first three reflections, it is possible to derive a Laplace Transform that expresses the resultant waveform.

$$V_{meas} = \frac{V_g}{2}\left(1 + \left(\rho + t(1-\rho)e^{-sT} - t(1-\rho)\rho e^{-2sT} + t(1-\rho)\rho^2 e^{-3sT} + ...\right)e^{-sT1}\right) \text{….} \quad (4.4)$$

Equation (4.4) needs some clarification:

- The exponential terms are used to describe each time delay
- T1 is introduced to account for the measurement of the voltage as it occurs at the output of the step generator and is time displaced from the probes by the distance required to travel along the length of the coaxial transmission line. An equation to express this relationship for T1:

  $$T_1 = \frac{2L_{coax}\sqrt{\varepsilon_{rCoax}}}{c} \qquad \text{……...….……...……} \quad (4.5)$$

  where ε_{rCoax} is the dielectric permittivity of the coaxial cable.

- The initial voltage that appears on the transmission system will only be half of the generated voltage due to the fact that the output impedance of the step generator is matched to the characteristic impedance of the coaxial transmission line $(Z_0 = Z_g)$, namely:

  $$V_{initial} = V_g \frac{Z_0}{Z_0 + Z_g} = \frac{V_g}{2} \qquad \text{……...…} \quad (4.6)$$

Combining the mathematical relationships with the lattice diagram methodology, a graphical representation can be derived, shown in Figure 4.3.

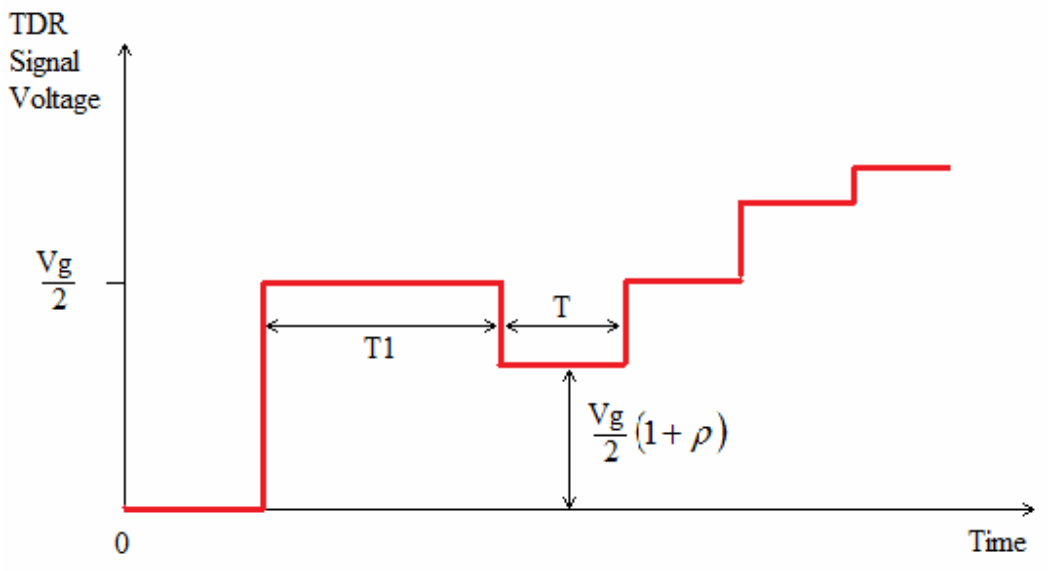

Figure 4.3 *Concept TDR Waveform*

In the next section, the time domain response of a standard 3-wire probe of length 10cm $\left(L_{probe} = 0.1m\right)$ and connected to the TRASE TDR equipment via a 2.2m coax $\left(L_{coax} = 2.2m\right)$ will be modeled using lattice diagrams. The coax used will be RG58U for which the manufacture specifies a dielectric constant $\varepsilon_r = 2.16$ and characteristic impedance $Z_0 = 50\,\Omega$. Two cases will be considered, first with the probe in air and secondly with the probe immersed in water. These two cases will assist with the calibration process of the new probe once it is designed and constructed.

4.3 Standard Probe in Air

At this stage it will be beneficial also to calculate the impedance of the probe itself and equation (2.15) derived by Ball (2002) and presented earlier in chapter 2 will be used:

$$Z_{0\,probe} = \frac{1}{2\pi}\sqrt{\frac{\mu_0}{\varepsilon_0}}\left[\ln\left(\frac{s}{a_i}\right)+\frac{1}{n}\ln\left(\frac{s}{a_0 n}\right)\right] \qquad \text{……...……..…} \quad (4.7)$$

where n = number of outer conductors
s = separation
a_o = radius of outer conductor
a_i = radius of inner conductor

For permeability and permittivity constants $\mu_0 = 1.26\times10^{-6}\,H/m$
$\varepsilon_0 = 8.85\times10^{-12}\,F/m$

The equation is reduced to:

$$Z_{0\,probe} \approx 60\left[\ln\left(\frac{s}{a_i}\right)+\frac{1}{2}\ln\left(\frac{s}{2a_0}\right)\right] \qquad \text{……...……...…….} \quad (4.8)$$

For the 3-wire probe, there are two outer conductors ($n = 2$), equal wire size ($a_o = a_i = 3mm$) and with equal separation ($s = 25mm$). Substituting these values into equation (4.8), the impedance of the probe will be:

$$\begin{aligned} Z_{0\,probe} &= 60\left[\ln\left(\frac{s}{a_i}\right)+\frac{1}{2}\ln\left(\frac{s}{2a_0}\right)\right] \\ &= 60\left[\ln\left(\frac{0.25}{0.03}\right)+\frac{1}{2}\ln\left(\frac{0.25}{2\times0.03}\right)\right] \\ &= 170.03\,\Omega \end{aligned} \qquad \text{.....} \quad (4.9)$$

In air $K_a = \varepsilon_r = 1$, therefore:

$$\begin{aligned} Z_{pSoil} &= \frac{Z_{0\,probe}}{\sqrt{K_a}} \\ &= 170.03\,\Omega \end{aligned} \qquad \text{.....} \quad (4.10)$$

The difference between the impedances of the probe and the coaxial line will create a mismatch at the interface of the two such that the reflection coefficient will be:

$$\rho = \frac{Z_{pSoil} - Z_0}{Z_{pSoil} + Z_0} = 0.546 \quad \text{..... (4.11)}$$

Also, the transmission coefficient at the mismatch is calculated as:

$$t = 1 + \rho = 1.546 \quad \text{..... (4.12)}$$

Time delays along the length of the coaxial cable (T1) and along the probe are:

$$T_1 = \frac{2 \times 2.2\sqrt{2.16}}{3 \times 10^8} = 21\,ns \quad \text{..... (4.13)}$$

$$T = \frac{2 \times 0.1\sqrt{1}}{3 \times 10^8} = 0.7\,ns \quad \text{..... (4.14)}$$

If generator step voltage is assumed to be 2V then:

$$V_{initial} = V_g \frac{Z_0}{Z_0 + Z_g} = \frac{V_g}{2} = \frac{2}{2} = 1\,\text{V} \quad \text{..... (4.15)}$$

With the values now calculated, the lattice diagram can be constructed and waveform produced, shown in Figures 4.4 and Figure 4.5 respectively.

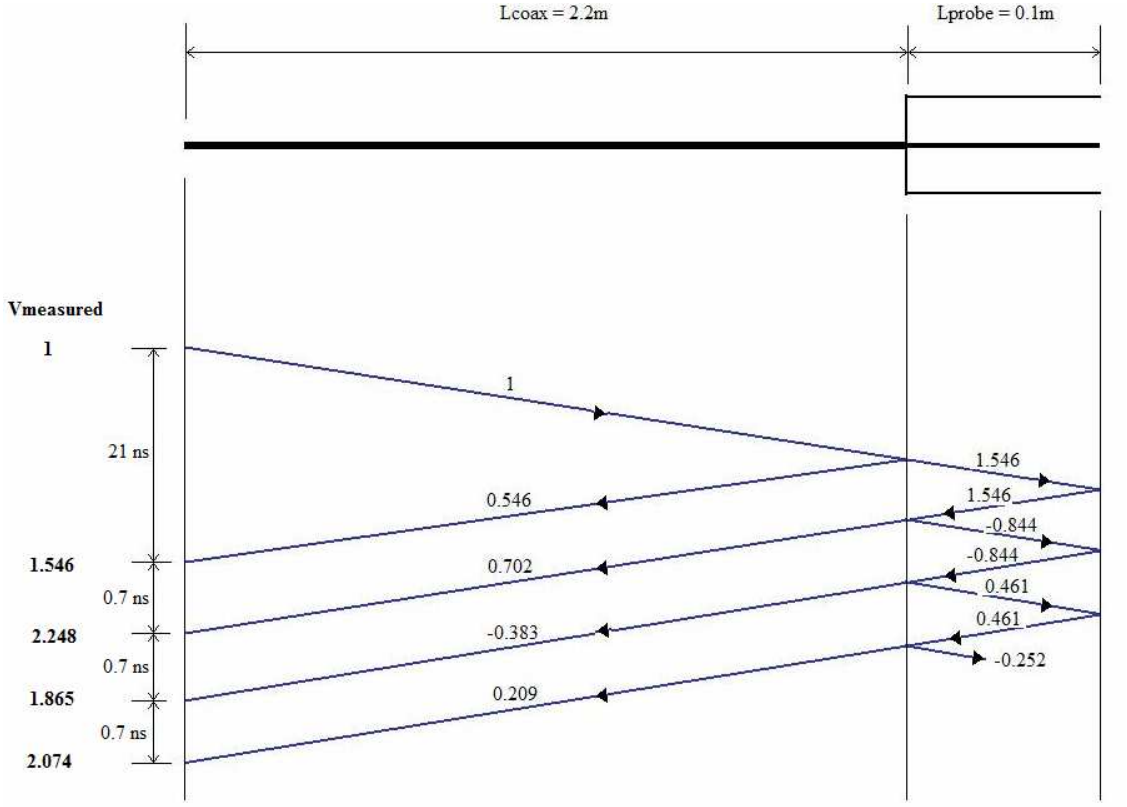

Figure 4.4 *Lattice Diagram (Standard Probe in Air)*

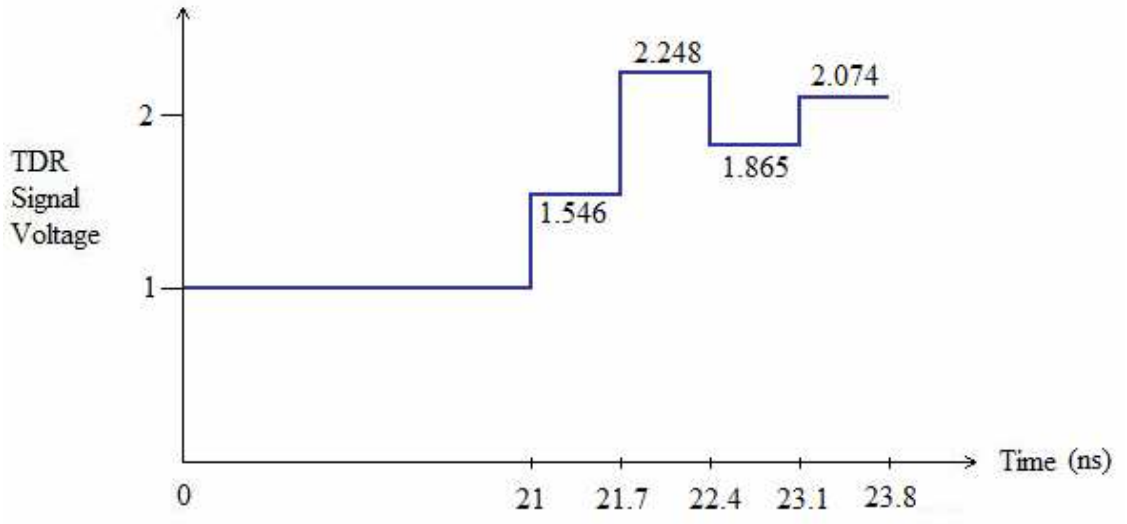

Figure 4.5 *TDR Waveform (Standard Probe in Air)*

4.4 Standard Probe in Water

All previous calculated attributes will be the same as in the previous scenario, except for the effect of the water permittivity on probe impedance. For water, it will be assumed relative permittivity $\varepsilon_r = K_a = 81$, therefore effective probe impedance will be:

$$Z_{pSoil} = \frac{Z_{0\,probe}}{\sqrt{K_a}} = 18.9\,\Omega \quad \text{..... (4.16)}$$

The variation of impedances of the probe and the coax will create a mismatch at the interface of the two such that the reflection coefficient will be:

$$\rho = \frac{Z_{pSoil} - Z_0}{Z_{pSoil} + Z_0} = -0.452 \quad \text{..... (4.17)}$$

Also, the transmission coefficient at the mismatch is calculated as:

$$t = 1 + \rho = 0.548 \quad \text{..... (4.18)}$$

Time delays along the length of the probe will be:

$$T = \frac{2 \times 0.1\sqrt{81}}{3 \times 10^8} = 6\,ns \quad \text{..... (4.19)}$$

A lattice diagram can now be constructed and TDR waveform produced, shown if Figures 4.6 and 4.7 respectively.

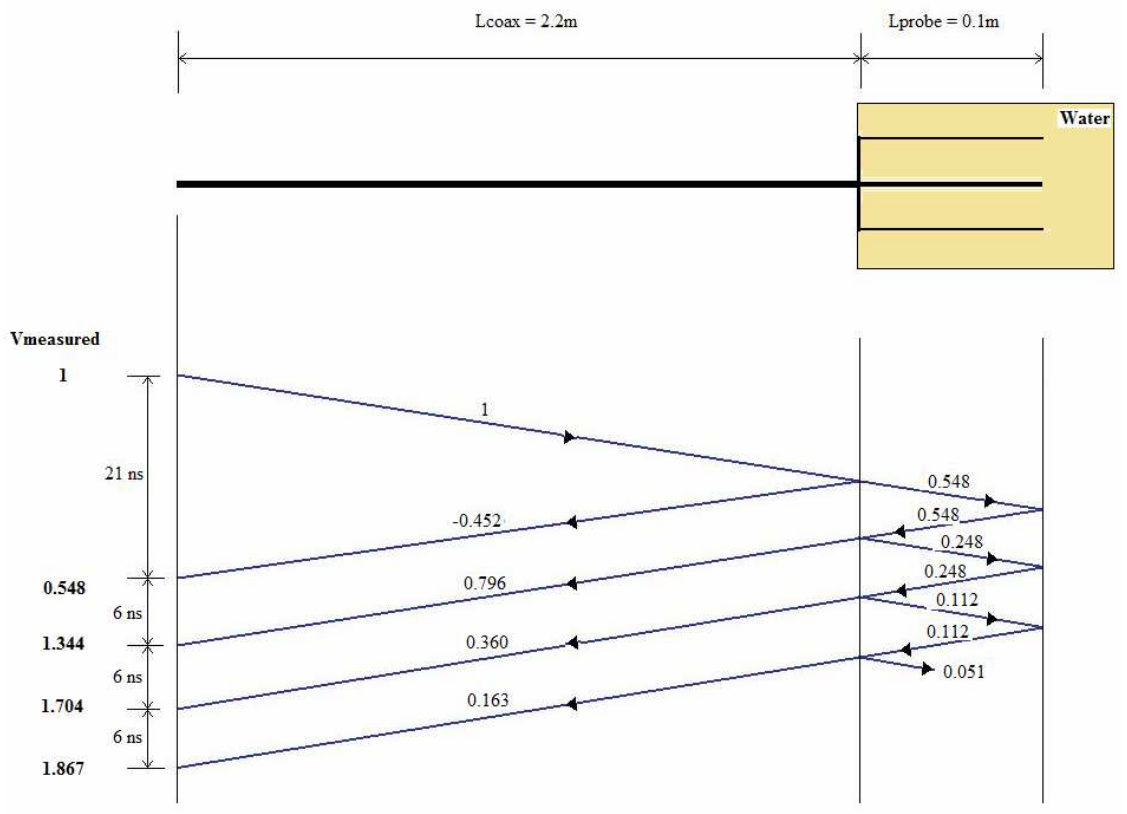

Figure 4.6 *Lattice Diagram (Standard Probe in Water)*

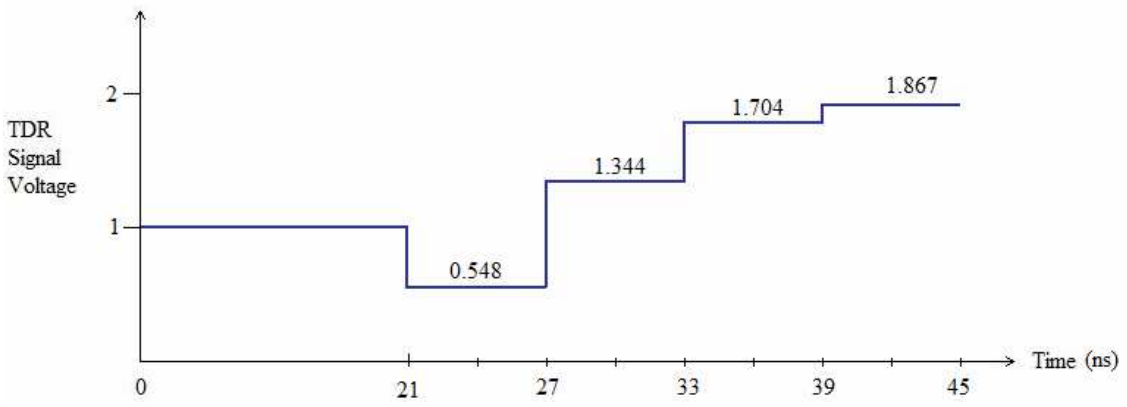

Figure 4.7 *TDR Waveform (Standard Probe in Water)*

It is necessary to note that these TDR waveforms are representations of a lossless transmission system. Lattice diagram methods are simply a tool that lead to an

understanding of the basic nature of signal response, since in a real application, the entire transmission line system is subject to frequency dependent losses. It is the high frequency components of the fast rise time pulse that are most affected by losses during transmission. Other losses are caused by the DC conductivity of the soil (due to the presence of minerals, salts, etc.) and also by the dielectric polarisation losses of the various soil constituents, especially the water. In general, the effect of losses will contribute significantly to rounding of square edges within the waveform, signal attenuation and final DC values.

One of the important features to note in the two previous TDR waveforms is that the amplitude of each subsequent reflection decreases, with the final voltage approaching that of the generator output voltage (V_g). This is intuitive of DC considerations for an open circuit; that is the transmission line is terminated in an open-circuit. As expected then, after only a few reflections the step generator eventually sees an open circuit and thus voltage measured at the sampling receiver $V_{meas} = V_g$. Also of importance is the effect that the relative permittivity characteristics of water and air have on the impedance characteristics of the probe and subsequent waveforms. The first implication is for the creation of an impedance mismatch that affects the reflection properties of the transmission line when the incoming signal encounters the mismatch. Secondly is the effect on timing of reflections. The transit times for reflections are seen to increase with the relative permittivity of the medium surrounding the probe. In this case the transit time increased from 0.7ns for air (Ka=1) to 6ns for water (Ka=81). The next section will investigate these properties when the signal is injected at a point along the length of the probes rather than at the probe's head.

4.5 Conclusions: Chapter 4

A signal that passes along a transmission line system is subject to reflections where any impedance mismatches occur. This chapter has investigated TDR waveform behaviour by

development of a lossless transmission line model and use of lattice diagrams. TDR signal behaviour was examined under various conditions of air and water dielectric properties surrounding standard TDR probes. It was found that as the relative permittivity of the material surrounding the probe increases, that the transit time also increases. The surrounding material has significant implications for the effective impedance of the probe section of the transmission line and consequently for signal reflection properties. The greater the impedance mismatch, the greater is the reflection coefficient. Transmission line principles will be used in the design of the alternate probes in the next chapter.

Chapter 5 Prototype Probe Design

5.1 Introduction

Probe design requirements will be investigated in this chapter such that an effective prototype probe can be constructed. Arbitrary requirements determine overall size and shape while transmission line considerations reveal information about the expected behaviour of an incident signal that is launched from a position two thirds the distance along the probe's centre conductor. Lattice diagrams are again used to determine this behaviour. Workshop production of the designed prototype probe is then detailed.

5.2 Standard Probe Construction

Conventional 3-wire and 2-wire probes in use are represented in Figure 5.1

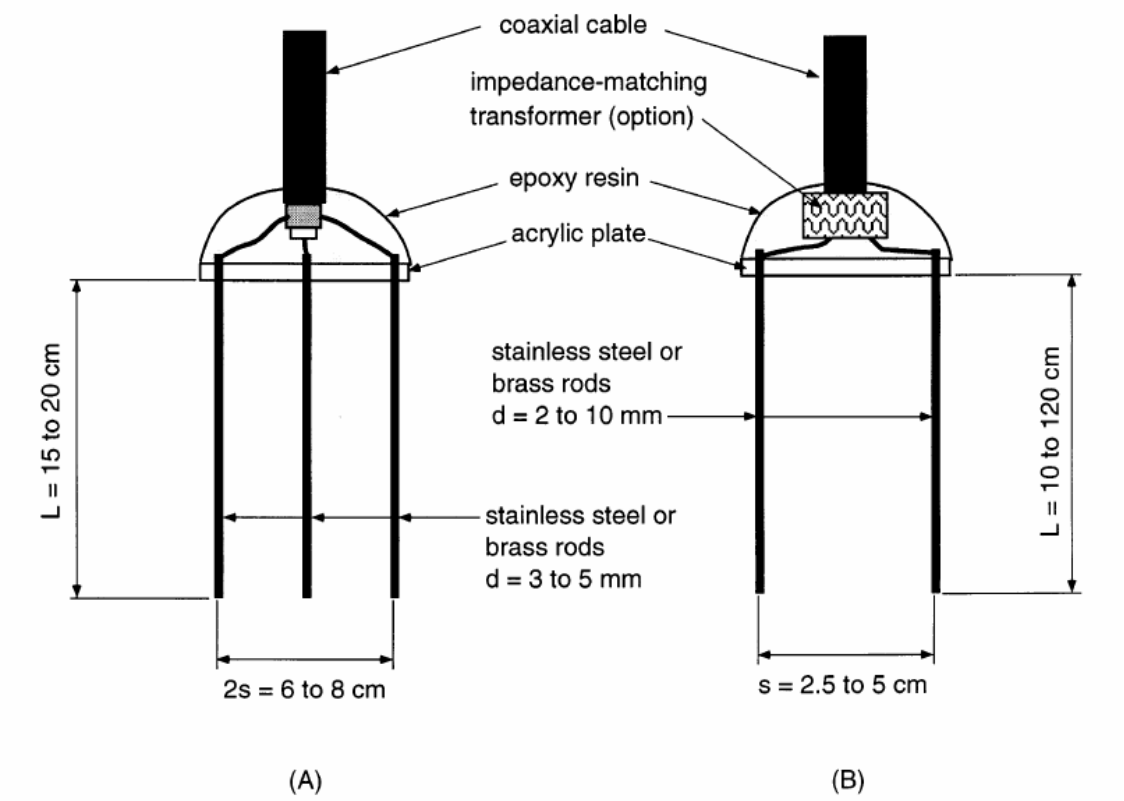

Figure 5.1 *Structural Diagrams of Standard Probes (A) 3-Wire and (B) 2-Wire*

(*Source*: Noborio 2001, p.225)

The three-wire probe is a good approximation of a coaxial cell (Zeglin, White & Jenkins 1989) and does not need an impedance matching transformer as does the two-wire. For this reason it was decided to design a prototype based on the 3-wire concept. Of particular notice in Figure 5.1 is the point of signal injection at the top of the centre wire. The centre wire is electrically isolated from the rest of the structure. The probes are pushed full length into the soil.

5.3 Arbitrary Design Requirements

To reach the top of the zone of interest in the soil, it is desired that the launch of the signal be delayed until it has reached a position approximately two thirds of the distance down the waveguide. This will be achieved by continuing the 50Ω coax inside the probe's centre wire to the new launch point at the start of the root zone area of interest. When the fast rise-time pulse reaches this position, it will begin propagation through the soil. The concept structure for the prototype probe is shown in Figure 5.2.

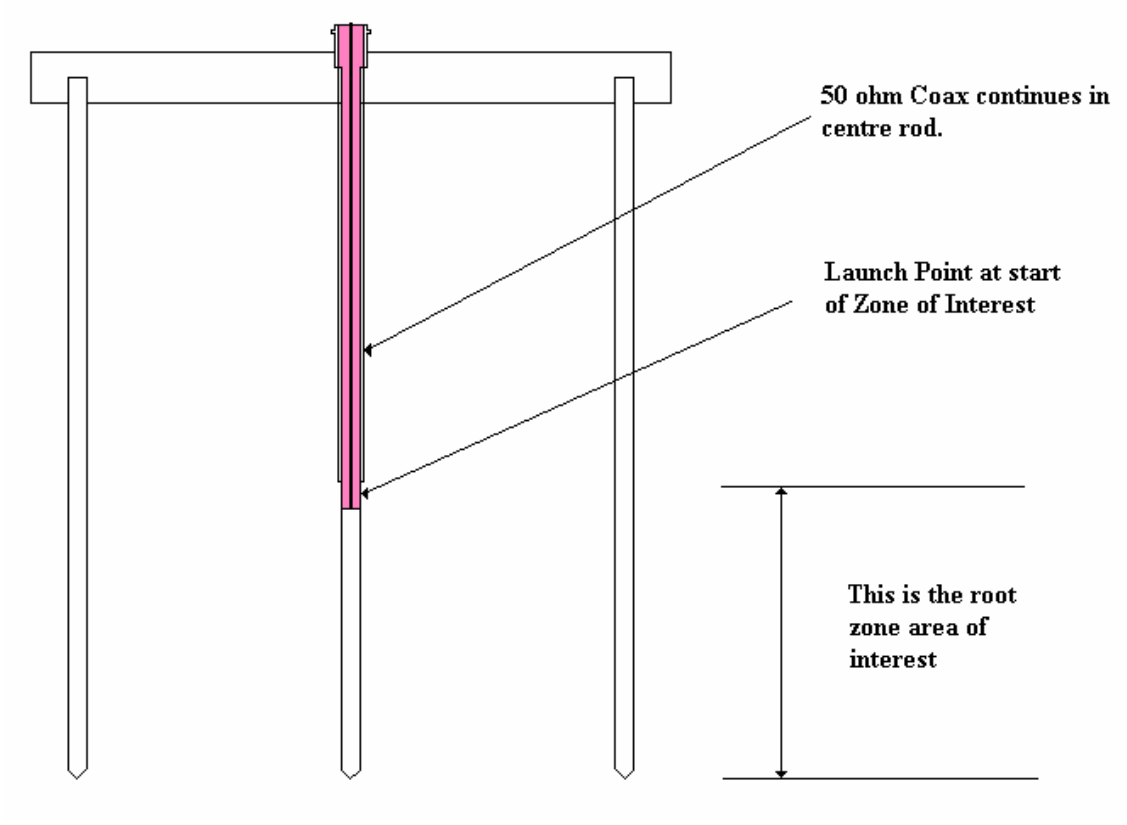

Figure 5.2 *Concept Structure for 3-wire Prototype Probe*

The accuracy of 3-wire probes is reduced when the overall length is less than 10cm. For this reason it was decided to design a probe with at least 10cm wire length after the signal injection point. At the injection point, the TDR signal would emerge as a wavefront, propagating in two directions; one that would travel back up the wires and the other downwards. By constructing probes that have a first section longer than the end section, the part of the TDR signal in the wavefront traveling downwards (that part of the signal that passes through the zone of interest) can easily be distinguished from the wavefront traveling upwards (since the timing of its reflection is much greater). To achieve this it was decided to construct the probes with a 20cm first section that would house the coaxial transmission line to the point of injection. Keeping the probes to an overall length of 30cm would also be of advantage so that later soil testing in the laboratory could be compared to the TRASE's standard 30cm 'connector' probe used as a control. A square panel mount BNC connector is fitted on the head of the new probe. What then about wire

sizes and separation dimensions? The next section will investigate design implications for characteristic impedance.

5.4 Transmission Line Considerations

5.4.1 Transmission Line Modeling

Transmission line theory can be utilised to analyse the connection of a single 50 Ω coaxial transmission line to a parallel 3-wire transmission line. Figure 5.3 gives a representation of the direction of waves at the emergence from the launch point and at the end of the probes.

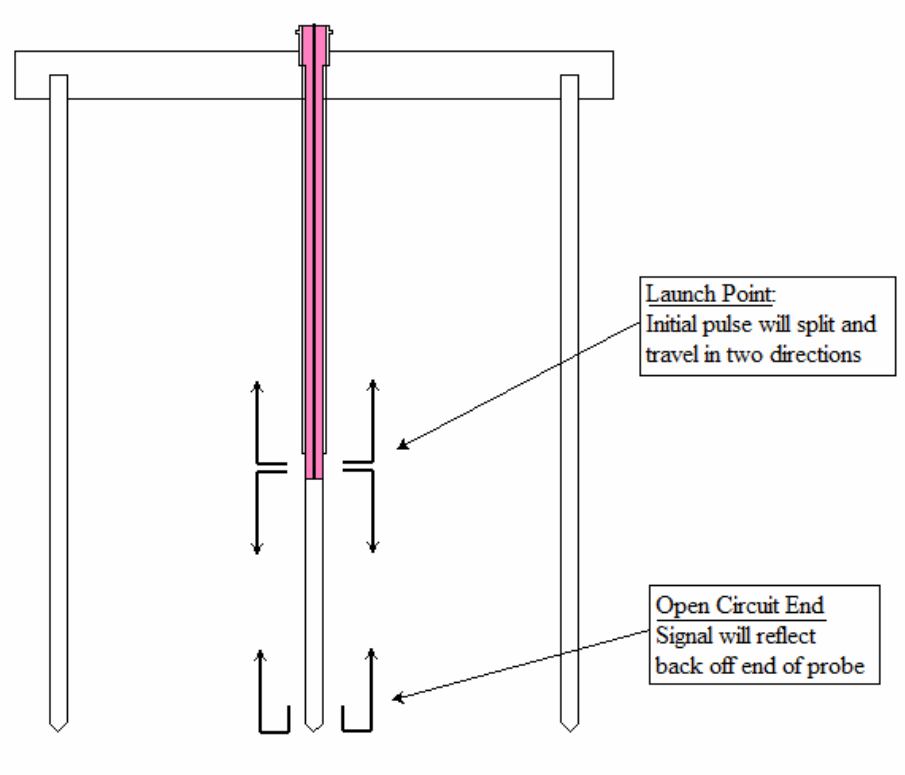

Figure 5.3 *Signal Splitting at Launch Point*

The characteristic impedance of the parallel 3-wire transmission line is the same in both directions and is dependant on the probe structural dimensions and the dielectric properties of the soil present. It is necessary then to use a transmission line model to

investigate the behaviour of the wave at this point. Figure 5.4 shows the direction of signal travel at the launch point while Figure 5.5 displays an equivalent circuit diagram.

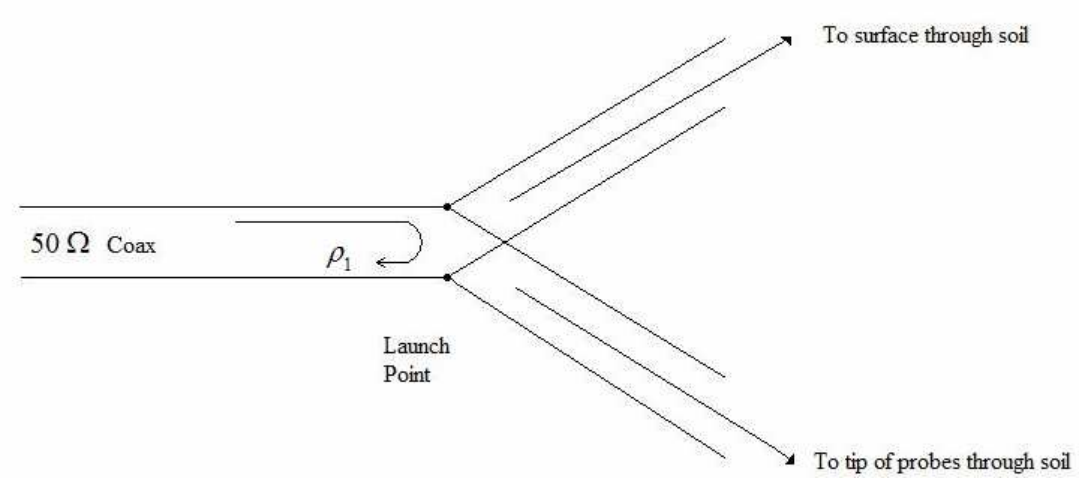

Figure 5.4 *Direction of Signal Travel at Launch Point*

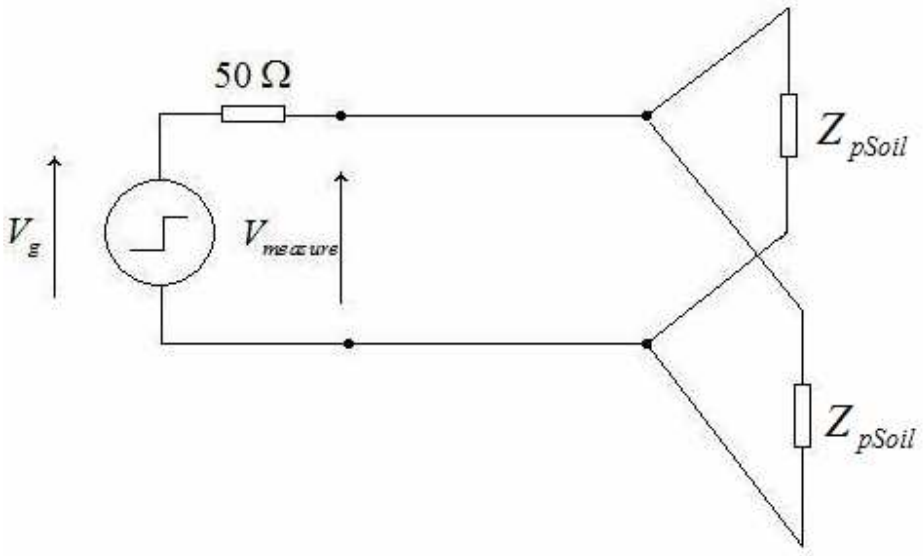

Figure 5.5 *Equivalent Circuit for Initial Launch of Wave*

The launched wave will see a parallel 3-wire transmission line of equal impedance in each direction. This will effectively halve the initial signal power. The wave that travels back up through the soil to the head of the probe has a much greater distance to travel

than the wave traveling through the soil to the end of the probe. For this reason, the upward traveling wave can be ignored since any reflections will not be seen until much later. It is the downward traveling wave that is of importance and will be tracked.

The voltage reflection coefficient of the incident wave off the mismatch shown in Figure 5.4 will be labeled ρ_1 and can be determined as:

$$\rho_1 = \left(\frac{\left(Z_{pSoil} // Z_{pSoil}\right) - Z_0}{\left(Z_{pSoil} // Z_{pSoil}\right) + Z_0} \right)$$

$$= \left(\frac{\frac{Z_{pSoil}}{2} - Z_0}{\frac{Z_{pSoil}}{2} + Z_0} \right) \qquad \text{..... (5.1)}$$

For each of the two waves the transmission coefficient will be:

$$t_1 = (1 + \rho_1) \qquad \text{..... (5.2)}$$

The signal reflecting off the end of the probe wires will encounter a different scenario when it arrives back at the launch point. Some of the energy will travel back into the coax and continue back to the TRASE unit. Some of the energy will continue to travel through the soil back towards the surface, while some will be reflected off the mismatch and back down through the soil to the probe tip again. Figure 5.6 shows the direction of signal travel when the reflected signal returns to the launch point, and Figure 5.7 displays an equivalent circuit diagram.

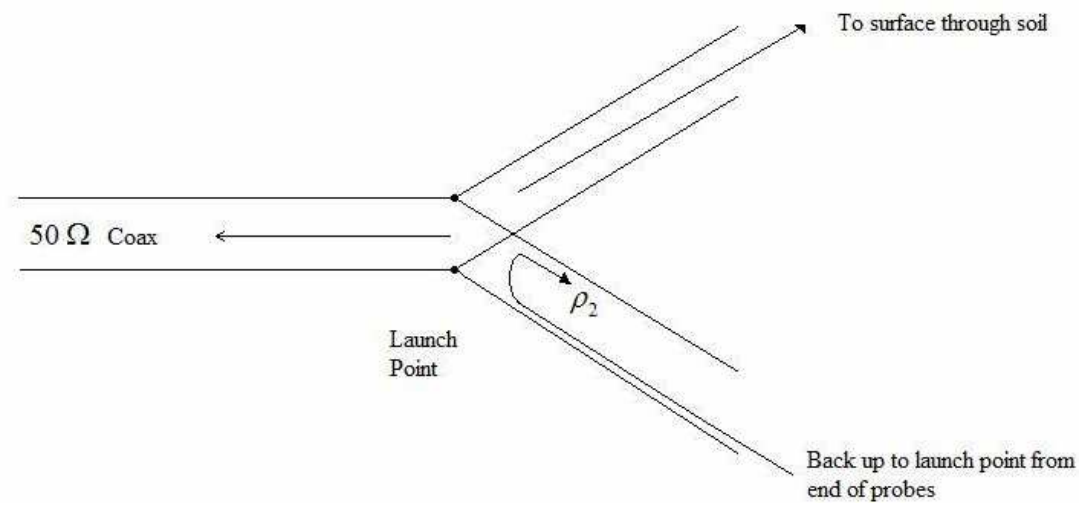

Figure 5.6 *Direction of Signal travel when returning to Launch Point*

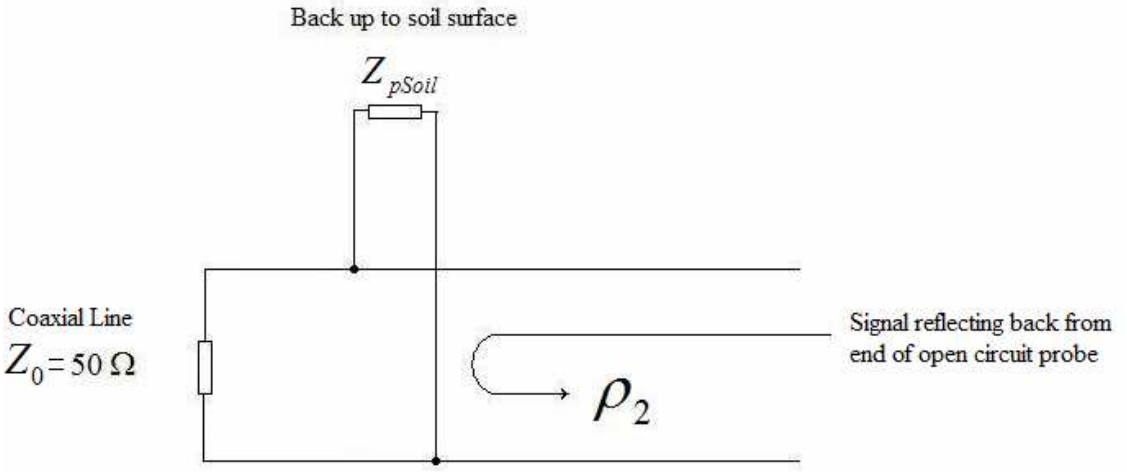

Figure 5.7 *Equivalent Circuit for Wave reflected back off Open Circuit End*

Some of the first reflected wave will again be reflected off the mismatch of Figure 5.6 back down through the soil to the tip of the probe and will be labeled ρ_2 and can be determined as:

$$\rho_2 = \left(\frac{\left(Z_0 // Z_{pSoil}\right) - Z_{pSoil}}{\left(Z_0 // Z_{pSoil}\right) + Z_{pSoil}} \right)$$

$$= \left(\frac{\left(\frac{Z_0 Z_{pSoil}}{Z_0 + Z_{pSoil}} \right) - Z_{pSoil}}{\left(\frac{Z_0 Z_{pSoil}}{Z_0 + Zp_{Soil}} \right) + Z_{pSoil}} \right) \quad \text{..... (5.3)}$$

The new transmission coefficient will be:

$$t_2 = (1 + \rho_2) \quad \text{..... (5.4)}$$

where 1 represents the first reflected wave $t_1 = (1 + \rho_1)$, thus:

$$t_2 = \left(t_1 + \rho_2\right) = \left(1 + \rho_1 + \rho_2\right) \quad \text{..... (5.5)}$$

The effect of the two connected transmission lines on the amount of signal transmitted into the coaxial line back towards the TRASE unit can be given as:

$$t_2 \left(\frac{Z_0}{Z_0 + Z_{pSoil}} \right) \quad \text{..... (5.6)}$$

This will not be the same for the amount of signal transmitted back up the soil to the surface; this will in fact be equivalent to:

$$t_2 \left(\frac{Z_{pSoil}}{Z_{pSoil} + Z_0} \right) \quad \text{..... (5.7)}$$

5.4.2 General Lattice Diagram

A general lattice diagram (Figure 5.8) will now be developed so that the previously derived relationships between incident and subsequent reflected waves at the launch point can be clearly understood.

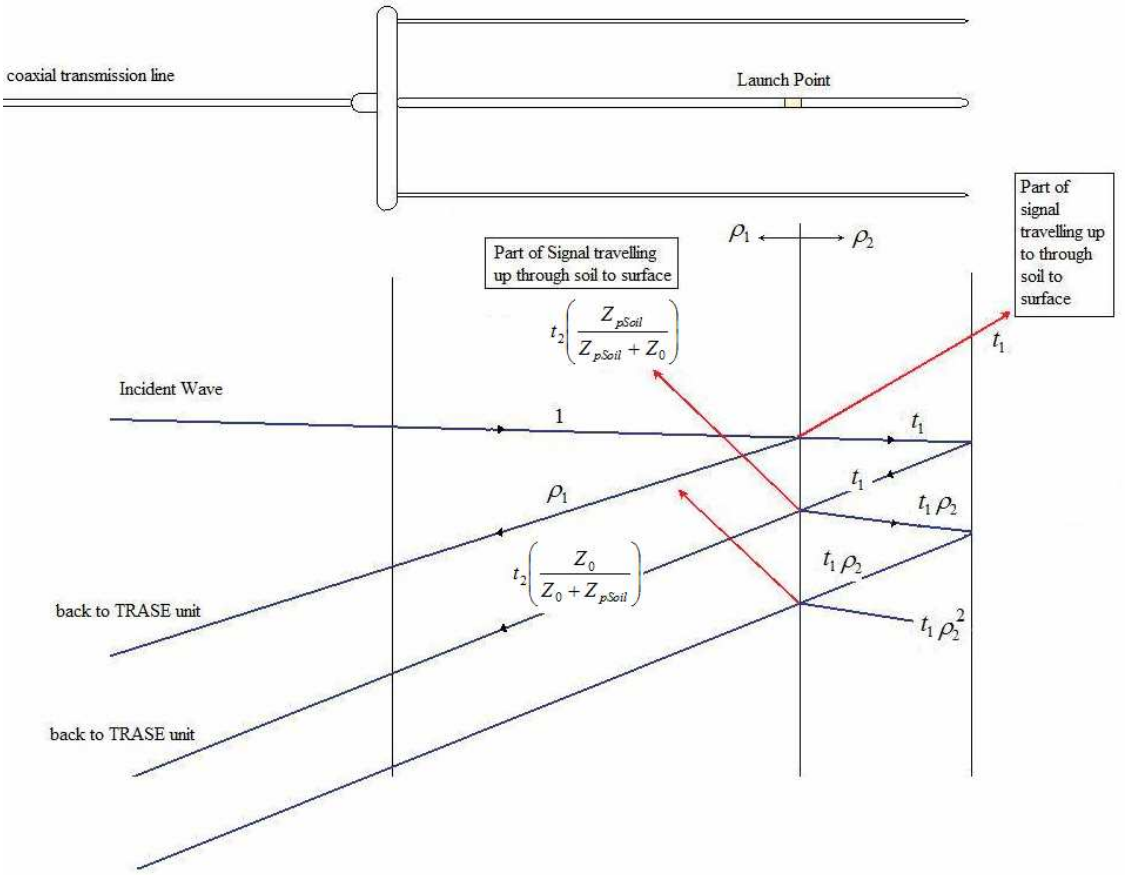

Figure 5.8 *General Lattice Diagram for Prototype Probe*

5.5 Probe Characteristic Impedance

The probe will be required to give good signal transfer from the coaxial transmission line under a range of various conditions; that is relative permittivity will vary according to the amount of moisture present in the soil. Maximum signal transfer will occur if the impedance mismatch at the launch point is minimised such that:

$$Z_0 \cong Z_{pSoil} // Z_{pSoil} = 50\,\Omega \qquad \text{..... (5.8)}$$

Therefore it is desirable that $Z_{pSoil} \cong 100\,\Omega$.

From earlier chapters it was established that:

$$Z_{pSoil} = \frac{Z_{0\,probe}}{\sqrt{\varepsilon_r}} \qquad \text{..... (5.9)}$$
$$Z_{0\,probe} = Z_{pSoil}\sqrt{\varepsilon_r}$$

In dry soil, apparent dielectric permittivity may be as low as $K_a = 2$. Substitution of $K_a = 2$ for ε_r into (5.9) gives:

$$\begin{aligned} Z_{0\,probe} &= Z_{pSoil}\sqrt{K_a} \\ &= 100 \times \sqrt{2} \\ &= 141\,\Omega \end{aligned} \qquad \text{..... (5.10)}$$

The extreme of the range would be experienced in a situation where soil is saturated. Using the Topp Equation (2.9) and knowledge of soil properties that determine saturation at around 30%, Ka can be calculated as 16.5. In this case:

$$\begin{aligned} Z_{0\,probe} &= Z_{pSoil}\sqrt{K_a} \\ &= 100 \times \sqrt{16.5} \\ &= 406\,\Omega \end{aligned} \qquad \text{..... (5.11)}$$

Following on from the above it is desirable then that the characteristic impedance of the probe be somewhere in the middle of the range, say $200 - 250\Omega$.

Investigations of some variations of wire separation and diameter will determine their effect on characteristic impedance. The earlier equation (4.7) by Ball (2002) will be used for the calculation.

Recalling that:

a_i = radius of inner conductor
a_0 = radius of outer conductors
s = separation distance between inner and outer conductors
n = number of outer conductors

Sizing and spacing of conductors is also limited by the material sizing available commercially, and also in keeping with some of the arbitrary considerations earlier in the

chapter. In general it was decided to design a probe of similar dimensions to the commercially available ones. A further consideration was that the hollow centre conductor must have sufficient internal dimensions capable of housing the RG58U coaxial cable.

Table 5.1 *Design Variations of Prototype Probe*

Design Variation	a_i mm	a_0 mm	s mm	n	$Z_{0\,probe} \approx 60\left[\ln\left(\frac{s}{a_i}\right)+\frac{1}{2}\ln\left(\frac{s}{2a_0}\right)\right]$
1	3.175	1.575	25	2	$186.0\,\Omega$
2	3.175	3.175	25	2	$164.9\,\Omega$
3	3.175	1.575	50	2	$248.3\,\Omega$
4	3.175	1.925	30	2	$196.3\,\Omega$
5	5.0	1.925	30	2	$169.1\,\Omega$

From the table it can be seen that increasing separation between conductors results in an increase in characteristic impedance. Conversely, increasing the size of the outer conductors decreases characteristic impedance, as does increasing the size of the internal conductor. Design variation No.4 was selected as being most suitable for satisfying the most number of design requirements as outlined previously. With this design, impedence matching can be calculated to occur at a specific apparent permittivity, namely:

$$\begin{aligned} K_a &= \left(\frac{Z_{0\,probe}}{Z_0}\right)^2 \\ &= \left(\frac{196.3}{50}\right)^2 \\ &= 15.41 \end{aligned} \qquad \text{..... (5.12)}$$

which occurs for volumetric water content (via Topp equation) θ_v =28%.

5.6 Lattice Diagram and TDR Waveform

Information has been derived in sections 5.4 and 5.5 to construct a lattice diagram from which a TDR waveform can be derived. The remaining information required is that of timing of the incident wave and subsequent reflections.

The coaxial cable length will be 2.2m to the top of the head of the probe and then can be considered to continue into the first 20cm of the probe. Therefore the total length can be considered as $L_{coax} = 2.4m$. Timing for signal propagation from the step generator to the launch point via the coaxial transmission line (and back) will therefore be:

$$T_1 = \frac{2 \times L_{coax}\sqrt{\varepsilon_r}}{c} = \frac{2 \times 2.4\sqrt{2.16}}{3 \times 10^8} = 23ns \quad \text{..... (5.13)}$$

The lower section of the probe after the launch point is 10cm long. Timing for signal propagation from the launch point to the end of the probes (and back) via the 'probe in soil' transmission line will therefore be:

$$T = \frac{2 \times L_{\text{Pr}obe}\sqrt{\varepsilon_r}}{c} \quad \text{..... (5.14)}$$

As in Chapter 4, two separate cases will be considered. First with the probe in air and secondly with the probe submersed in water.

5.6.1 Prototype Probe in Air

In air $K_a = \varepsilon_r = 1$, therefore timing for the lower section transit can be made using eqn.(5.14) such that:

$$T = \frac{2 \times 0.1\sqrt{1}}{3 \times 10^8} \quad \text{..... (5.15)}$$
$$= 0.7\ ns$$

Also the impedance of the probe in soil can be found:

$$Z_{pSoil} = \frac{Z_{0\,probe}}{\sqrt{K_a}} = \frac{196}{\sqrt{1}} = 196\ \Omega \quad \text{..... (5.16)}$$

The reflection coefficient of the incident wave at the launch point was determined in (5.1) to be:

$$\rho_1 = \left(\frac{\frac{Z_{pSoil}}{2} - Z_0}{\frac{Z_{pSoil}}{2} + Z_0} \right) = \left(\frac{\frac{196}{2} - 50}{\frac{196}{2} + 50} \right) = 0.324 \quad \text{..... (5.17)}$$

The transmission coefficient (using equ. 5.2) will be:

$$t_1 = (1 + \rho_1) = 1.324 \quad \text{..... (5.18)}$$

The arrival of the first reflection back at the launch point experiences a different reflection shown in eqn. (5.3) as ρ_2, and can be determined as:

$$\rho_2 = \left(\frac{\left(\frac{Z_0 Z_{pSoil}}{Z_0 + Z_{pSoil}} \right) - Z_{pSoil}}{\left(\frac{Z_0 Z_{pSoil}}{Z_0 + Zp_{Soil}} \right) + Z_{pSoil}} \right) = -0.662 \quad \text{..... (5.19)}$$

The second transmission coefficient (eqn. 5.5) can be determined as:

$$t_2 = 1 + \rho_1 + \rho_2 = 0.662 \quad \text{..... (5.20)}$$

With the values now calculated, the lattice diagram can be constructed and waveform produced, shown in Figures 5.9 and Figure 5.10 respectively.

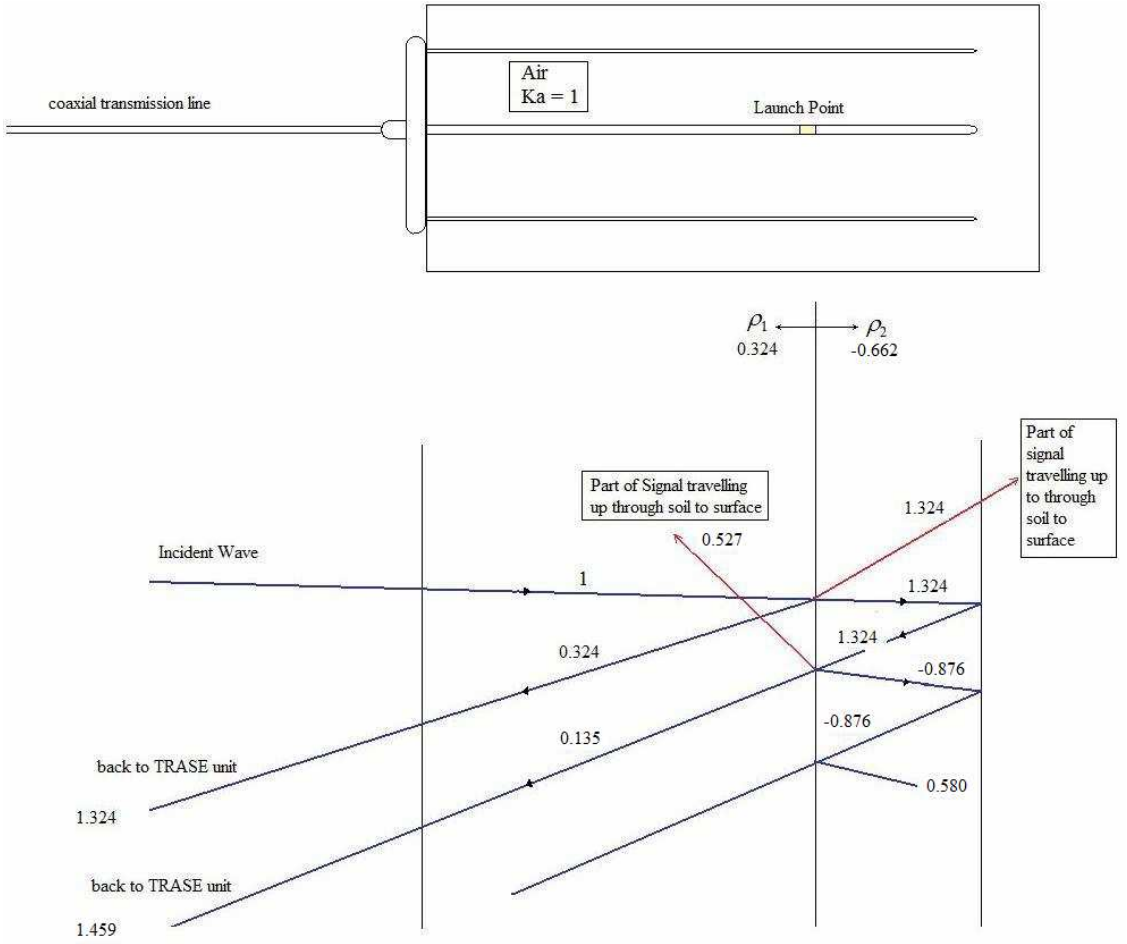

Figure 5.9 *Lattice Diagram for Prototype Probe in Air (Ka = 1)*

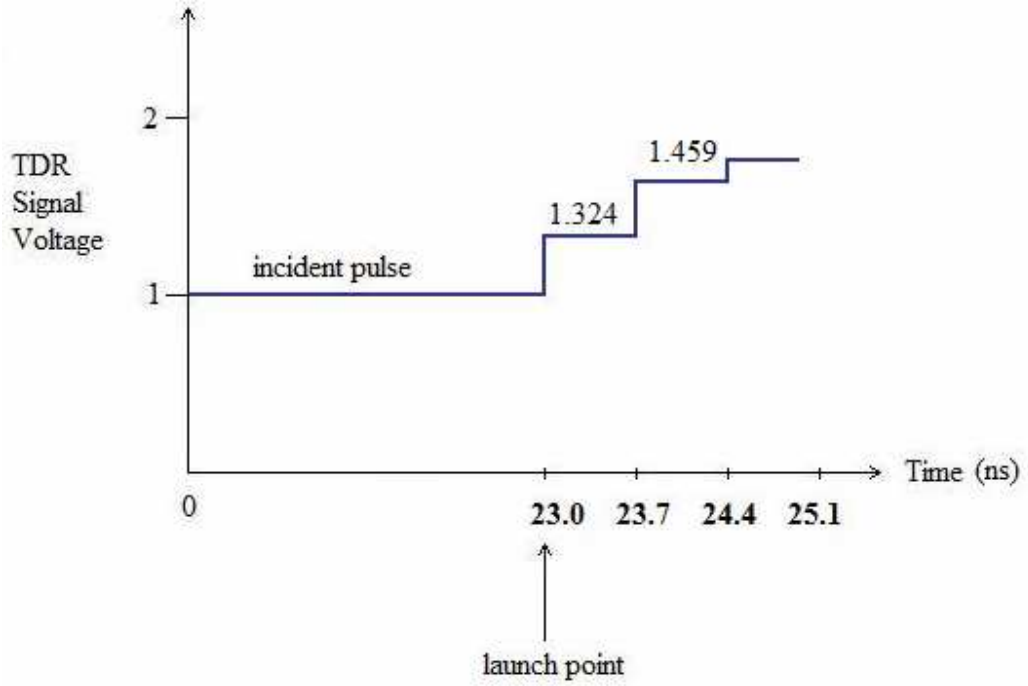

Figure 5.10 TDR *Waveform for Prototype Probe in Air (Ka=1)*

5.6.2 Prototype Probe in Water

All previous calculated attributes will be the same in this scenario as previous, except for the effect of the water permittivity on probe impedance. For water, it will be assumed relative permittivity $\varepsilon_r = K_a = 81$, therefore timing for the lower section transit can be made using (5.14) such that:

$$T = \frac{2 \times 0.1\sqrt{81}}{3 \times 10^8} \qquad \text{…….....……. (5.21)}$$
$$= 6\,ns$$

Also the impedance of the probe in soil can be found:

$$Z_{pSoil} = \frac{Z_{0\,probe}}{\sqrt{K_a}} = \frac{196}{\sqrt{81}} = 21.8\ \Omega \quad \text{..... (5.22)}$$

The reflection coefficient of the incident wave at the launch point can be determined by use of eqn. (5.1), such that:

$$\rho_1 = \left(\frac{\frac{Z_{pSoil}}{2} - Z_0}{\frac{Z_{pSoil}}{2} + Z_0} \right) = -0.642 \quad \text{..... (5.23)}$$

The transmission coefficient (using equ. 5.2) will be:

$$t_1 = (1 + \rho_1) = 0.358 \quad \text{..... (5.24)}$$

The arrival of the first reflection back at the launch point experiences a different reflection shown in eqn. (5.3) as ρ_2, and can be determined as:

$$\rho_2 = \left(\frac{\left(\frac{Z_0 Z_{pSoil}}{Z_0 + Z_{pSoil}} \right) - Z_{pSoil}}{\left(\frac{Z_0 Z_{pSoil}}{Z_0 + Zp_{Soil}} \right) + Z_{pSoil}} \right) = -0.179 \quad \text{..... (5.25)}$$

The second transmission coefficient (using eqn. 5.5) can now be determined as:

$$t_2 = 1 + \rho_1 + \rho_2 = 0.179 \quad \text{..... (5.26)}$$

With the values now calculated, the lattice diagram can be constructed and waveform produced, shown in Figures 5.11 and Figure 5.12 respectively.

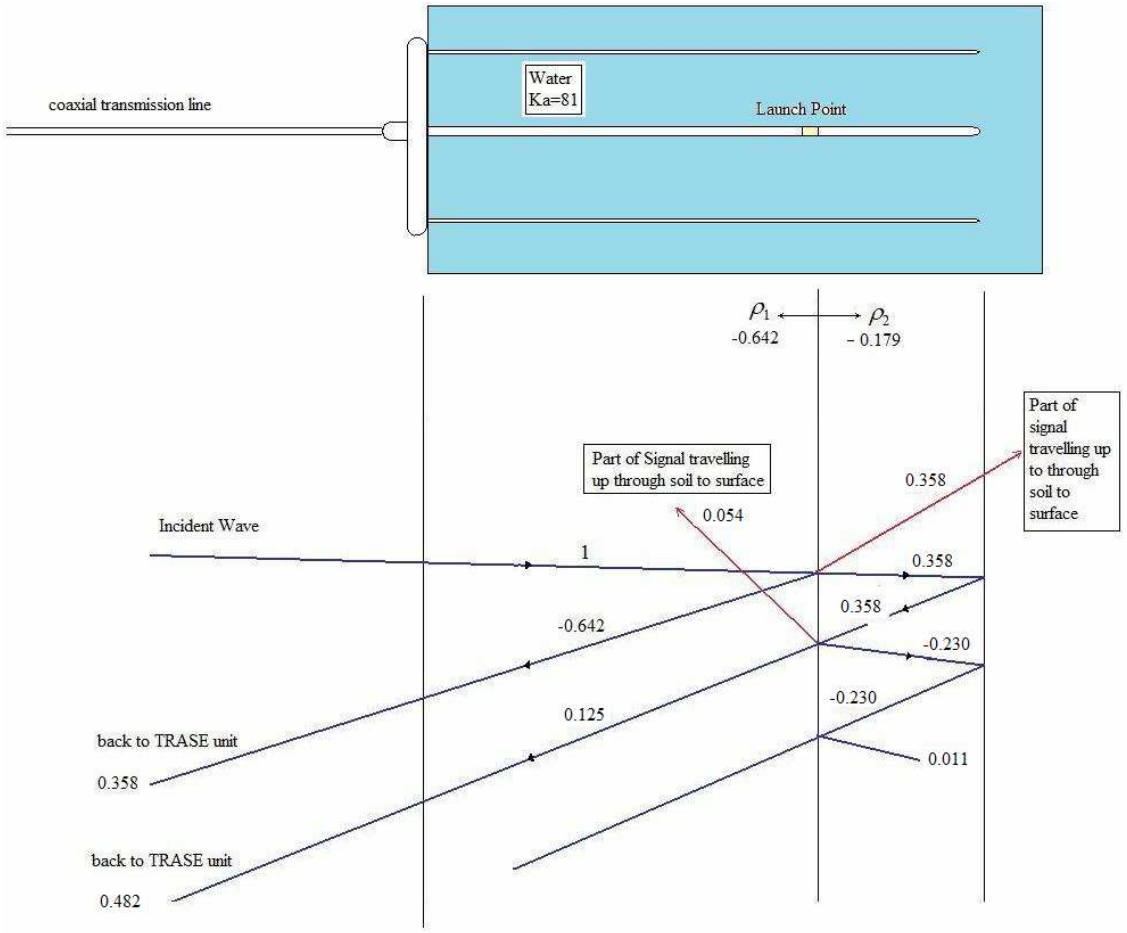

Figure 5.11 *Lattice Diagram for Prototype Probe in Water (Ka=81)*

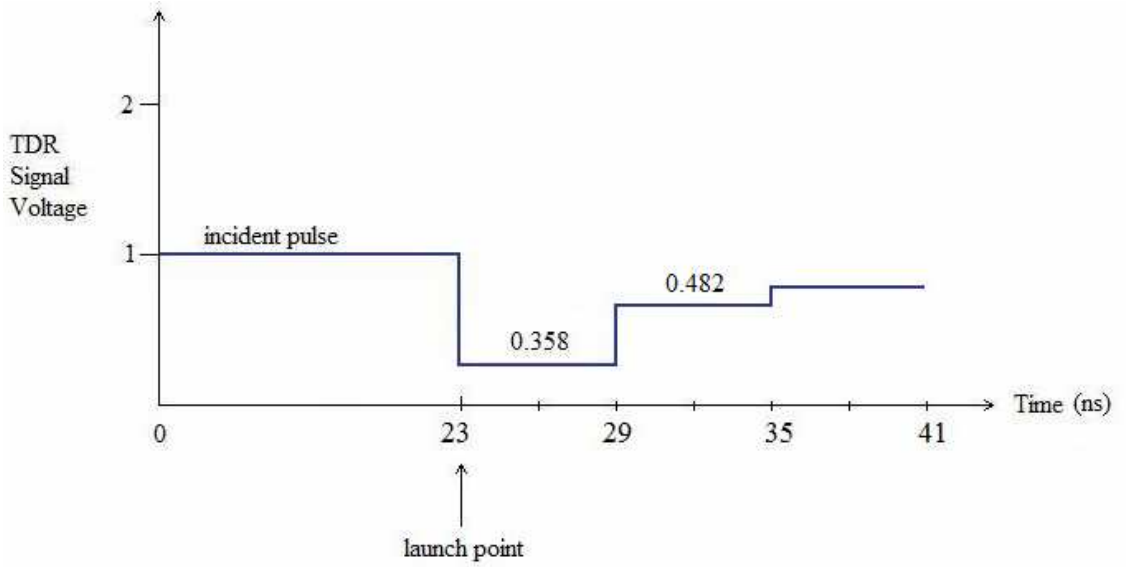

Figure 5.12 *TDR Waveform for Prototype Probe in Water (Ka=81)*

5.7 Mechanical Construction

All materials chosen for construction of the prototype are stainless steel of Grade 316 quality. Workshop construction of the probe included the use of milling machine to produce a suitable arbor, and silver soldering of the inner and outer conductors to the arbor. The centre conductor was chosen with sufficient inner diameter to accommodate the coaxial cable to the launch point. The launch point itself would need to be of insulating material, transferring the injection signal from the coaxial transmission line to the probe end section, thus allowing propagation into the soil medium. It would also have to be mechanically robust such that a threaded connection between the upper section and the solid end section could be achieved. Some HDPE (high density polyethylene) material was found to be most suitable for turning and threading to the desired dimensions. The inner conductor of the coax is passed through the launch point connection into the solid end section, secured in place by a stainless steel grub screw. As stated in section 5.3, the connection of the coax to the probe is via a panel mount BNC connector which is secured in place by four screws. Threads are tapped into the arbor to accommodate the mounting screws.

Figures 5.13 - 5.15 that follow show details of the above mentioned mechanical design statements. In particular the overall size and appearance, a disassembled view and the launch point connector are displayed. Further details of the prototype probe construction and mechanical drawings are found in Appendix D

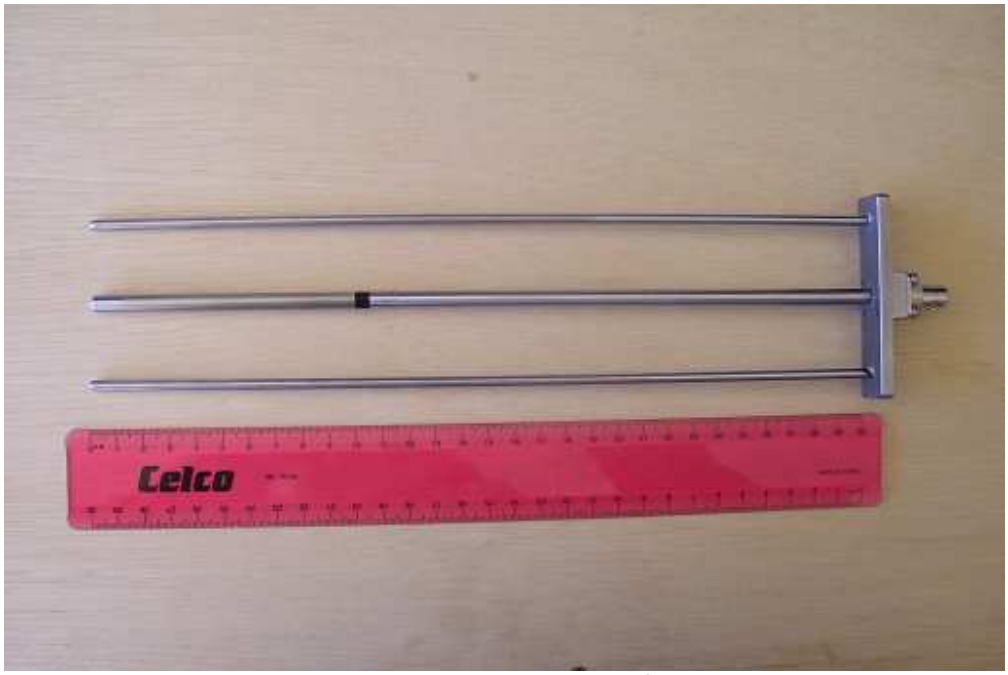

Figure 5.13 *Overall Size and Appearance of Prototype Probe*

Figure 5.14 *Disassembled View of Prototype Probe*

Figure 5.15 *Launch Point Connector of Prototype Probe*

5.8 Conclusions: Chapter 5

Transmission line considerations and the application of lattice diagrams have been useful in the determination of TDR responses that support the design of a prototype probe. It was discovered that the impedance mismatch that occurs at the launch point must be minimised in order to obtain maximum signal transmission into the soil under test. The signal is severely attenuated due to a splitting into two directions at this point. Probe conductor separation and dimensions can be altered to vary the characteristic impedance of the probe. A stainless steel prototype was then constructed in the workshop. Laboratory procedures and calibration of the probe will be addressed in the next chapter such that it can be analysed under soil testing conditions.

Chapter 6 Laboratory Procedures and Calibration of Prototype Probe

6.1 Introduction

Utility and performance of the prototype probe needs to be investigated by laboratory testing of soil samples. This chapter will first establish the soil preparation and laboratory testing procedures to be used. Problems associated with use of an unfamiliar probe to the TRASE system are highlighted, discussed and overcome. The calibration process is conducted in conjunction with the expected waveforms that were derived by theory in Chapters 4 and 5. Although it will be shown that excess signal loss is experienced, the prototype probes in general perform in close alignment with the expected behavior.

6.2 Soil Used for TDR Measurements

To test the functionality of the new probe, measurements will need to be conducted on a soil type somewhat consistent with 'standard' soil types used in other empirical testing procedures (Sabburg 1993, Topp, Davis & Annan 1980). The soil chosen was available in the USQ's Geology Workshop and was of a sandy soil type. This soil was not subject to any noticeable expansion with increasing moisture content as do some heavy clay soils. The soil however was initially quite lumpy and solid. To provide a more consistent and homogeneous structure, and to aid probe insertion it was decided to first pulverise the soil and then sieve it to 10mm. This was in keeping with other laboratory testing procedures (Habash 1994).

6.3 Laboratory Procedures

The testing equipment used to test the prototype probe was the same as described previously in Chapter 3. This section will give further details of the equipment and experimental procedures used.

The TRASE instrument was used to measure the TDR response of the prototype probe in a tube filled with soil samples. The tube constructed for this thesis is made of UPVC, 5mm wall thickness, 250mm outside diameter and 500mm deep. The soil testing tube is shown in Figure 6.1 with prototype probes shown, and in Figure 6.2 (top view).

Figure 6.1 *Laboratory Testing Tube (with Prototype Probe shown)*

Figure 6.2 *Laboratory Testing Tube (top view)*

The dimensions of the testing tube were chosen such that the 300mm probes could be fully inserted into soil samples with sufficient depth of soil beneath the probes and surrounding them such that the test signal would not be influenced by any materials other than the soil. Research by Habash (1994) asserts that measurements are unaffected if they are positioned approximately 5cm from the outer boundaries of the testing tube. If these limits are encroached then reliability of measurements is decreased. The cylindrical nature of the testing tube with a flat PVC base plate was also desirable since it provided accurate measurement of the soil sample volume. The experimental setup used in the laboratory to conduct all measurements is shown in Figure 6.3. Shown is the TRASE measurement instrument connected to the probe via a 2.2m coaxial cable. The probe is inserted into a soil sample in the testing tube; measurements are then taken by the TRASE.

Figure 6.3 *Measurement System including TRASE and Soil Testing Tube*

As a means of calibration, the prototype probe was first tested suspended in free air, then in water. Subsequent to these 'calibration' tests, a thorough and systematic set of tests in soil samples of varying moisture contents were then conducted. For each set of tests conducted on a particular soil sample, the probes were placed in three different positions around the centre area of the testing tube, with five measurements recorded in each position. The information recorded was then averaged to produce a reliable representation. In addition, the TRASE supplied 30cm 'connector' type probes and 10cm 'buriable' probes were also used in the same manner to test each soil sample, providing

comparison, or 'standard' measurements. Distilled water, rather than town supply or rain water was chosen for all tests to ensure consistency with established laboratory testing procedures. The process used will now be described.

First, the soil was oven dried for 24 hours at $105^{o}C$ to remove all water content and weighed. Mixing of the desired amount of water was performed to ensure even distribution of the water throughout the sample. This was achieved by placing the dried soil into a 200 litre plastic tub and application of the water with a spray bottle. This procedure is depicted in Figure 6.4. As the moisture is added the soil is cultivated and turned frequently with a small trowel.

Figure 6.4 *Application of Water to Soil Sample in 200litre Tub*

The wet soil was then placed into the testing tube. In an attempt to maintain even soil density throughout the tube, approximately 50mm of soil was placed in at a time and

lightly compacted with a long-handled ramming device. This process is depicted in Figure 6.5.

Figure 6.5 *Compacting Soil Sample to Ensure Even Density*

Once filled, the testing tube was sealed and put aside for 24hours. This was done in order to achieve even curing of the sample so that any expansion of the soil was allowed for. This procedure aligns well with real world conditions whereby certain soil types are quite expansive under wet conditions.

Following the curing process, the soil samples were then measured with the TRASE TDR equipment, using the fore mentioned procedures. Readings of apparent dielectric constant (Ka) and volumetric water content (θ_v) were recorded, along with graphs of the signal waveform as it was passed through the transmission system. Measurements are stored

within the TRASE's internal memory; each reading is labeled by the user. All measurements recorded were then downloaded via RS232 serial cable to a laptop computer (shown in Figure 6.6). Transfer of data was facilitated by use of the HyperTerminal communication protocol (Hilgraeve Inc. Detroit, Michigan). This protocol allows download of only one file at a time. All files of graphs and data are stored and transferred in ASCII format.

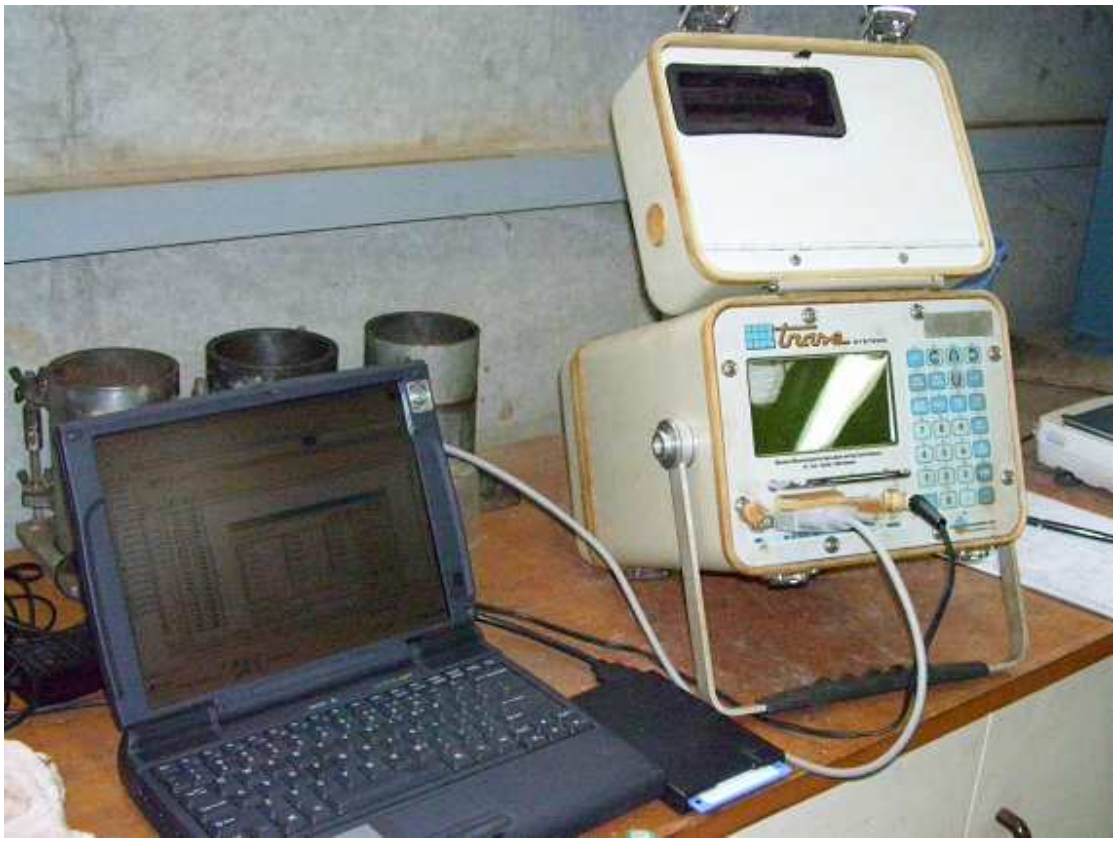

Figure 6.6 *Downloading of TDR Waveforms to Laptop via RS232 Serial Port*

At the completion of testing, the complete soil sample is weighed before return to the oven for 24 hour drying. After drying the soil is again weighed. In this way the gravimetric content of the moisture present in the sample could be identified and used in comparison to the TRASE measurements of volumetric content. In addition, a 400cc sample was removed each time and independently dried and weighed to assess

volumetric content (Figure 6.7). This ensured that effects of any evaporation during curing might be accounted for.

Figure 6.7 *Accurate Weighing of Soil Sample After 24 Hours Drying*

The test procedure can be summarised in six distinct steps:

1. Oven dry soil sample at $105^{o}C$ for 24 hours.
2. Determine the amount of water required to produce specific water content level.
3. Add and mix measured quantity of water with soil.
4. Leave soil sample to cure for 24 hours and measure volume,
5. Use the TRASE instrument to gather measurements in three different probe positions, using both prototype and standard TRASE probes.
6. Take an oven dried soil sample to verify the water content.

6.4 TRASE Testing Problems

The TRASE makes an adjustment for the two-way travel time of the TDR wave such that recorded transit time is half of the actual value. The manufacturers of the TRASE have obviously decided to display signal travel time in this fashion so that graphs represent the one-way travel time as it relates to the actual length of probe and coax. This is unnecessary but is easily accounted for by halving all calculated times in previous chapters.

The next problem encountered with making measurements with the TRASE is that it has an inbuilt zero-set feature that doesn't recognise the geometry of the prototype probe. This feature will be explained so that a solution can be derived.

Before making a series of readings it is necessary to 'zero set' the TDR Processor for the particular waveguide that will be used. This process establishes the zero time reference at the start of the pulse as it reaches the start of the waveguide. The zero set point is used by the TRASE for two purposes. Firstly it formats the capture window such that the arrival at the head of the waveguide, the travel through along the waveguide, and the first reflection point are displayed. These are the parts of the waveform of most interest to the user. Secondly it uses the zero set to calculate the transit time between the start of the waveguide and the point of first reflection. The internal software process that establishes the zero set point is unknown and inaccessible.

When using the prototype probe the TRASE would capture a part of the waveform that was not necessarily associated with the part required, in effect it was floating without an anchor point. Returned measurements of apparent dielectric constant and volumetric water content were completely erroneous. This necessitated manual setting of TRASE controls such that the capture window would display that part of the waveform desired. The location of the start of the probes in this case coincides with the end of the connecting coax. The time taken to travel to the end of the coaxial transmission line was easily established by connection of a short circuit to the end of the coax and performing a

measurement with capture window manually set to 0-50ns range. The waveform produced is displayed in Figure 6.8 and shows a sharp reflection at the point 19.32ns. This became the focus of all further zero set measurements with the capture window being set to either 15-45ns for a look at multiple reflections (and final DC value) or 15-25ns for the most detailed look possible of the first reflection (the manual controls of the TRASE only allow capture window settings in 10ns steps).

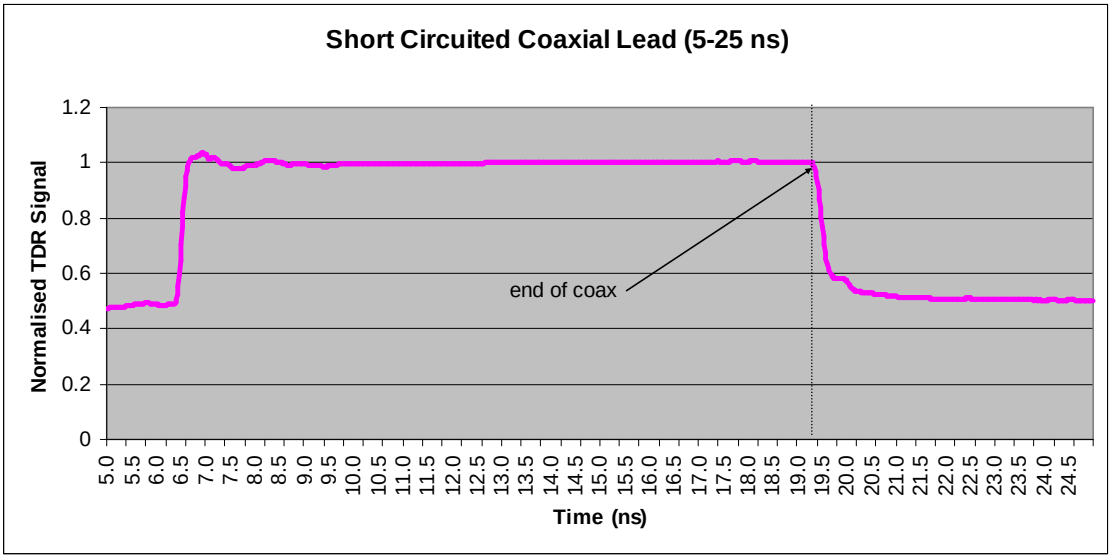

Figure 6.8 *TDR Waveform of Short-Circuited Coaxial Transmission Line*

Further, manual selection of a capture window meant that interpreting the waveform became process that relied heavily on knowledge of expected waveform behaviour as it varies under given conditions of soil moisture content. In particular it meant that location of the first reflection point initially became a manual event whereby once the zero set position was established, the anticipated travel time would point to the location of the reflection point. Two time bars in the TRASE capture window could be manually shifted to these two locations and one-way transit time calculated. Apparent dielectric constant (Ka) could then be calculated manually and subsequently volumetric water content calculated with a Matlab script based on the Topp equation (see Appendix C for Matlab script).

Another problem presented in the way in which the TRASE would capture and store data. For each measurement taken, the TRASE would not only determine the area of the waveform for capture, but it would also vary the amplitude such that a full screen image of the waveform would be displayed. This meant that each graph would be reconfigured in amplitude and the data would be stored with this change also. To be able to compare waveforms with each other and with the theory derived in Chapters 4 and 5, it became necessary to normalise each waveform such that the amplitude of the incident pulse was set to one. This was achieved by determining the area of the waveform representing the incident pulse, then calculating an average value over that range, and then application of this average to the entire waveform. This was achieved in the spreadsheet formatting used to store and interpret the waveforms once downloaded from the TRASE to personal laptop.

6.5 Calibration of Prototype Probe in Air and Water

The work done in Chapters 4-5 established the expected behaviour of the waveform under conditions of air (Ka=1) and water (Ka=81). Using the information about timing that was derived, comparisons can be made between expected and actual measured waveforms. Figures 6.9 and 6.10 show comparisons of expected and actual waveforms for the prototype probe in both air and water respectively. Initially, the most obvious difference is the rounding of the measured waveform due to the influence of complex components of materials. Recall that the former theory centered on lossless line characteristics. What is important for calibration purposes then is interpreting the timing and general waveform shape of the measured results. In general the shape of the waveform is similar; reflections are in the correct direction and are approximately of correct magnitude. Secondly the timing aligns well with the expected behaviour although there is some evidence of slightly longer than expected travel time.

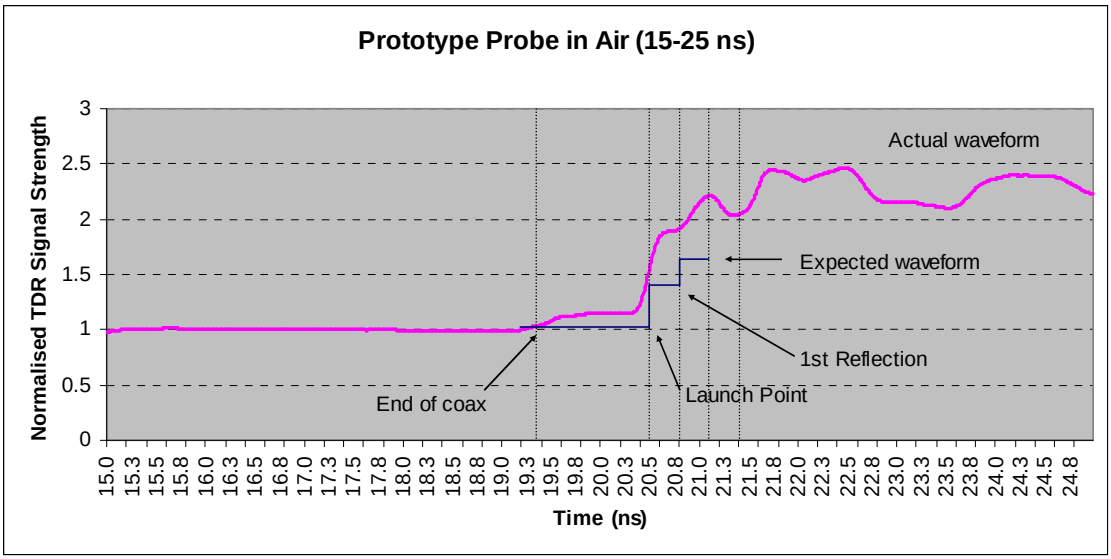

Figure 6.9 *Prototype Probe TDR Waveform Comparisons (in Air)*

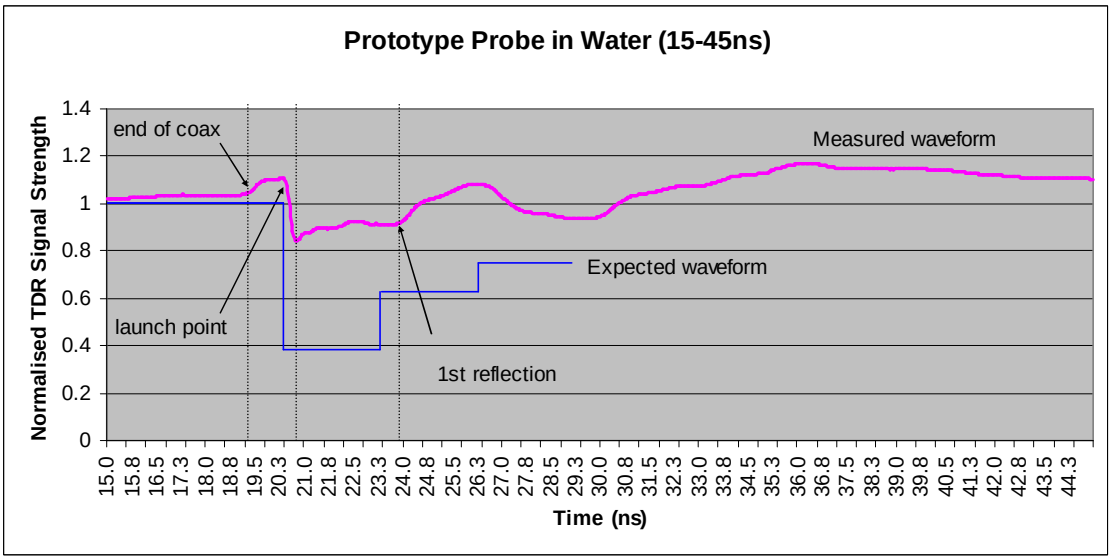

Figure 6.10 *Prototype Probe TDR Waveform Comparisons (in Water)*

The TDR waveform of Figure 6.10 is in a long enough capture window to show the effect of reflections subsequent to the first. The general trend however is a rather quick attenuation of the signal to a final DC level. The area of interest can be more closely examined by setting a 15-25ns capture window and is displayed in Figure 6.11.

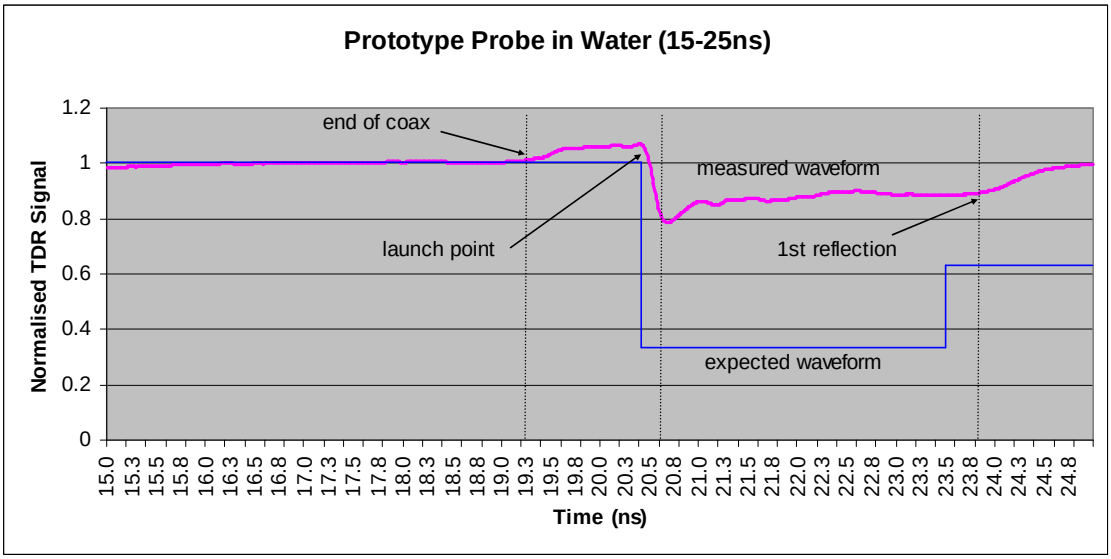

Figure 6.11 *Prototype Probe TDR Waveform Comparisons in Water (15-25ns)*

Although there is agreement with expected timing of the waveform, the most noticeable difference is the loss of signal strength transferred from the launch point into the soil traveling downwards to the tip of the probe. This gives rise to further implications for probe design due to impedance matching under varying moisture levels, to be further examined in the next section with testing of soil samples.

There is also a noticeable delay through the launch point connector. This will be due to the length of the connector (being 5mm) and an impedance mismatch between it and that of the coaxial transmission line in the hollow section of probe. Neither of these factors was taken into account in the derivation of the expected waveforms.

Another point of note is the change in waveform as it leaves the coaxial transmission line at the head of the probe into the coaxial system housed within the hollow section of the probe. There is obviously a change in characteristic impedance away from the $50\,\Omega$ expected creating an unwanted impedance mismatch. The cause of this will be investigated in the next chapter during TDR testing of soil

6.6 Conclusions: Chapter 6

Laboratory testing and calibration of the prototype probe was described in this chapter. First, soil preparation and laboratory testing procedures were established. Next, problems associated with the use of an unfamiliar probe to the TRASE system were discovered. The timing readings displayed by the TRASE are half of what was expected, and also the 'zero set' function was found to be incompatible. Calibration of the prototype probe was achieved by careful determination of the arrival time of the impulse wave at the start of the probe and subsequently with TDR measurements performed in both air and water. The capture window of the TRASE had to be manually set each time to the area of the waveform that was of interest, based on the above calibration process. Amplitude adjustments were found to be necessary to normalise each waveform so that comparisons between each other and with that of the expected behaviour as determined in Chapters 4 and 5 could be made. In general it was found that the probes were responding as expected although the signal strength was weaker. Performance and utility of the prototype will be examined in the next chapter through results of a series of tests in a range of moist soil samples, using the soil testing procedures described in this chapter.

Chapter 7 TDR Soil Measurements and Analysis

7.1 Introduction

Utility and performance of the prototype probe needs to be investigated by laboratory testing of soil samples. This chapter reports on measurements attained after conducting a comprehensive series of tests on soils of increasing levels of water content (described in Chapter 6). The test results will then be displayed and discussed. Discrepancies between expected and actual behaviour are explained. The probe is proved to be mechanically robust. However, interpretation of the results displayed by the TRASE is not intuitive. It is only by careful analysis of the results that water content information can be extracted. Results after analysis are found to be accurate.

7.2 TDR Measurements in Soil

The measurement process was only able to cover the range of 0 to 35% volumetric water content since at 35% the soil type used became heavily saturated and it was considered that attempts to increase moisture levels would not yield accurate results. In particular, most of the water would rise to the top of the testing tube and distribution throughout the soil was uncertain. Also, the bulk density of the soil also altered. As the water content reached saturation levels, the soil would collapse into a muddy form that reduced noticeable in volume. In all, the range 0-35% was covered in twelve steps with increasing amounts of water being added each time. The graph in Figure 7.1 shows a compilation of TDR waveforms of increasing wetness, and over a time scale of 0 – 50 ns, for the prototype probe.

Examination of the waveforms reveals several features of TDR theory. First there is a noticeable increase in the time delay as soil wetness increases. Over this span of soil wetness the time delay increases more than double from 0.7ns to 1.7ns. Figure 7.2 shows a closer look at the full range of tests with a 15-25ns capture window and in particular the first reflection is highlighted by a line of best fit.

An immediately noticeable feature, particularly in Figure 7.1 is the dramatic drop in DC final values with increasing water content. This is due to the fact that the DC reflection coefficient (ρ_{DC}) is inversely proportional to the DC conductivity (σ_{dc}) of the material as shown in equations 6.1-6.3 below (Habash 1994):

$$\rho_{DC} = \frac{1-T}{1+T} \quad \text{..... (7.1)}$$

$$\text{where } T = \frac{120\pi Z_{0Coax}\sigma_{dc}L_{\text{Pr}obe}}{Z_{0\,probe}} \quad \text{..... (7.2)}$$

By substitution and rearrangement:

$$\sigma_{dc} = \frac{Z_{0\,probe}}{120\pi Z_{0Coax}L_{probe}}\left[\frac{1-\rho_{dc}}{1+\rho_{dc}}\right] \quad \text{..... (7.3)}$$

Therefore it can be said that the decrease in DC value is attributable to an increase in the conductivity of the soil.

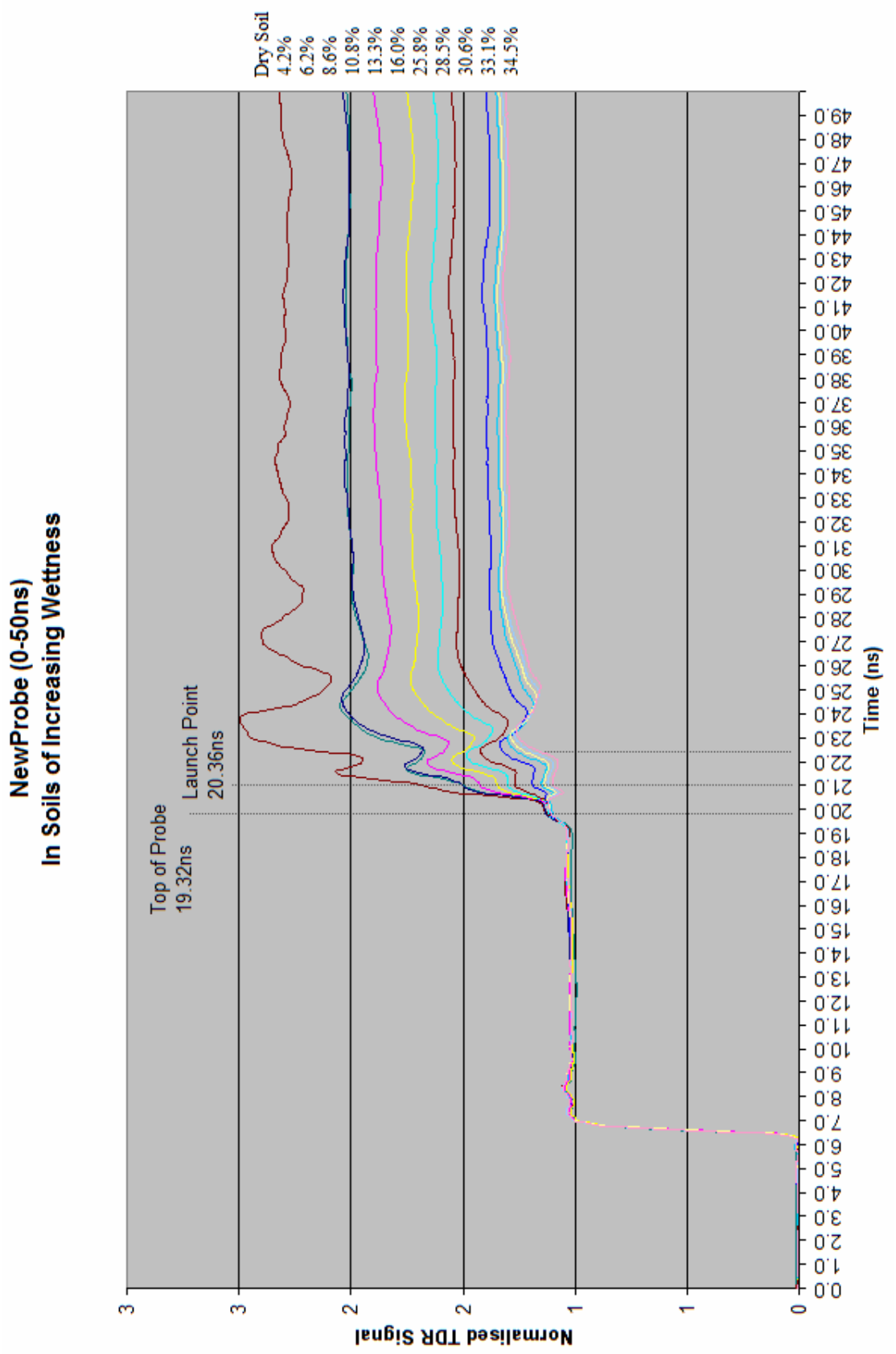

Figure 7.1 *TDR Waveforms for Prototype Probe (0-50 ns)*

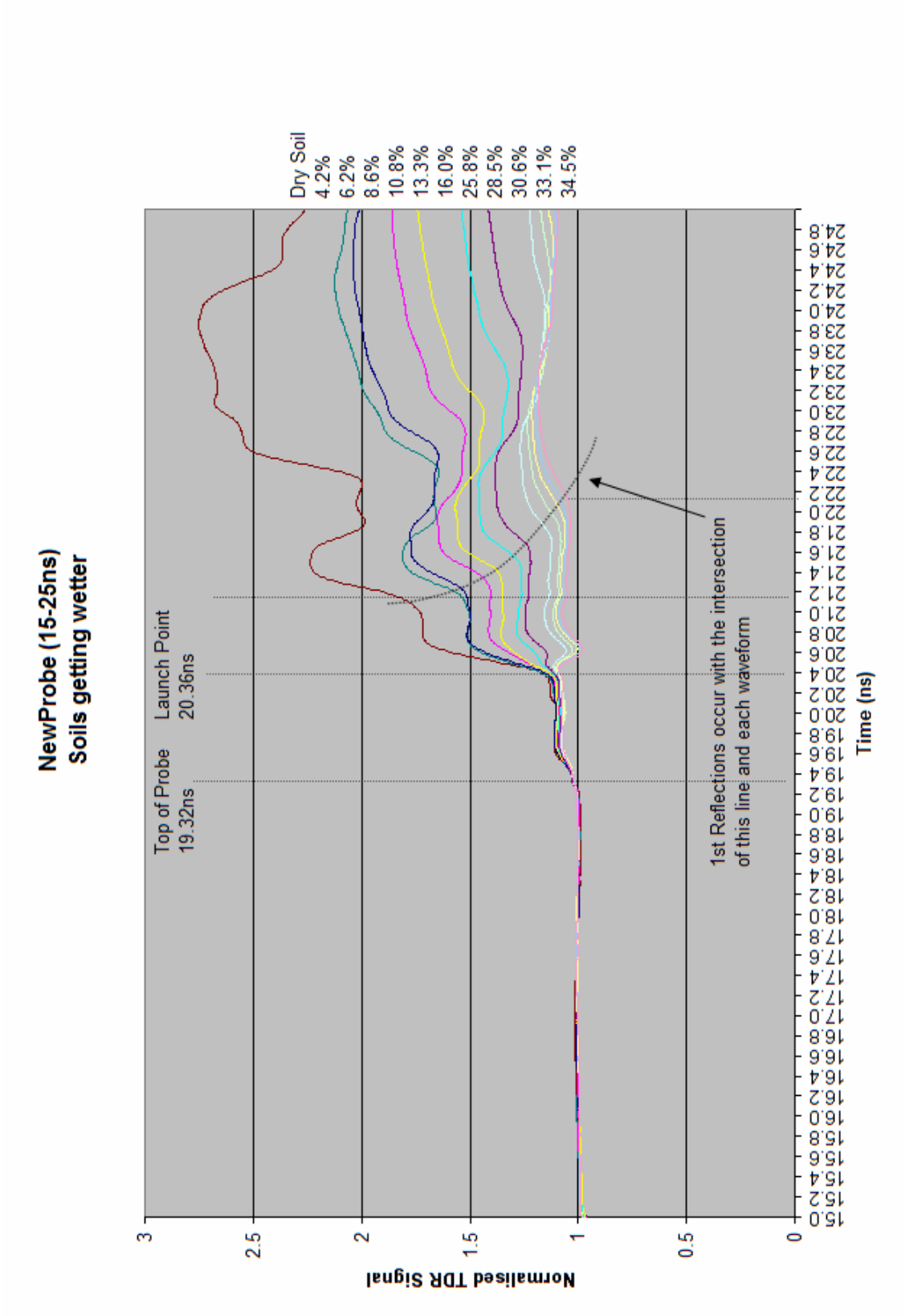

Figure 7.2 *TDR Waveforms for Prototype Probe (15-25 ns)*

Another feature that the waveforms share in common is that determination of secondary reflections is ambiguous. The first graph in dry soil does show a secondary reflection but this is increasingly difficult to distinguish with waveforms of increasing wetness. This feature is a primary reason that TDR for soil measurement is conducted on the basis of timing of the first reflection. Signal losses under the influence of wet soils tend to attenuate the signal very quickly. This is another reason why reflections returning from the initial upward traveling wave are ignored in the lattice diagram and transmission line modeling of Chapter 5 since they will return at a time when they become indistinguishable from final DC values that are being realised.

Careful investigation of the graph of one of the results will be useful, say somewhere mid range that is reflective of where actual field use might be most aimed. The graph of 16% water content is shown if Figure 7.3

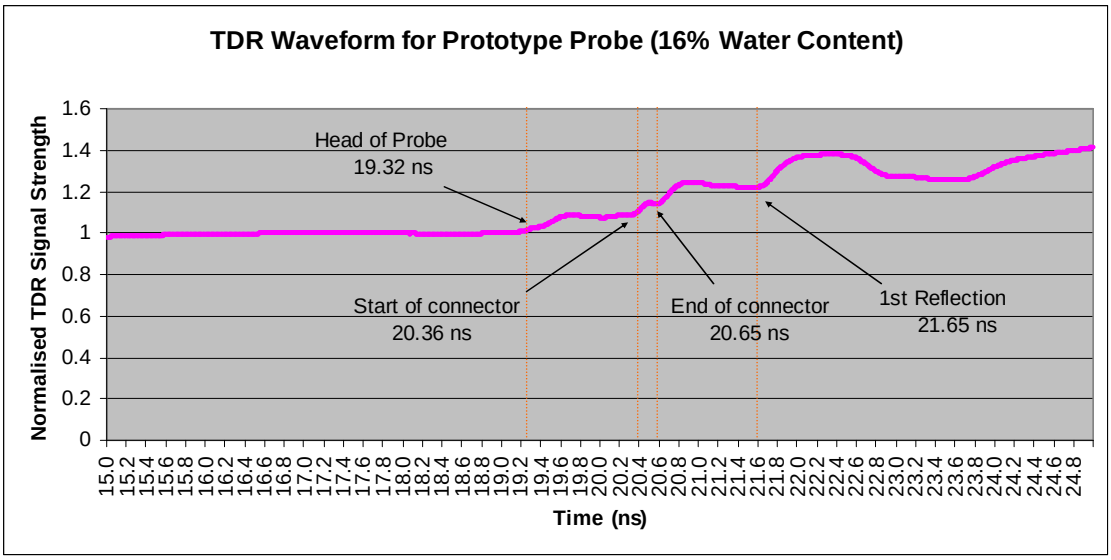

Figure 7.3 *TDR Waveform for Prototype Probe (16% Water)*

The transit time in Figure 7.3 is determined to be 21.65 - 20.65 ns = 1 ns. Using equation (2.8) apparent dielectric permittivity is calculated as:

$$K_a = \left(\frac{\Delta t \times c}{2L}\right)^2$$
$$= \left(\frac{1\times10^{-9}\times3\times10^{8}}{0.1}\right)^2 \quad \text{..... (7.4)}$$
$$= 9$$

By use of Topp equation, volumetric water content is calculated as θ_v = 18.3%. This percentage is not very well aligned with the actual water content of 16%. Reasons for this will become more obvious as results of soil testing are discussed in the rest of this chapter. Most obvious again in Figure 7.3 is the dramatic amount of signal attenuation indicating a relatively poor transfer of signal energy through the launch point into the soil in the downwards direction.

Having conducted a full range of tests, the relationship between apparent dielectric permittivity and water content measured by the prototype probe can be graphed and compared with the results of the TRASE's 30cm 'buriable' probes (Figure 7.4). It is clear that there is almost complete concurrence between the two. The overall performance of the prototype can therefore be said to be good provided careful interpretation of the waveform is conducted.

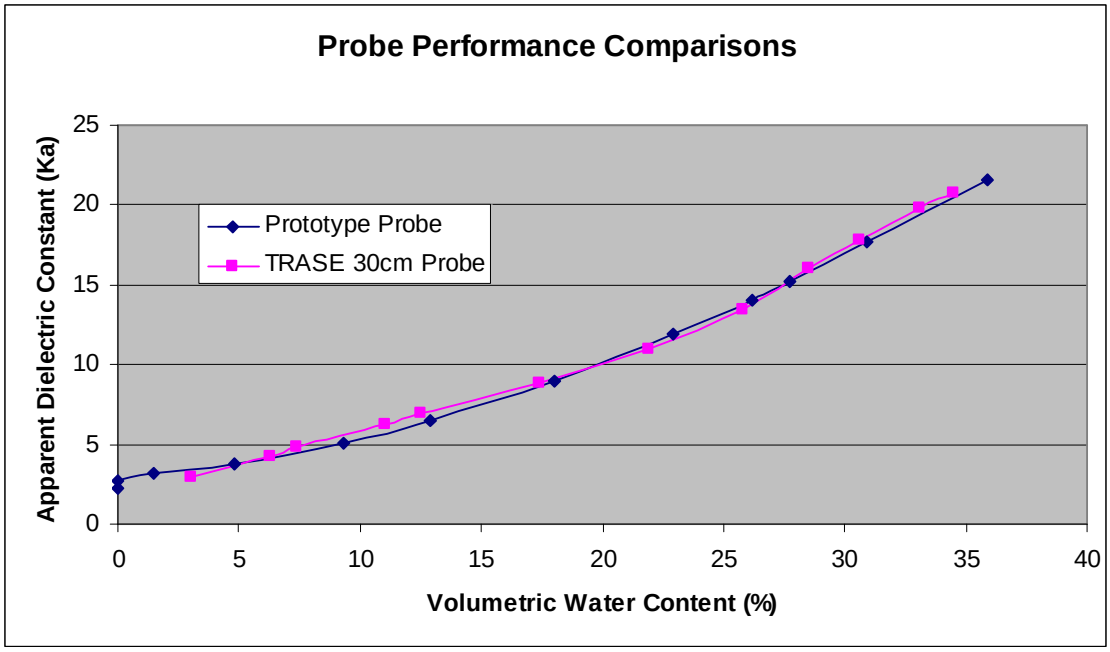

Figure 7.4 *Comparison of Measured Water Content to Topp Equation (Prototype Probe to TRASE Probe)*

Discrepancies seem to exist however between the data collected of measured vs. actual water contents. The comparison is shown in Figure 7.5. The data points show extremely good alignment about the line of best fit in the higher water content soils. The coefficient of determination for linear fit is good: R^2 =0.9858.

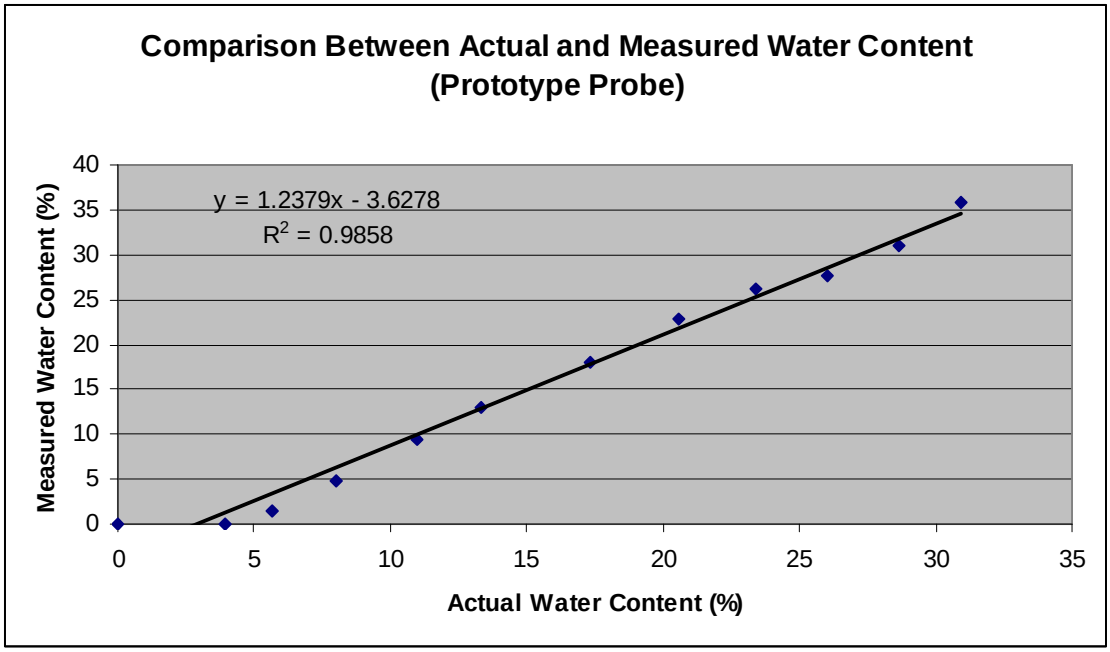

Figure 7.5 *Comparison of Measured Water Content by Prototype Probe to Actual*

The problem of alignment however lies in the displacement away from zero at the bottom of the graph. For example, when there is 5% water present, the prototype probe only measures approximately 2% (working off the line of best fit). Part of the problem in this lower region is that the Topp Equation $K_a = 3.03 + 9.3\theta_v + 146.0\theta_v^2 - 76.7\theta_v^3$ used to calculate θ_v from Ka presents some limitations in this area. Ka readings of 2.3 and 2.7 were calculated from the first two measurements taken by the probe which would return negative moisture readings when using the Topp Equation. Since negative moisture is an unreality, the readings were rounded off to zero.

The behaviour of this data is consistent with the behaviour of clay soils as was observed during laboratory testing of different soil types by Habash (1994). He found that when testing clay type soils in comparison to sandy loam type soils that in the lower region of the graph that clay type soils exhibited a behaviour whereby the water in the soil displayed different response to TDR signals dependant on whether the water was in a 'bound' or 'free' state. This is due to the fact that water in soil does not behave in the

same manner. Baver, Gardner and Gardner (1977) state that 'bound' water molecules are contained in the first few layers surrounding the soil particle and are held tightly by the influence of matric and osmotic forces. Since the matric forces decrease rapidly away from the soil-particle surface, water molecules located several molecular levels away are able to move with relative ease and are hence referred to as 'free'.

In the presence of an incident electromagnetic wave, the high intensity forces acting on the bound water molecule will produce a dielectric dispersion spectrum different to that of the free water (Hallikainen et al. 1985). The relative complex dielectric constant of a soil sample can be stated as:

$$\varepsilon_r = \varepsilon' + j\varepsilon'' \quad \text{..... (7.5)}$$

As a result of their research, Hallikainen et al. (1985) concluded that for a given volumetric moisture content:

a) ε' decreases with increasing clay content
b) ε'' increases with increasing sand content due to the ratio of free water to bound water, which is greater for sandy soils than for clays.

Bound water particles therefore behave more like the soil itself in terms of TDR measurements. In effect, the bound water molecules are characterised by lower dielectric permittivity than free water and TDR measurements will therefore yield lower than expected levels of water content. Zeglin, White and Russell (1992) also discovered similar behaviour when comparing their work to Topp's empirical curve. They were able to determine that certain soils yield different results especially at low levels of water content. In that region the permittivity of the particular soil dominates. The results obtained in laboratory testing of the prototype probe indicate clearly then that the soil type used was not consistent with that of Topp's empirical testing, but was more consistent with that of a high clay content soil.

7.3 Impedance Mismatch inside First Probe Section

The variation in the TDR graph as it encounters the start of the probe and travels to the launch point indicates that an impedance mismatch is present. The hollow section that carries the coax along this section has introduced a variation in characteristic impedance departing from that of the 50Ω RG58U coaxial cable that carries the signal to it. This is due to an air gap that is present between the outer coaxial dielectric and the inner of the hollow stainless steel tubing. It was proved to be problematic during construction to assemble the probe section with the outer shielding and PVC coating in place. This was because the fit was 'tolerance' and hindered sliding in of the coax. Having removed the outer layers of the coax, what then is the effect of this air gap on the characteristic impedance of the first section of the probe?

Dimensions of the coax and stainless steel tubing are shown in Figure 7.6. The stainless steel hollow tubing is 6.35mm outer diameter with a wall thickness of 1.2mm, therefore c = 1.975mm. Manufacturer's specifications for RG58U coax are helpful in determination of the remaining variables. The coax polyethylene dielectric outside diameter is 2.95 mm, therefore b = 1.475 mm. The copper inner conductor is rated at 0.9mm, therefore a = 0.45 mm.

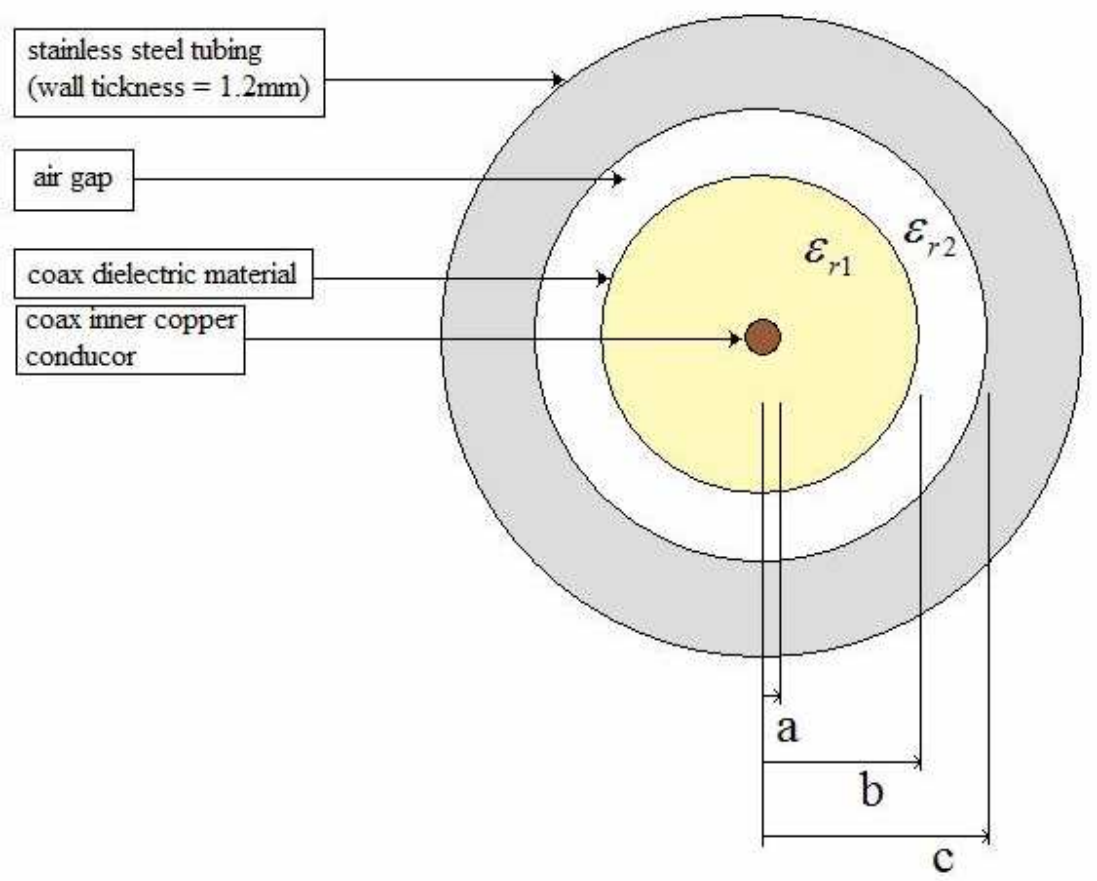

Figure 7.6 *Investigation of Air Gap on Characteristic Impedance*

The manufacturer specifies that the cable has lumped capacitance value of 101pF/m. This will be useful for calculating the permittivity of the coax dielectric and subsequently the characteristic impedance of this section of transmission line that we will call Z_{0gap}. Relative permittivity of the coaxial dielectric material ε_{r1} will need to be calculated. For the air gap, relative permittivity ε_{r2}=1.

Distributed parameters of capacitance per unit length of a coaxial transmission line (as shown in Figure 7.6) can be stated (ELE4605 Fields and Waves Study Book 1, p.2.5) as:

$$C = \frac{2\pi\varepsilon}{\ln\left(\frac{b}{a}\right)} \qquad \text{..... (7.6)}$$

where permittivity of the medium $\varepsilon = \varepsilon_0\varepsilon_{r1}$

and permittivity of free space $\varepsilon_0 = 8.854\times10^{-12}\ Fm^{-1}$

and ε_{r1} is the relative permittivity (often stated as dielectric constant)

Substituting values and rearrangement of (7.6) gives:

$$\begin{aligned}\varepsilon_{r1} &= \frac{C\ln\left(\frac{b}{a}\right)}{2\pi\varepsilon_0} \\ &= \frac{101\times10^{-12}\ln\left(\frac{1.475}{0.45}\right)}{2\pi\times8.854\times10^{-12}} \\ &= 2.155\end{aligned} \qquad \text{..... (7.7)}$$

Distributed capacitance for the line can now be stated (ELE4605 Fields and Waves Study Book 2, p.9.4) as:

$$\begin{aligned}C &= \frac{2\pi\varepsilon_0}{\frac{1}{\varepsilon_{r1}}\ln\left(\frac{b}{a}\right)+\frac{1}{\varepsilon_{r2}}\ln\left(\frac{c}{b}\right)} \\ &= \frac{2\pi\times8.854\times10^{-12}}{\frac{1}{2.155}\ln\left(\frac{1.475}{0.45}\right)+\ln\left(\frac{1.975}{1.475}\right)} \\ &= 66\ pFm^{-1}\end{aligned} \qquad \text{..... (7.8)}$$

Distributed inductance for the line can also be stated (ELE4605 Fields and Waves Study Book 1, p.2.5) as

$$L = \frac{\mu}{2\pi}\ln\left(\frac{b}{a}\right) Hm^{-1} \quad \text{..... (7.9)}$$

where permeability of the medium $\mu = \mu_0\mu_r$

and permeability of free space $\mu_0 = 4\pi\times10^{-7}\,Hm^{-1}$

and μ_r is the relative permeability (since the material is non-magnetic μ_r =1)

Substituting values into (7.9):

$$L = \frac{4\pi\times10^{-7}}{2\pi}\ln\left(\frac{1.475}{0.45}\right) \quad \text{..... (7.10)}$$
$$= 237\ \text{n}Hm^{-1}$$

At high frequencies the characteristic impedance of a transmission coax can be stated (ELE4605 Fields and Waves Study Book 1, p.3.3) as:

$$Z_0 = \sqrt{\frac{L}{C}} \quad \text{..... (7.11)}$$

Then for the transmission line with the air gap present, characteristic impedance is:

$$Z_{0gap} = \sqrt{\frac{237\ \text{nH/m}}{66\ \text{pF/m}}} \quad \text{..... (7.12)}$$
$$= 60\,\Omega$$

This will cause a reflection of:

$$\rho = \frac{Z_{ogap} - Z_0}{Z_{0gap} + Z_0}$$
$$= \frac{60-50}{60+50} \quad \text{..... (7.13)}$$
$$= 0.091$$

A lattice diagram could be constructed to aid drawing of the waveform, but it is sufficient to know that the small change in waveform measured at the start of the probe

head is as a result of the mismatch between the two coaxial transmission lines. This could be overcome by increasing the inner diameter of the probe's hollow centre conductor such that it could house the coaxial line with shielding and outer PVC layer intact. However this would in turn have implications for the outer diameter and consequently the characteristic impedance of the probe itself. Alternatively a coaxial line of characteristic impedance $50\,\Omega$ with a smaller diameter if available could be used.

7.4 Conclusions: Chapter 7

Utility and performance of the prototype probe was determined under conditions of laboratory testing of soil samples. The probe proved to be mechanically robust, and in general, the results were shown to be useful and somewhat consistent with the expected behaviour. Discrepancies between actual and measured water volume at low levels was explained by an investigation of the variable behaviour of water in different soil types, in particular the 'free' and 'bound' characteristics associated with certain soils such as clay. Also, an unexpected impedance mismatch caused by an air gap surrounding the coax carried in the hollow section of the probe to the launch point was discussed. Loss of signal strength and impedance matching are areas that need further addressing in making any design alterations that might yield more defining TDR waveforms. This is an area that can be investigated through the use of computer simulated design and testing. The next chapter introduces an appropriate software package capable of assisting the ongoing design process.

Chapter 8 Simulation Design and Testing

8.1 Introduction

Empire EM Modeling is produced by the German company IMST. A 3D drawing interface allows the user to draw a model for simulation testing. Empire is a 3D electromagnetic field simulator based on the 3D Finite Difference Time Domain (FDTD) method which has become a standard for RF component design (IMST GmbH 2007). The FDTD algorithm solves the Maxwell's equation and is of the general form:

$$E^{n+1} = E^{n} + \frac{\delta t}{\varepsilon} \sum_{o} \frac{H_0^{\,n+\frac{1}{2}}}{\Delta_0} \qquad \text{..... (8.1)}$$

where E is the electric field component associated with a node

H is the magnetic field component associated with a node

Δ is the node of interest

With a certain time step that ensures stability, the algorithm steps forward in time, updating the electric and magnetic field nodes from the old ones under constraints of boundary fields and exciting field. The time step value is derived from the smallest cell size and guarantees the stability of the solving algorithm. In order to speed up a simulation, the user can enlarge the smallest cell size. The time step is generally represented as:

$$\delta t = \frac{\Delta_{\min}}{c\sqrt{3}} \qquad \text{..... (8.2)}$$

where $\Delta_{\min}$ is the smallest cell size

This chapter will investigate the operation of Empire 3D electromagnetic simulation software. In particular, the prototype probe already constructed will be drawn and tested. Time domain waveforms will be shown. The 3D simulation reveals something of the nature of the traveling wave through the soil, and the lumped conductance end effect is visually displayed.

8.2 Drawing Environment

8.2.1 Preference Setting

The probe structure is drawn in Empire's '***Draft***' mode. This is a 3D drawing environment whereby the prototype probe is drawn to scale. The first requirement of the ***Draft*** mode is to set basic global parameters that define the simulation domain in terms of x.y.and z distances and number of cells within. The number of cells is termed 'discretisation'. Because Empire excites the structure with a time pulse the frequency range is entered at the beginning which determines the pulse width. The upper frequency and the resolution entered are a measure for the grid accuracy used for the automatic meshing. During simulation the material can be treated as either lossless or lossy for a selectable frequency band. The loss band is centered to the target frequency. Figure 8.1 shows the setting of preferences for the drawing environment of the prototype probe.

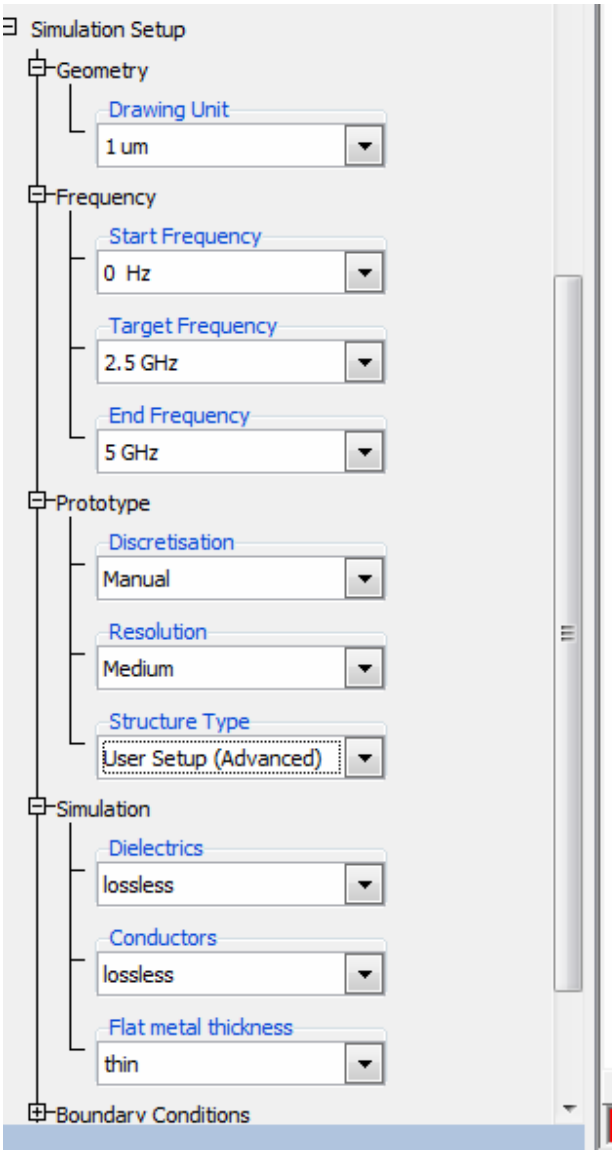

Figure 8.1 *Empire Draft Environment: Setting of Preferences*

8.2.2 Structure Definition

Empire uses a layer concept to group objects with common properties. Objects include boxes, wires, polygons and solids. Properties can be physical (such as material permittivity), geometrical (such as height) or functional (such as animation). More than one property can be set to a layer, for example field dump box and animation plane. All objects on this layer inherit these properties by default. The sequence of layers is

important for rendering purposes and can be controlled by the assignment of layer numbers. The drawing environment is displayed in Figure 8.2. Note the x,y,z axis definition in the lower right corner of the drawing area; the length of the probes extends in the z direction.

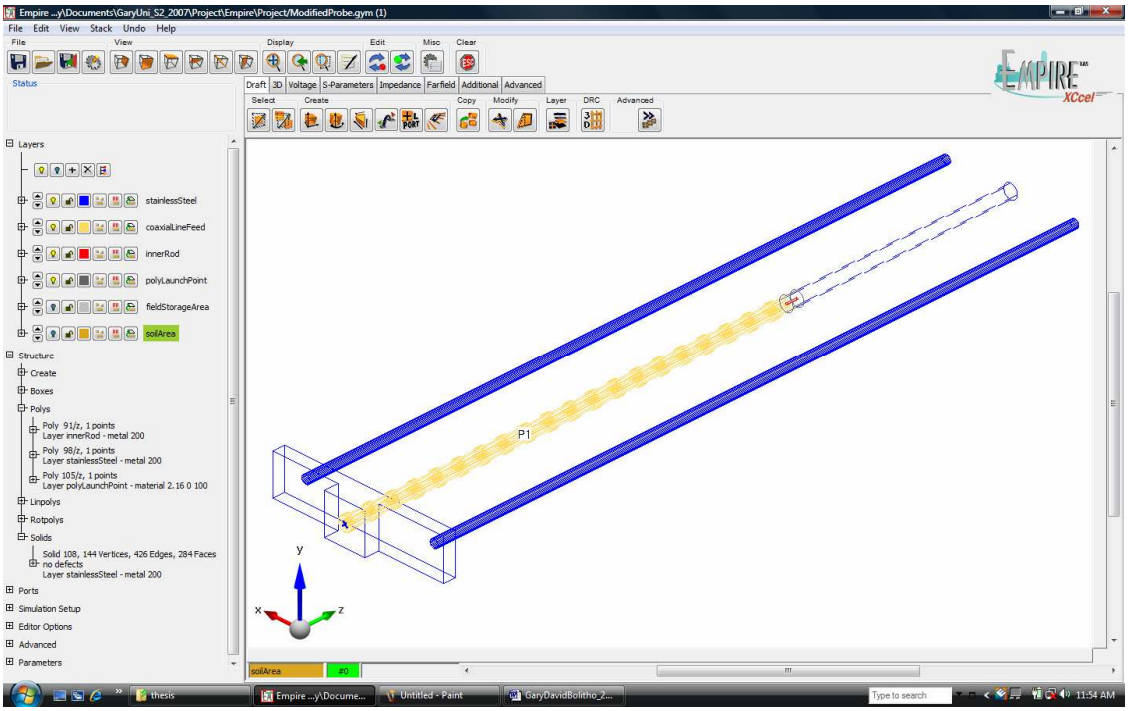

Figure 8.2 *Empire Draft Environment: Structure Definition using Layers*

Views within the ***Draft*** environment allow observation of the structure from any angle. Also a 'clip' function allows looking in to the structure by defining slicing planes. At the left of the drawing area in Figure 8.2 is the layer list. The lists provide for creation and control of layers, objects, simulation parameters and ports. The properties for each layer are set individually, and each layer can be locked or hidden to prevent modification of objects. Figure 8.3 takes a closer look at the layers created for the prototype probe.

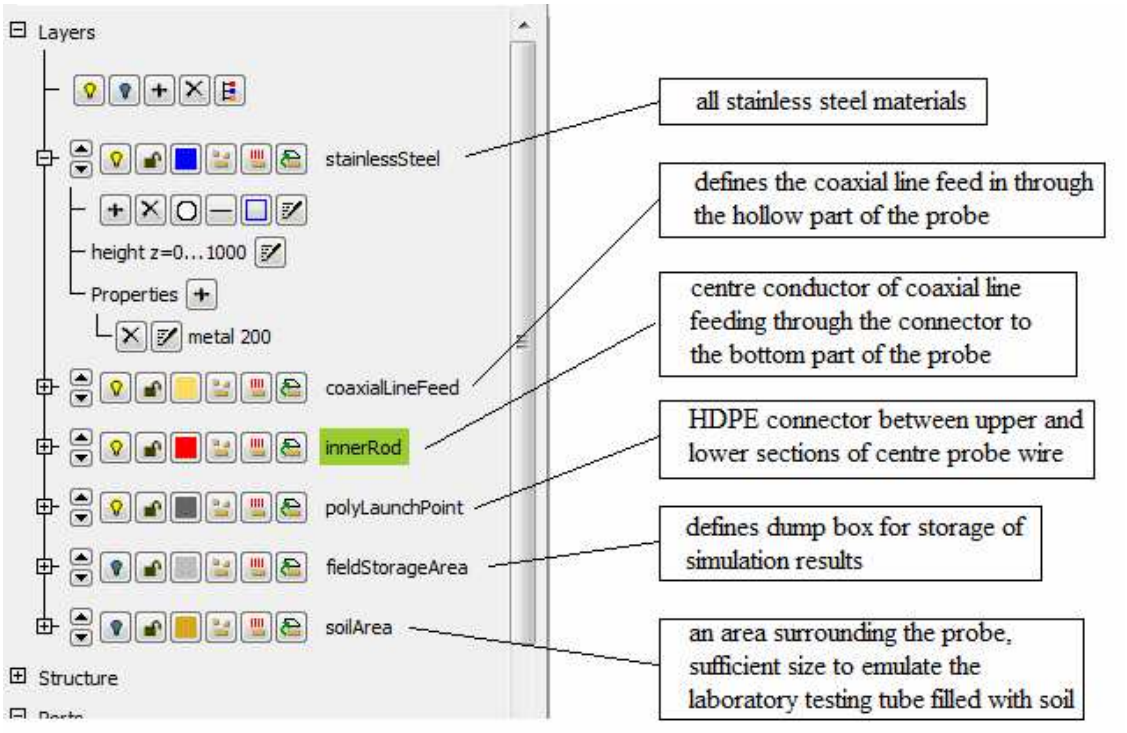

Figure 8.3 *Layer List: Creation of Layers for Different Materials*

The layers created for the prototype probe are as follows:

- *stainlessSteel*
- *coaxialLineFeed*
- *polyLaunchPoint*
- *fieldStorageArea*
- *soilArea*

Each of these layers is assigned different properties. The *stainlessSteel* layer in Figure 8.3 has been expanded to reveal the height of the layer (z=1000) and the material property of 'metal'. Within the Object Property Editor, specific material properties such as permittivity, conductivity and priority are set. The priority ranking assigned to either an object or layer determines which takes precedence in any intersecting volume. Priority is assigned anywhere on a scale of 0 to 256. Figure 8.4 shows the Object Property Editor settings for the layer *polyLaunchPoint*. This layer is for the HDPE connector that

constitutes the launch point. Note that permittivity $\varepsilon_r = 2.16$ has been selected as it is considered to be of similar material to that of the coaxial transmission line dielectric (for which the manufacturer has specified $\varepsilon_r = 2.16$). This property can be varied to investigate its impact on the reflection coefficient at this point in the transmission system.

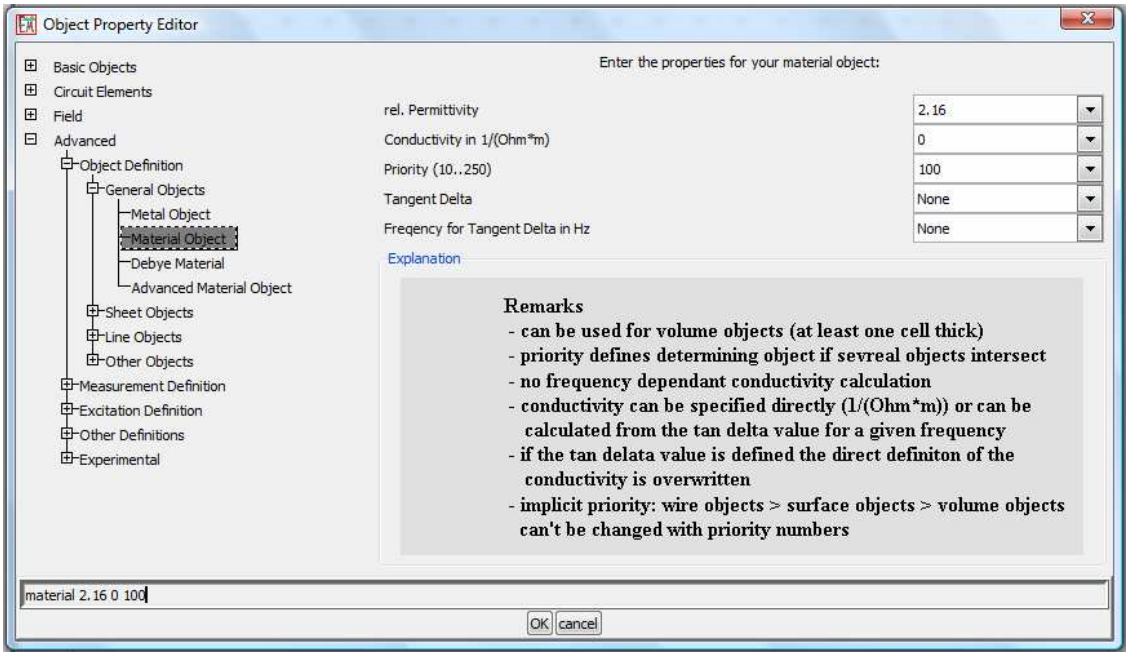

Figure 8.4 *Property Editor: Setting Material Properties for Launch Point Connector*

The port layer *coaxiaLineFeed* has been defined with dimensions and properties set to match those of the coaxial cable manufacturer's specifications. This layer facilitates the injection of the excitation into the structure. The coaxial port properties are adjusted in the Library Element Editor and are displayed in Figure 8.5. Besides geometry, particular attributes include:

- characteristic impedance $Z_o = 50\,\Omega$,
- dielectric permittivity $\varepsilon_r = 2.16$,
- priority settings graduated from the centre wire, through the dielectric to the outer sheath, and

- discretisation that gives field recording emphasis to the port area over the rest of the structure.

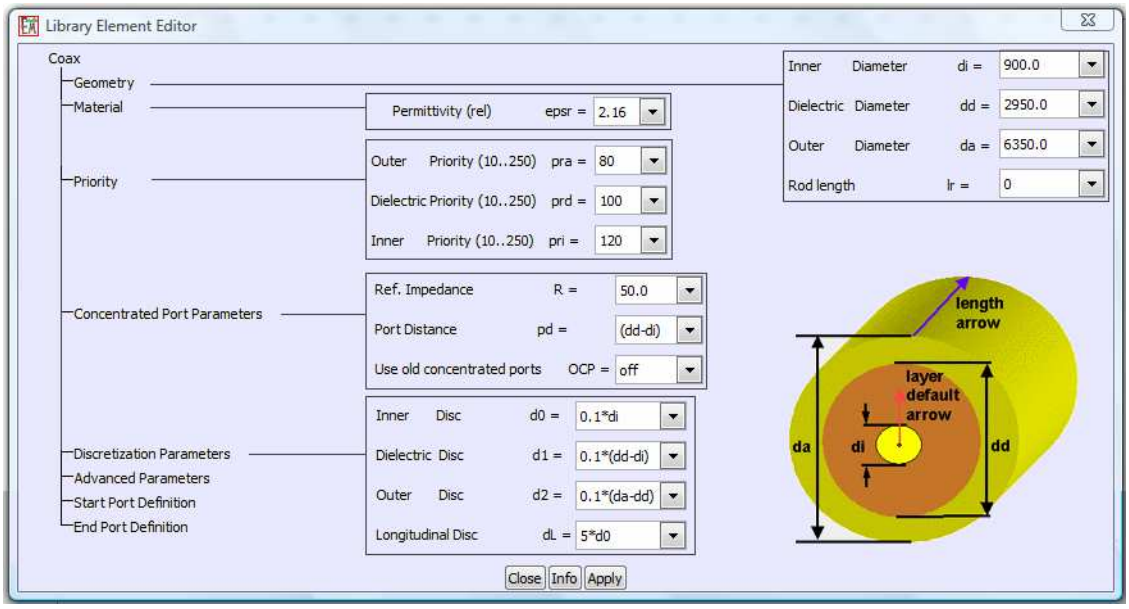

Figure 8.5 *Library Element Editor: Coaxial Port Properties*

The *fieldStorageArea* layer defines a volume around the probe in which the simulation information is recorded. To obtain near fields, this recording box has to be defined on a layer with the property 'Field Distribution'. Various frequency points or time steps can be specified and *E* or *H* fields can be omitted to save memory. The number of frequency points used for field recording will effect the amount of memory used during the simulation and needs to be selected carefully. The near field will be stored inside this recording box and can be visualised post-processing with animation planes. The recoding box volume is displayed in Figure 8.6.

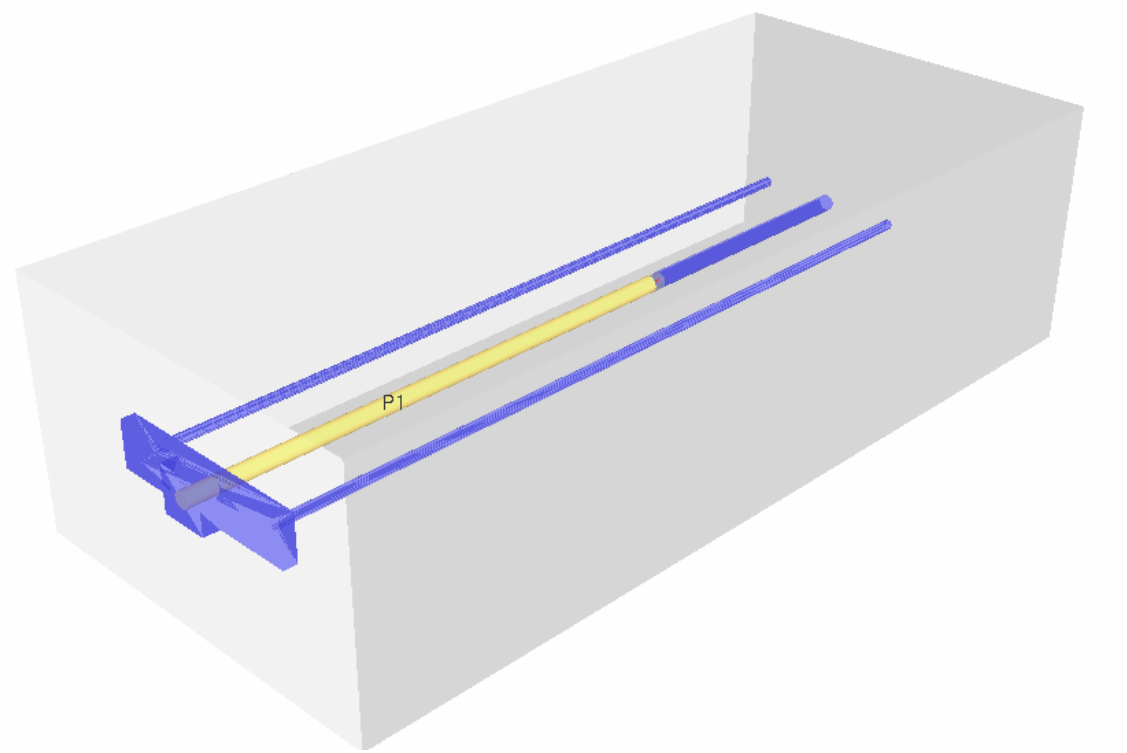

Figure 8.6 *Field Storage Area: Transparent View*

The *soilArea* layer is identical in volume to the *fieldStorageArea* recording box. The purpose of this box is such that the dielectric permittivity can be manually changed to mimic soil conditions of variable wetness.

8.2.3 Discretisation and Drawing Conversion

The final procedure for the structure set-up is to define or adjust the mesh according to the entered geometry and ports. Empire provides an automatic discretisation facility that determines a suitable mesh. The mesh of cells may be equidistant or graded. This allows resolution of the finer structural details with many cells. Rather than automatic discretisation, the grid can be adjusted manually to place more emphasis on the launch point area. After setup is complete and the structure is mapped to a grid, the drawing is converted to an input file (.acad) ready for the simulator.

8.3 Simulation Environment

8.3.1 Pre Processing

With the structure and mesh now defined as an input file, certain parameters that control the simulation environment will need to be chosen. In particular, boundary conditions, excitation shape and simulation end criterion will be set.

The outermost gridlines define the borders of the simulation area where boundary conditions are applied. For the simulation of open structures such as soil probes, the finite calculation domain needs to be truncated by boundary conditions with absorbing properties. Perfectly matched layer (PML) boundary conditions are chosen such that any radiating field effects are absorbed. The ground plane however (in the xy plane at the start of the probes, i.e. z min) is set differently with *Electric* boundary conditions. Application of *Electric* wall conditions forces the tangential electric field components on the outer of the plane to zero. In other words, only normal electric field components exist, so the electric field is perpendicular to this wall. Setting of boundary conditions is shown if Figure 8.7. Note the number 6 that follows the PML setting; this is an absorption quality level. Selection of a larger number enlarges the conducting thickness at the boundary (i.e. the number of layers used for absorption). The trade-off for selecting higher levels is of course processing time. The available range is from PML4 – PML12.

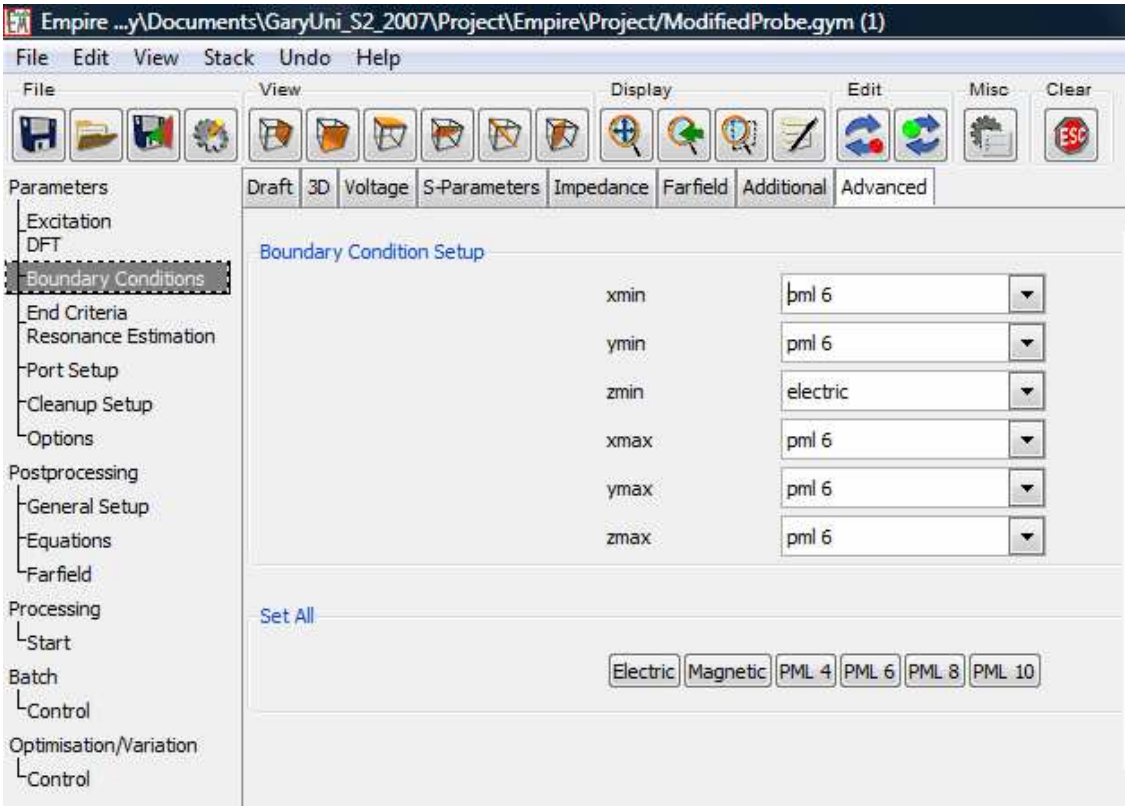

Figure 8.7 *Boundary Conditions: Set to be Perfectly Matched (Absorbing)*

Excitation is impressed on certain field nodes originating at the defined port. The port is defined as coaxial and allows parameters of current, voltage and resistance to be manually set. The excitation voltage itself is set as a fast rise-time pulse (rise time = 200ps) and is shown if Figure 8.8.

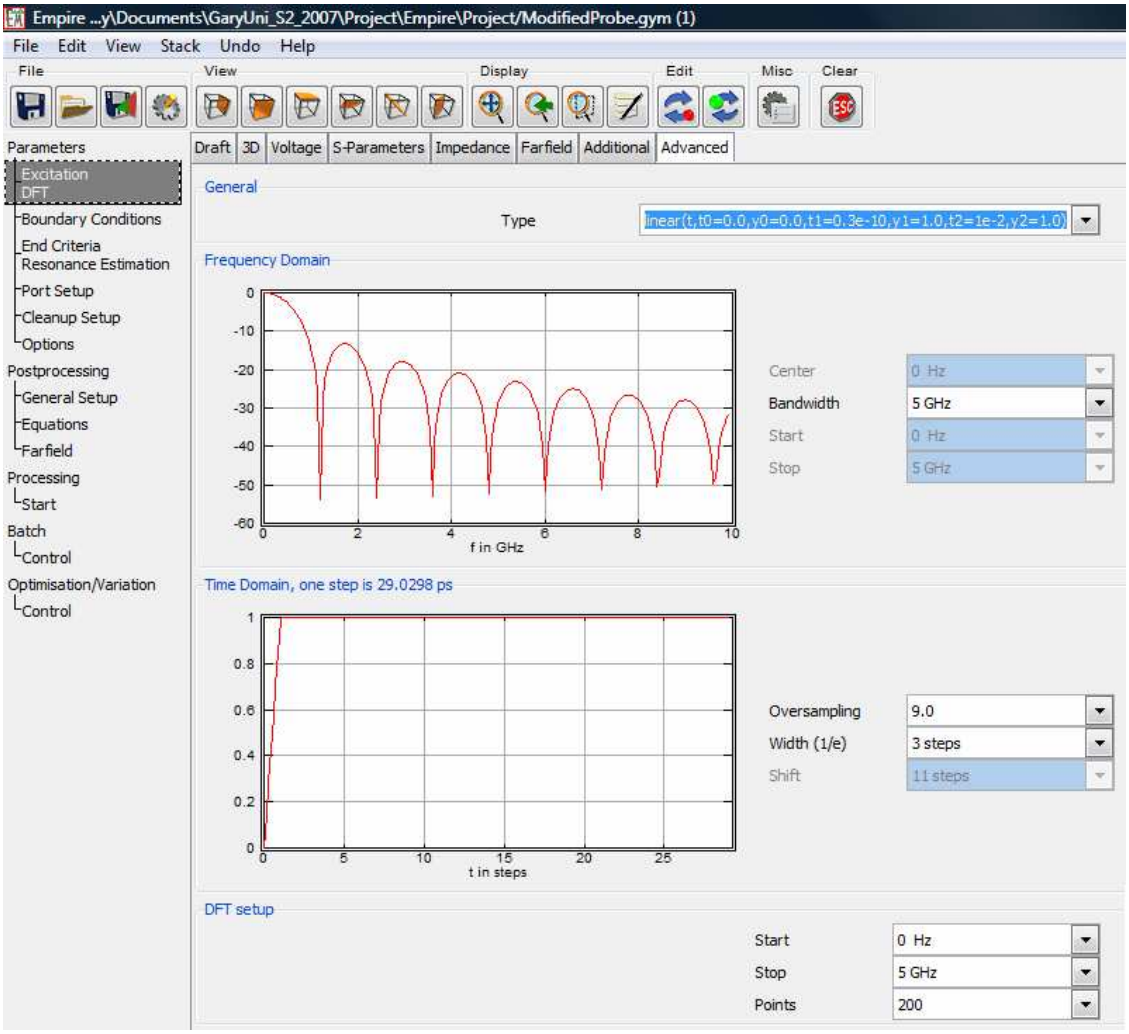

Figure 8.8 *Excitation Defined: Fast Rise-Time Pulse*

An end criterion must be set to determine termination of the simulation. Simply a set number of steps can be allocated, sufficient to deliver the required accuracy. Alternatively, the decay of energy inside the simulation domain can be monitored; simulation is stopped when the preset checksum decrement is reached. The user can also manually cease simulation at any time. The setting of end criterion for the prototype probe is shown in Figure 8.9.

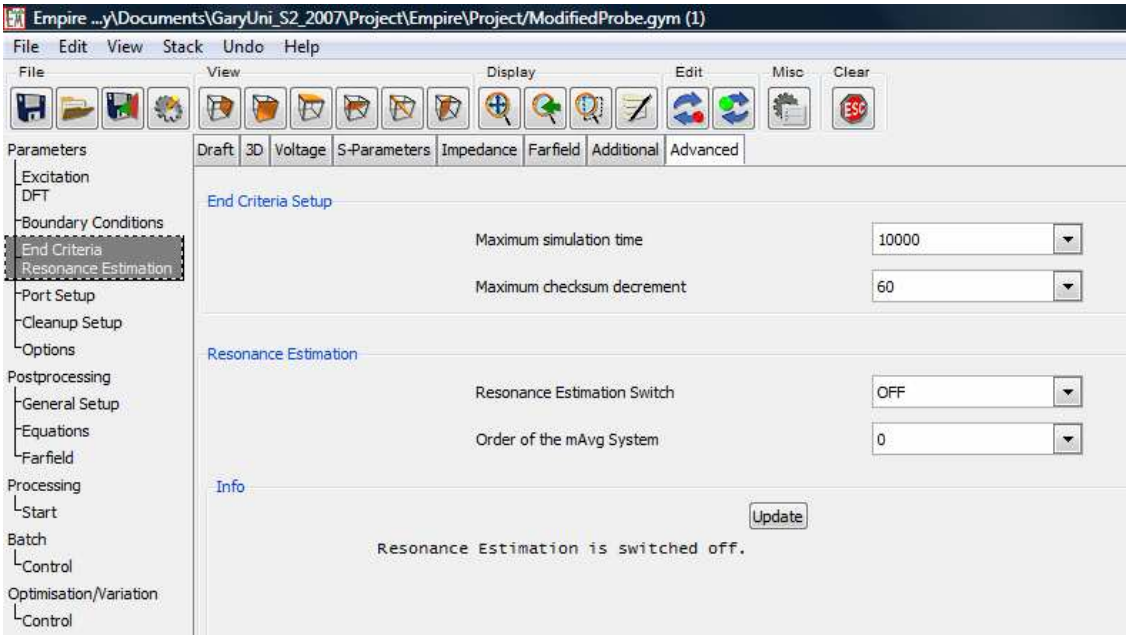

Figure 8.9 *Simulation End Criterion: Number of Steps and Energy Decay Checksum*

8.3.2 2D Post Processing

The structure is excited by the pulse and the simulation is carried out in the time domain. Frequency domain results are complex values, derived from the time domain signals by a Discrete Fourier Transformation (DFT). The DFT is applied after simulation to obtain impedances or s-parameters, the frequency range being a function of the time domain pulse width. The DFT is also used to calculate frequency domain near fields, and is generally described as:

$$\sum_n u(t) e^{-i2\pi fn\delta t} \delta t \qquad \text{..... (8.3)}$$

Empire produces a range of 2D graphs resulting from simulation. Time domain voltage and current waveforms of both incident and reflected waves are available. Smith charts and polar charts are also generated. In the frequency domain, voltage, current, impedance, admittance, power and s-parameters can be displayed. All graphs can be customised for presentation by selection of parameters in the setup screen, as shown if Figure 8.10. Note in the lower left area is a list of files that Empire has automatically created after simulation for each type of graph selected.

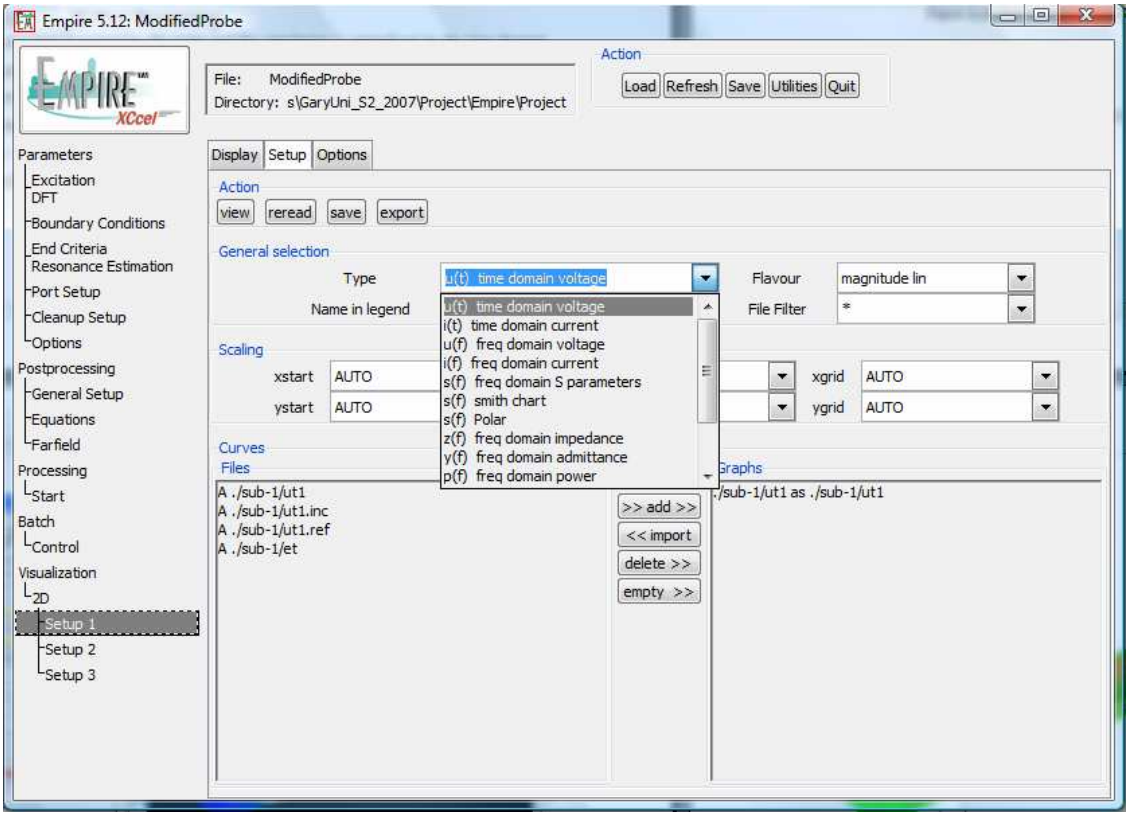

Figure 8.10 *2D Graph Selection and Setup*

A typical voltage waveform in the time domain is displayed in Figure 8.11. The reflections as they occur from the end of the probes are clearly evident.

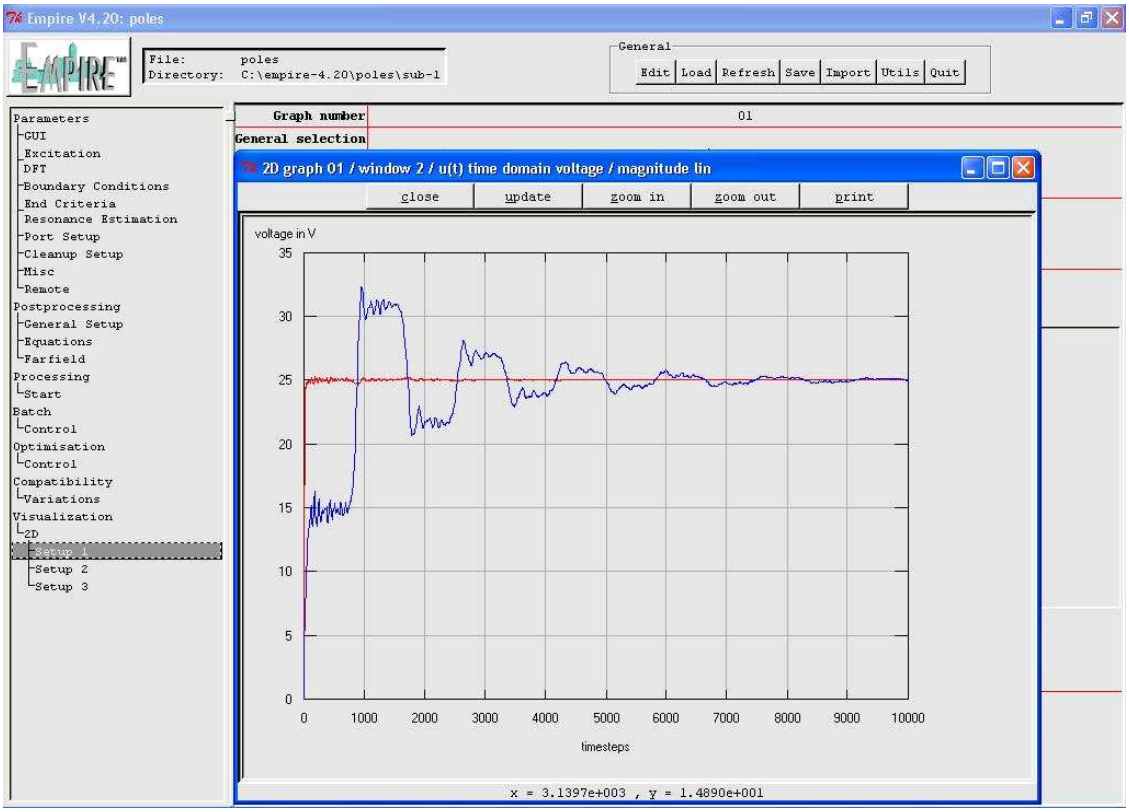

Figure 8.11 *2D Graph: Time Domain Voltage Waveform for Probes*

8.3.3 3D Post Processing

3D field animations are possible after simulation. This is achieved by accessing the *fieldStorageArea* layer that was created during the structure definition process earlier. Within the properties for this layer, the 'Field Display' is chosen and '3D Field Animation Box' controls are accessed. Figure 8.12 displays the animation controls.

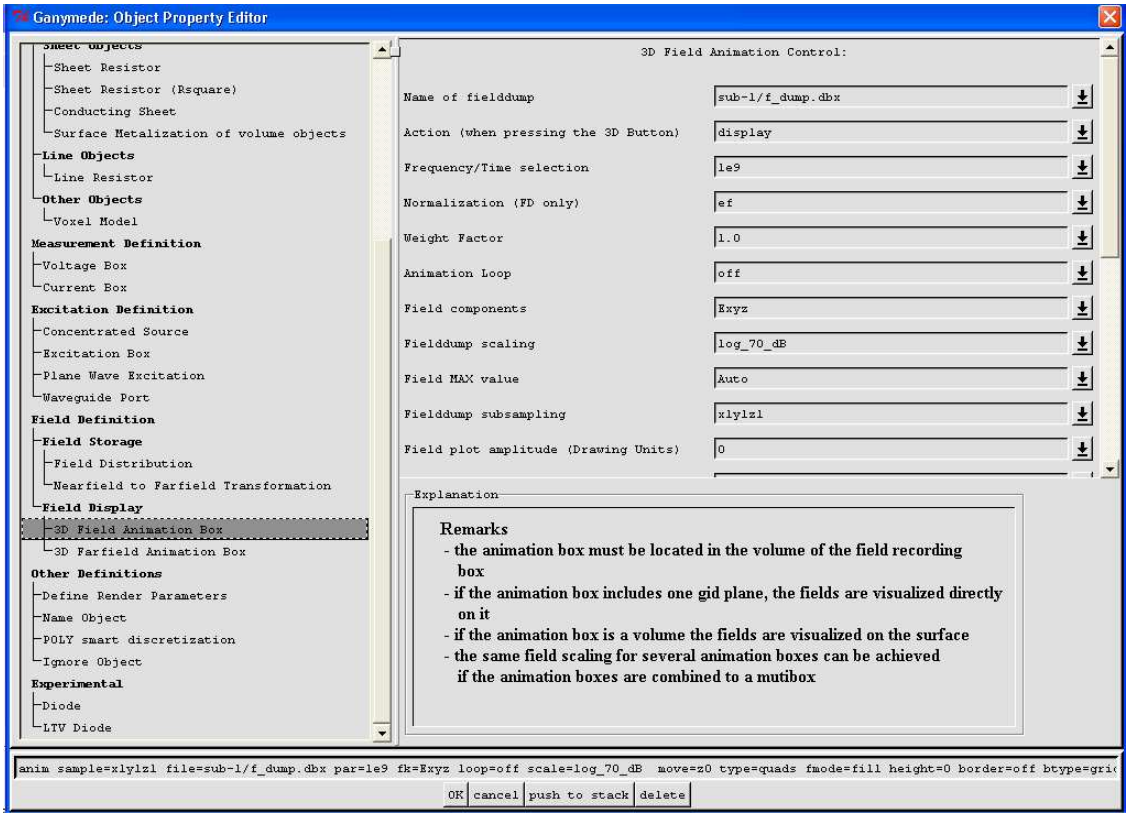

Figure 8.12 *3D Simulation: Field Animation Controls*

The animation controls are set such that Electric field components in xyz planes will be displayed. All other animation visualization controls, such as scaling, amplitude, rendering, are all manually set. Figure 8.13 shows a snapshot of the propagating electromagnetic field along the probes during the 3D animation loop.

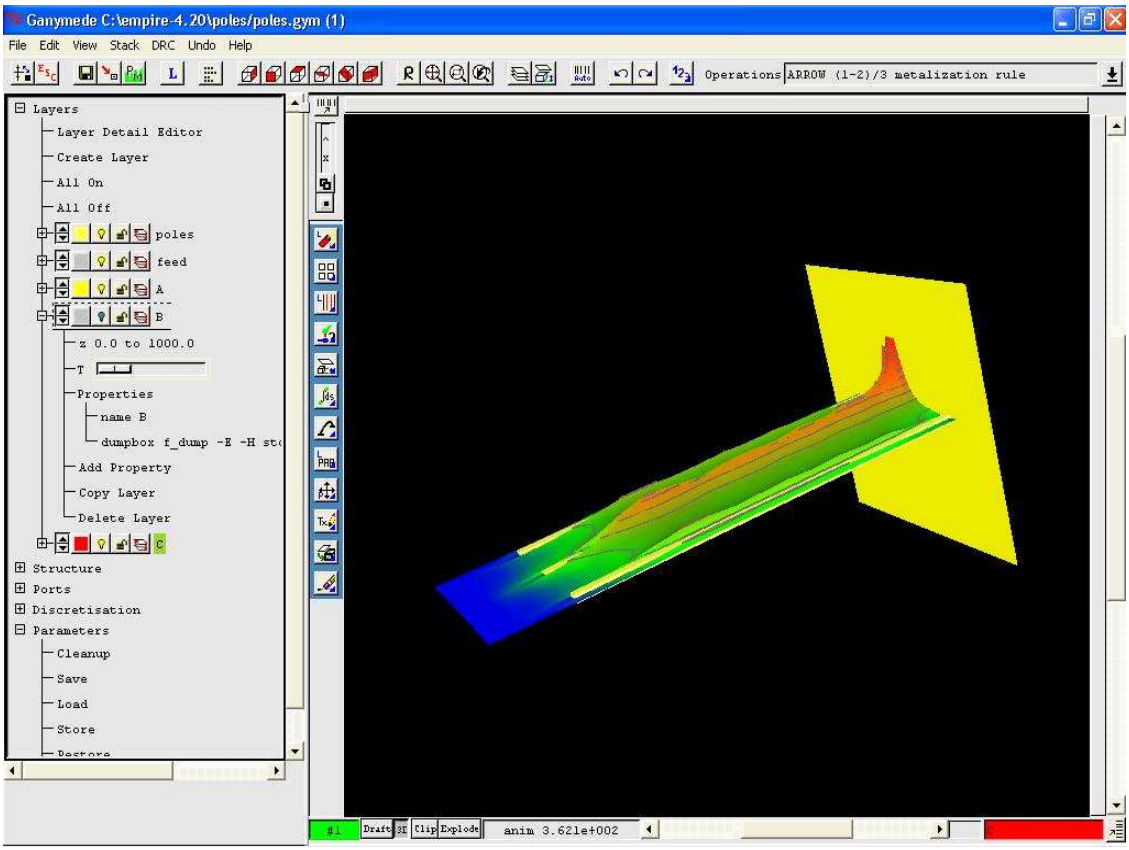

Figure 8.13 *3D Simulation Snapshot: Propagation of Electromagnetic Fields*

Closer examination of the animation at the time the exciting wave propagates to the end of the probes is shown in Figure 8.14. An interesting feature here is the extension of the wave past the end of the probe wires. This effectively increases the length of the probes as used in all previous chapter calculations when determining expected behaviour. The simulation delivers a practical example of the 'end effect' as explained in Chapter 2. Recall assertions provided by Pentinellia et al. (2002) that reactive end effects present as a stored electrical energy relating to the fringing of the electric field at the open-circuit end of the transmission line. The equivalent distributed circuit would be seen as end shunt capacitance, related to frequency. The time-domain effect of the distributed capacitance is to create a delay, the net effect being equivalent to a 'lengthening' of the line.

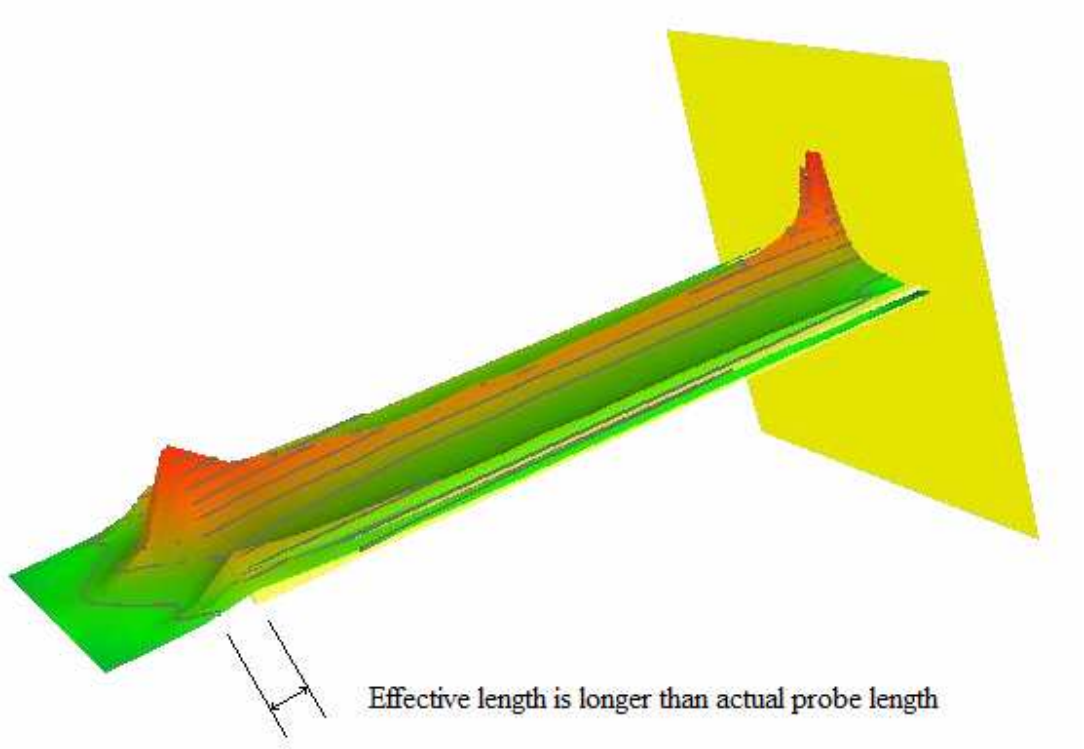

Figure 8.12 *3D Simulation: Effective Length of Probe is Longer*

8.4 Conclusions: Chapter 8

This chapter investigated the operation of Empire 3D EM simulation software. A prototype probe was drawn in the *Draft* environment with layers created to describe different geometrical, physical and functional properties. In particular, layers were created for the stainless steel materials, the coaxial line feed (as a port), the HDPE launch point connector material, a simulation storage area and a soil volume space around the probe. Pre-simulation requirements of absorbing boundary conditions, fast rise-time excitation pulse and suitable simulation end criteria were determined. Discretisation of the mesh grid is concentrated about the launch point area. 2D simulation results include both time and frequency domain behaviour. A time domain voltage reflection wave was presented. 3D simulation results were presented as animations of the propagating electric field in xyz directions. Something of the nature of the traveling wave as it encountered

the open-circuited end of the probe in soil was revealed. The effective length of the probe is longer than its physical length due to reactive end effects. Unfortunately due to time constraints, detailed simulations for the prototype probe have not been achieved. Conclusions for the thesis and recommendations for further work will be addressed in the next chapter.

Chapter 9 Conclusions and Recommendations

9.1 Introduction

The TDR approach to the in-situ measurement of soil moisture content is today accepted as a most reliable and accurate method in comparison to alternatives such as neutron probe or dual gamma ray methods (see Chapter 1). The need for more specific measurements such as in the root zone area has set objectives for this project, namely:

- Design and construct a soil probe that yields soil profile information rather than averaged information.
- Gain familiararity with simulation software; used to aid in the design and testing of potential probe configurations.
- Assess the new probe for accuracy and functionality.

This final chapter will highlight the outcomes of each of the preceding chapters in relation to the stated objectives. Problems that were encountered will be summarised and recommendations for ongoing work made. It will be seen that problems encountered included calibration of the prototype probe and accurate analysis of the recorded waveforms. Whilst the prototype probe delivered results reasonably matched with that of the design criteria and was found to be mechanically robust, there were a number of areas identified for improvement. Further work would include simulation modeling to fine tune impedance matching criteria such that the reflection coefficient can be minimised and signal transfer maximized. When implemented this would provide more distinctive waveforms that could facilitate less intuitive-based interpretation.

9.2 Overview of Thesis Work Carried Out

A review of literature in Chapter 2 investigated TDR principles and applications to soil moisture measurement. Theory of TDR in general was evaluated from a mathematical perspective and development of its practice examined with an investigation of empirical work by others in this field. It is the transit time of signal propagation through the soil (guided by the probe) that is directly related to water content, since soil and mineral particles have a much lower permittivity than that of water. The evidence suggested that the TDR method for soil moisture determination is a mature science, although probe

design for the extraction of more precise information of soil structure is still an area of interest today.

The TRASE TDR equipment that was used in laboratory testing for this thesis was examined in Chapter 3. Some familiarisation with its operation was gained through experiments in soils of variable water content using the standard probes.

TDR waveform behaviour was established theoretically in Chapter 4 through the use of transmission line modeling. Lattice diagrams proved useful in determination of expected behaviour of standard probes in air and water. The dielectric property of the medium in which the probe is placed was found to have significant implications for probe impedance characteristics. Arising variations in effective probe impedance contributes to an impedance mismatch with the transmission system characteristic impedance at the interface of the two. The extent of impedance mismatch determines a reflection coefficient, and consequently the amount of energy that is transmitted through the mismatch. For the design of the new probe it was desired to minimise this mismatch at the launch point.

The new probe design was influenced by transmission line modeling based on lossless line characteristics. The signal as it is launched from the point along the length of the probe would incur a splitting into two directions. The wave traveling in the direction towards the open-circuited end of the probe was the focus of design calculations since it would return information from the soil zone of interest. Supporting the design process was reliance on probe air-spaced characteristic impedance determination using a derived mathematical expression (Ball 2002). Having determined suitable design parameters a prototype probe was constructed using chiefly stainless steel materials and RG58U coaxial cable. The launch point connector was constructed of HDPE of assumed dielectric permittivity.

Laboratory testing and calibration of the prototype probe was described in Chapter 6. The TRASE system was not able to recognise a zero set point when taking measurements with the new probe. To overcome this all measurements had to be manually configured

and analysed for transit time. The zero set point was established by TDR measurement under conditions of a short circuit at the end of the connecting coaxial cable. The capture window of the TRASE was then manually set to the area of interest. Having captured desired data, waveforms were transferred via RS232 serial port to a laptop using HyperTerminal communication protocol. Once all tests were completed and downloaded, the resulting TDR waveforms required conditioning to normalise their amplitude. This was achieved in a spread-sheeting program. Interpretation of transit time was achieved after graphing each result and fitting tangent lines about the reflection point.

Utility and performance of the prototype probe was determined under conditions of laboratory testing of soil samples, described in Chapter 7. The probe proved to be mechanically robust, and in general, the results were shown to be useful and somewhat consistent with expected behaviour. Some discrepancies between actual and measured water volume at low levels was explained by an investigation of the variable behaviour of water in different soil types, in particular the ‘free’ and ‘bound’ characteristics associated with certain soils such as clay. Also, an unexpected impedance mismatch caused by an air gap surrounding the coax carried in the hollow section of the probe to the launch point was discussed.

A 3D electromagnetic simulation program was investigated in Chapter 8. The prototype probe was drawn in the *Draft* environment with layers created to describe different geometrical, physical and functional properties. Pre-simulation requirements of absorbing boundary conditions, fast rise-time excitation pulse and suitable simulation end criteria were determined. 2D simulation results include both time and frequency domain behaviour. A time domain voltage reflection wave was presented. 3D simulation results were presented as animations of the propagating electric field in xyz directions. Something of the nature of the traveling wave as it encountered the open-circuited end of the probe in soil was revealed. The effective length of the probe is longer than its physical length due to reactive end effects.

9.3 Interpretation of Results Achieved

Interpretation of data from the TDR waveforms is not an exact science. The critical aspect in the TDR measurement of permittivity is related to the identification of those points in the wave form used to determine the travel times. Determination of transit time points in this thesis relied on intuitive and careful examination of the waveforms. Any type of interpretation is made difficult by the fact that the waveform measured with a cable tester is significantly different from that of an idealised TDR trace, due to various factors as observed:

1. The experimental setup introduces non-ideal characteristics. These include measurement delays associated with the TRASE instrument itself, energy losses along conductor parts, and possible radiation and excitation of higher-modes in the transmission line that result in dispersion effects.
2. The presence of complex phenomena at line discontinuities. Any impedance mismatch along the transmission line results in signal reflection. The signal reflection can be largely related to reactive effects of electromagnetic energy storage, typically capacitive in nature. Differences between physical length and effective length of the prototype probe were explained in relation to capacitive end effects.
3. Dissipative and dispersive features of the soil (and its constituents of minerals, ‘free’ and ‘bound’ water, and air). The dielectric properties of the materials are all different and are dependant on frequency. This causes deformation of the signal in the time domain, observed by rounding off of the leading and trailing edges of the waveform shape. Again it is the higher frequency content of the pulse that is most subject to dispersion effects.

9.4 Further Research and Recommendations

Measured waveforms using the prototype probe suffered excess signal attenuation compared to calculated expectations. Impedance mismatch at the interface between the coaxial cable and the head of the probe was described in Chapter 7. Also the impedance mismatch at the launch point connector was discussed in Chapters 5 and 7. The effective impedance of the prototype probe in air was also based on some assumptions made in

Chapters 4, 5, and 7. Evaluation of these transmission line discontinuities and effective impedance of probes is an area that requires further investigation, in an effort to account for the excess signal loss. 3D simulation software is highly regarded as the means by which further analysis and design alterations can be implemented and assessed. The extent to which end effects and possibly radiated energy losses can be examined in this way.

The launch point connector is of unknown permittivity and could be assessed with the use of a network analyser. In addition the determination of transit time points from the measured waveforms could be extracted with use of commercially available analysis software.

9.5 Conclusions: Chapter 9

The thesis has delivered what it set it out to achieve. A prototype probe has been designed and constructed for the purpose of determining soil moisture content in a root zone area of the soil. Extensive laboratory testing reveals that the probe delivers specific information in this area of interest as opposed to average information over the length of the probe typically attained with the use of 'standard' probes. In addition, the prototype probe has proved to be mechanically robust and functional for field use, and could be considered for commercial application in conjunction with TDR cable testing equipment. The 3D EM simulation software 'Empire' by IMST is considered to be a comprehensive and useful program by which further development can be supported.

List of References

Baver, L.D., Gardner, W.H., & Gardner, W.R. 1977, *Soil Physics*, Wiley, New York.

Ball, J.A.R. 2002, *Characteristic Impedance of Unbalanced TDR Probes*, IEEE Transactions of Instrumentation and Measurement, Vol. 51, No. 3, pp. 532 – 536.

Dean, T.J., Bell, J.P. & Baty, A.J.B. 1987, *Soil Moisture Measurement by an Improved Capacitance Technique, Part I. Sensor Design and Performance*, Journal of Hydrology, Vol. 93, pp. 67-78.

ELE4605 Fields and Waves Study Book 1, 2003, Distance Education Centre, University of Southern Queensland, Toowoomba.

ELE4605 Fields and Waves Study Book 2, 2003, Distance Education Centre, University of Southern Queensland, Toowoomba.

Greacen, E.L. 1981, *Soil Water Assessment by Neutron Method*, CSIRO, Melbourne.

Habash, K.O. 1994, *An Investigation of TDR for Soil Measurements*, U/G Thesis, University of Southern Queensland.

Halikainen, M.T., Ulaby, F.T., Dobson, M.C., El-Rayes, M.A. & Wu, L. 1985, 'Microwave Dielectric Behaviour of Wet Soil – Part I: Empirical Models and Experimental Observations' in *IEEE Transactions on Geoscience and Remote Sensing*, Vol. GE-23, No. 1, pp. 25-34.

Heimovaara, T.J. 1993, *Time Domain Reflectometry in Soil Science, Theoretical Backgrounds, Measurements and Models, Amsterdam.*

Heimovarra, T.J. 1993, *Design of Triple-Wire Time Domain Reflectometry Probes in Practice and Theory*, Soil Science Society Am. J., Vol. 57, pp.1410 – 1417.

Hoekstra, P. & Delaney, A. 1974, *Dielectric Properties of Soils at UHF and Microwave Frequencies*, Journal of Geophysical Research, Vol. 79, No. 11, pp. 1699-1708.

Hook, W.R., Livingston, N.J., Sun Z.J. & Hook, P.B. 1992, *Remote Diode Shorting Improves Measurement of Soil Water by Time Domain Reflectometry*, SSSAJ., Vol. 56, pp. 1384-1391.

IMST GmbH, 2007, *Empire XCcel: The More Effective 3D EM Simulation Tool - Short Manual*, Kamp-Lintfort, Germany.

Laurent J.P. 1998, *Profiling Water Content of Soils with TDR: Experimental Comparison with the Neutron Prone Technique*, Laboratoire d'étude des Transferts en Hydrologie et Environment, France.

McKim, H.L., Walsh, J.E. & T. Pangburn, 1980, *Comparison of Radio Frequency, tensiometer and Gravimetric Soil Moisture Techniques,* State University of New York, Buffalo.

Moisture Point 2007, *Technical PaperMP-917 Technical Brief 1: Moisture•Point TDR SYSTEM* [Online], Available: http://www.esica.com, [Accessed 12 July 2007].

Noborio, K. 2001. *Measurement of soil water content and electrical conductivity by time domain reflectometry: A review*, [Online], Computers and Electronics in Agriculture Vol. 31, pp. 213-37. Available: http://www.sciencedirect.com/science/, [Accessed 30 May 2006].

Pettinellia E., A. Cereti, A. Galli, and F. Bella, 2002. *Time domain reflectometry: Calibration techniques for accurate measurement of the dielectric properties of various materials*, [Online], Review of Scientific Instruments, Vol. 73, pp. 3553-3562, Avaliable: http://weblinks2.epnet.com.ezproxy.usq.edu.au/ [Accessed 30 May 2006]

Robinson D.A., S.B. Jones, J.M. Wraith, D. Or & S.P. Friedman, 2003, *A review of advances in dielectric and electrical conductivity measurements in soils using time domain reflectometry*, Vadose Zone Journal, Vol. 2, pp. 444-475.

Selig, E.T. & S. Mansukhani, 1975, *Relationship of Soil Moisture to the Dielectric Property*, J. Geotech. Engng. Div.,Proc. ASCE Vol. 101:GT8, pp. 755-70.

Soilmoisture Equipment Corp., 1989, *Trase System 1: Operating Instructions*, Soilmoisture Equipment Corporation, Santa Barbara, California.

Topp, G.C., Davis, J.L. & Annan, A.P. 1980, *Electromagnetic Determination of Soil Water Content: Measurements in Coaxial Transmission Lines*, Water Resources Research, Vol. 16, No. 3, pp. 574-582.

Topp, G.C., Davis, J.L. & Annan, A.P. 1982a, *Electromagnetic Determination of Soil Water Content Using TDR: I. Applications to Wetting Fronts and Steep Gradients*, Soil Society of Am. J. Vol. 46, pp. 672 – 678.

Topp, G.C., Davis, J.L. & Annan, A.P. 1982b, *Electromagnetic Determination of Soil Water Content Using TDR: II. Evaluation of Installation and Configuration of Parallel Transmission* Lines, Soil Society of Am. J. Vol. 46, pp. 678 - 684.

Topp, G.C. & Davis J.L. 1985, *Measurement of Soil Water Content Using Time Domain Reflectometry (TDR): A Field Evaluation,* Soil Science Society Am. J., Vol 49, pp. 19-24.

Topp, G.C., Yanuka, M., Zebchuk, W.D. & Zegelin, S. 1988, *Determination of Electrical Conductivity Using Time Domain Reflectometry: Soil and Water Experiments in Coaxial Lines,* Water Resources Research, Vol. 24, No. 7, pp. 945-952.

Zegelin, S.J., White, I. & Jenkins, D.R. 1989, *Improved Field Probes for Soil Water Content and Electrical Conductivity Measurement Using Time Domain Reflectometry*, Water Resources Research, Vol. 25, No. 11, pp. 2367-2376.

Zegelin, S.J., White, I. & Russell, G.F. 1992, *A Critique of the Time Domain Reflectometry Technique for Determining Field Soil-Water Content*, Soil Science Society of America, Special Publication No. 30, pp. 187 – 208.

Bibliography

Arcone, S.A & Wills, R. 1986, *A Numerical Study of Dielectric Measurements Using Single-Reflection Time Domain Reflectometry*, Journal of Phys. E: Sci. Instrum., Vol 19, pp. 448-54.

Chudobiak, W.J., Syrett, B.A. & Hafez, H.M. 1979, *Recent Advances in Broad Band VHF and UHF Transmission Line Methods for Moisture Content and Dielectric Condatnt Measurement*, IEEE Transactions on Instrumentation and Measurement, Vol. IM-28, No 4, pp. 284-9.

Dalton, F.N. & Van Genuchten, M. 1986, *The Time-Domain Reflectometry Method for Measuring Soil Water Content and Salinity*, Geoderma, Vol. 38, pp237-50.

Dalton, F.N., Herkelrath, W.N., Rawlins, D.S. & Rhoades, J.D 1984, *Time Domain Reflectometry: Simulations Assessment of the Soil Water Content and Electrical Conductivity with a Single Probe*, Science, Vol. 224, pp. 989-90.

Hill, P.N. & Green, H.E. 1982, *In Situ Measurement of Soil Permittivity and Permeability*, Journal of Electric and Electronic Engineers Australia, IEAust. & IREEAust., Vol. 2, No. 4.

Kwok, B.P., Nelson, S.T. & Bahar, E. 1979, *Time Domain Measurements for Determination of Dielectric Properties of Materials of Agricultural Materials,* IEEE Transactions on Instrumentation and Measurements, Vol. IM-28, No. 2, pp. 109-12.

Topp G.C., Davis, J.L. & A.P. Annan, 1980, *Electromagnetic determination of soil water content: measurements in coaxial transmission lines*, Water Resources Research, Vol. 16, pp. 574-82.

Topp, G.C., Reynolds, W.D. & Green, R.E. 1992, *Advances in Measurement of Soil Physical Properties: Bringing Theory into Practice,* SSSAJ Special Publication, No. 30, pp. 143-208.

Topp G.C. & W.D. Reynolds, 1998, *Time domain reflectometry: a seminal technique for measuring mass and energy in soil,* Soil Tillage Research, Vol. 47, pp. 125-32.

Topp,G.C., Zegelin, S. & I. White, 2000, *Impacts of the Real and Imaginary Components of Relative Permittivity on Time Domain Reflectometry Measurements in Soils,* SSSAJ, Vol. 64, pp. 1244-1252.

Topp, G.C. & T.P.A. Ferre, 2002, *Water content, In, Methods of Soil Analysis. Part 4*. (Ed. J.H. Dane and G.C. Topp), SSSA Book Series No. 5, Soil Science Society of America, Madison WI.

Appendix A: Project Specifications

University of Southern Queensland
Faculty of Engineering and Surveying

ENG 4111/2 Research Project
PROJECT SPECIFICATION

STUDENT:	**Gary David BOLITHO**
PROJECT TITLE:	Time Domain Reflectometry (TDR) probes for the measurement of root zone soil moisture
SUPERVISORS:	Dr. Jim Ball, A/Prof, Faculty of Engineering and Surveying Dr. Steven Raine, A/Prof, Faculty of Engineering and Surveying
SPONSORSHIP:	Faculty of Engineering and Surveying, USQ
DATE:	1 August, 2007, Version 3.

1. Rationale

Time Domain Reflectometry (TDR) is a well established method of soil moisture measurement. A probe consisting of 2 or 3 parallel wires is pushed into the ground and connected to the TDR equipment. The latter produces a pulse of electrical energy, which travels down the probe, is reflected at the open ends of the wires, and returns to the surface. A measurement of the travel time can be converted into an estimate of soil moisture by means of a calibration curve stored within the instrument. The Faculty owns a TRASE instrument that is suitable for this project.

A soil moisture measurement obtained as above is an average over the length of the probe, which is typically 30 to 60cm long. It is however desirable that the moisture profile of the soil be attained, especially in the root zone area. It is feasible then that by careful probe design, a launch of the electrical pulse into the soil can be executed at a distance below the ground surface, thus yielding more specific information in the zone of interest.

2. Objectives

2.1. Design and construct one or more probes that yield soil profile information rather than averaged information.

2.2. Assess the new probes for accuracy and functionality.

3. Specific Tasks and Deadlines

3.1. Literature review of TDR application to soil testing, dielectric properties of water and wet soils, and soil measurement techniques.
Substantially complete by 13 April 2006 (to some extent this may be ongoing)

3.2. Familiarisation with the TRASE instrument, conventional TDR measurements, preparation of soil samples and calibration procedure.
Complete by 6 April 2006

3.3. Familiarisation with a commercially available software package for simulated design and testing of probes.
Complete by 11 May 2006 (depending on procurement by Faculty)

3.4. Assist with the design and manufacture of modified TDR probe
Complete by 18 May 2006 (depending on workshop production times)

NOTE: Part 2 of Project has been delayed for 12months. This has necessitated a review of Specification tasks and deadlines from S2 2006 to S2 2007.

3.5. Calibrate the new probe in air, water and one known soil. Signal processing programs using Matlab may be required.
Complete by 23 August 2007.

3.6. Comparison with conventional probes, in simulation and in practice.
Mostly complete by 6 September 2007, but ongoing in background during dissertation preparation.

As time permits:

3.7. Using 3D simulation software: make alterations to probe design and test.
Complete by 4th October 2007

3.8. Complete the thesis, with intermediate and final deadlines as follows:

Completion of First Draft by:	11 October 2007
Completion of Final Draft by:	25 October 2007
Deadline for submission:	1 November 2007

NB: The supervisor is to be shown each draft as it becomes available, and the supervisors comments should be incorporated in the next draft.

4. Assessment Guidelines

4.1. To be awarded a Pass (C) Grade the following work must be completed, as a minimum:

- A competent literature review
- Design of a new probe that demonstrates good attention to aspects of transmission line theory and mechanical robustness.
- Competent testing and calibration of the new probes in reference soils.
- An acceptable thesis, which conforms to the Faculty guidelines for thesis presentation

4.2. To be awarded a Credit (B) Grade, at least the following work must be completed:

- A comprehensive literature review with an attempt to relate the project topic to present state of the art in the specified areas.
- Calibration and testing results that are consistent with theory and software simulation

- A competent thesis, which in addition to the literature review as above contains a good description of the work undertaken, together with an analysis of the results obtained. The thesis must conform to Faculty guidelines for thesis presentation.

4.3. To be awarded the grade of Distinction (A) or High Distinction (HD) at least the following work must be completed:

- A comprehensive literature review together with a discussion of the relation of the present project to the present state of the art in the specified areas.
- Calibration and testing results that are highly consistent with theory and software simulation
- A thesis which is excellent in almost every respect

In addition, the student must be able to demonstrate a capacity for initiative and innovation, and an ability to function independently of the supervisors.

Acceptance by the student	Acceptance by the supervisors	
GARY BOLITHO 001992138	A/PROF J A R BALL	A/PROF S RAINE

Appendix B: Project Timelines

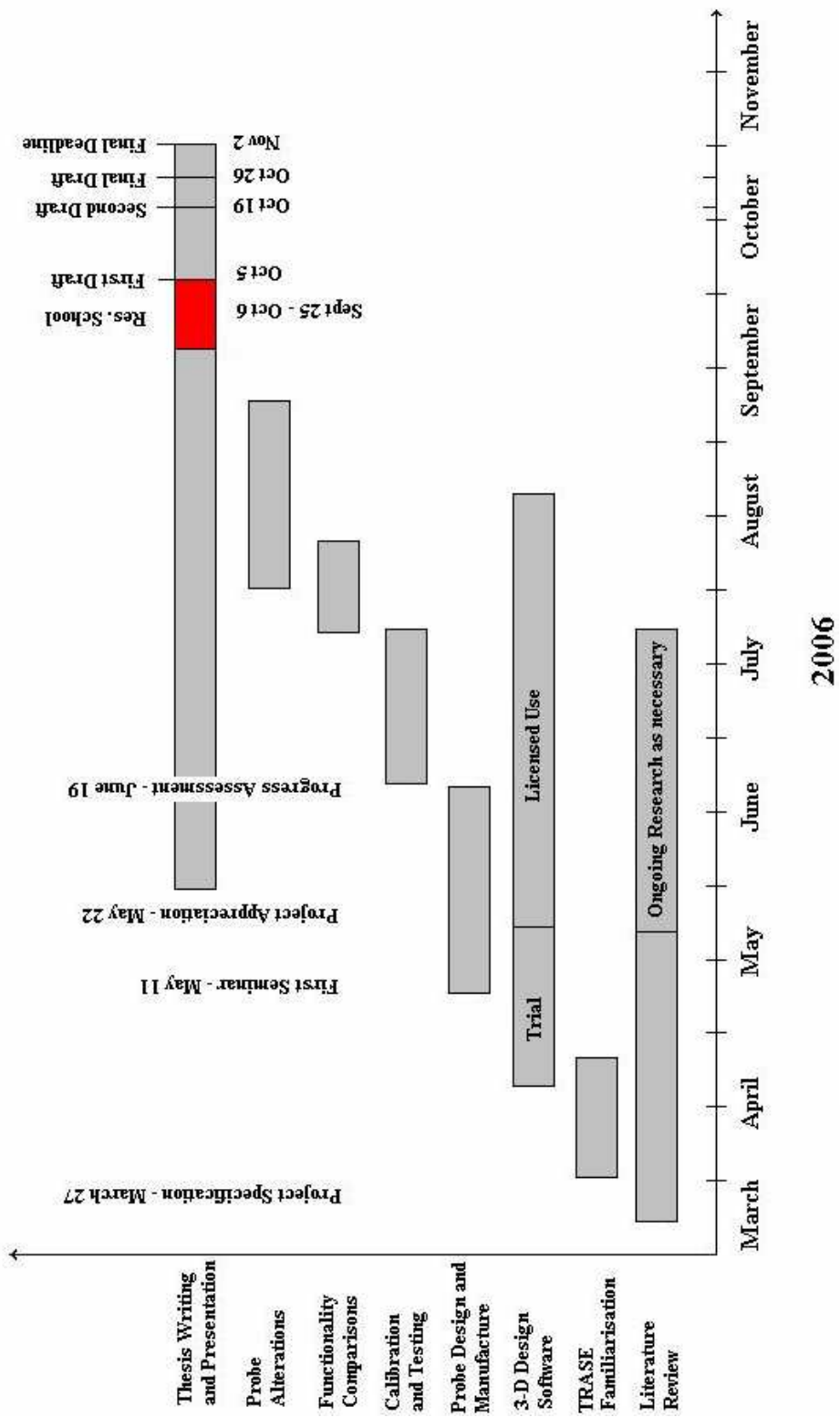

Figure B.1 *Proposed Timeline of Major Project Activities 2006*

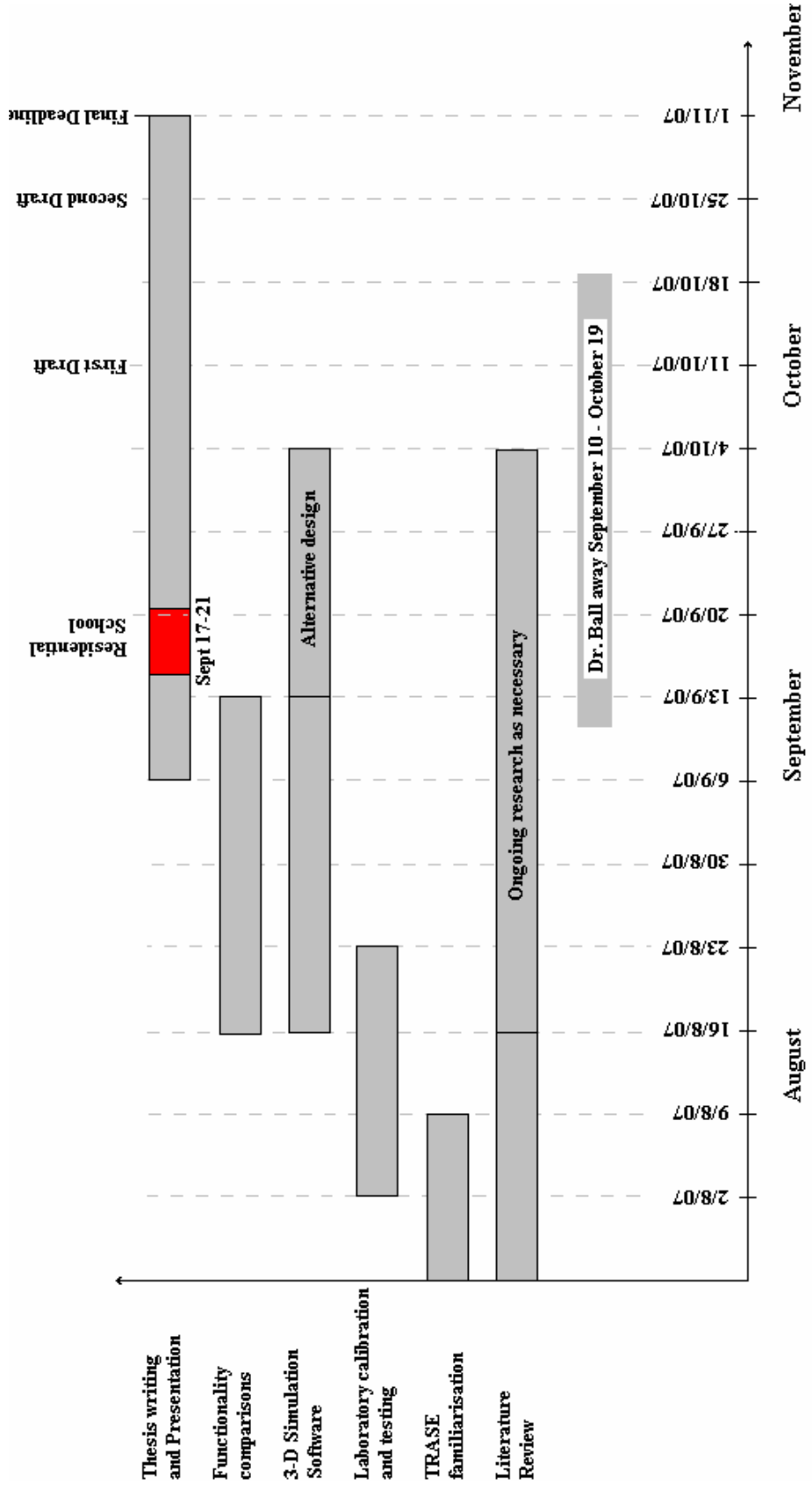

***Figure 8.2** Amended Project Timeline for S2 2007 (2nd part of Project delayed by 12 months)*

Appendix C: MATLAB Scripts

```
% Script:          Calculate Volumetric Water Content
% Purpose:         Script to calculate volumetric water content (thetaV),
%                  given the apparent dielectric constant (Ka)
%                  ThetaV is calculated by means of a lookup table
%                  created with values according to Topp Equation
%
% User Inputs:     Ka - apparent dielectric constant
%
% Output:          volumetric water content  (thetaV)
% Calls:           nil
%
% Source:          G. Bolitho September, 2007
%-------------------------------------------------------------------------------------------

clear all
thetaV=[0:0.0001:1];
ToppKa=3.03+9.3*thetaV+146*thetaV.^2-76.7*thetaV.^3;

% input calculated Ka
disp('Ka value must be between 0 and 81');
Ka=input(' Enter calculated Ka value: ')

i=0; checkKa=0;
while Ka>checkKa
   i=i+1;
   checkKa=ToppKa(i);
end

fprintf('Volumetric water content = %2.2f%%\n',thetaV(i)*100);
```

Appendix D: Probe Details

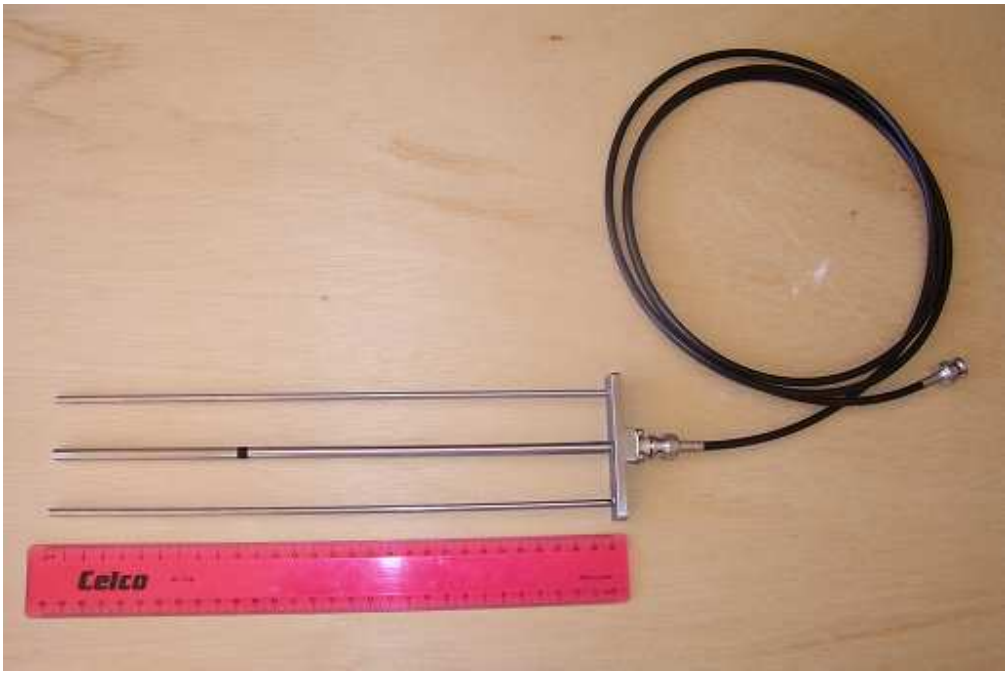

Figure D.1 *Prototype Probe with 50Ω Coaxial Connection Lead*

Figure D.2 *Details of Launch Point Connector Assembly*

Figure D.3 *Stainless Steel Arbour Showing Connection Details for Coaxial BNC Socket*

Figure D.4 *Panel Mount BNC Coaxial Socket with RG58U Cable*

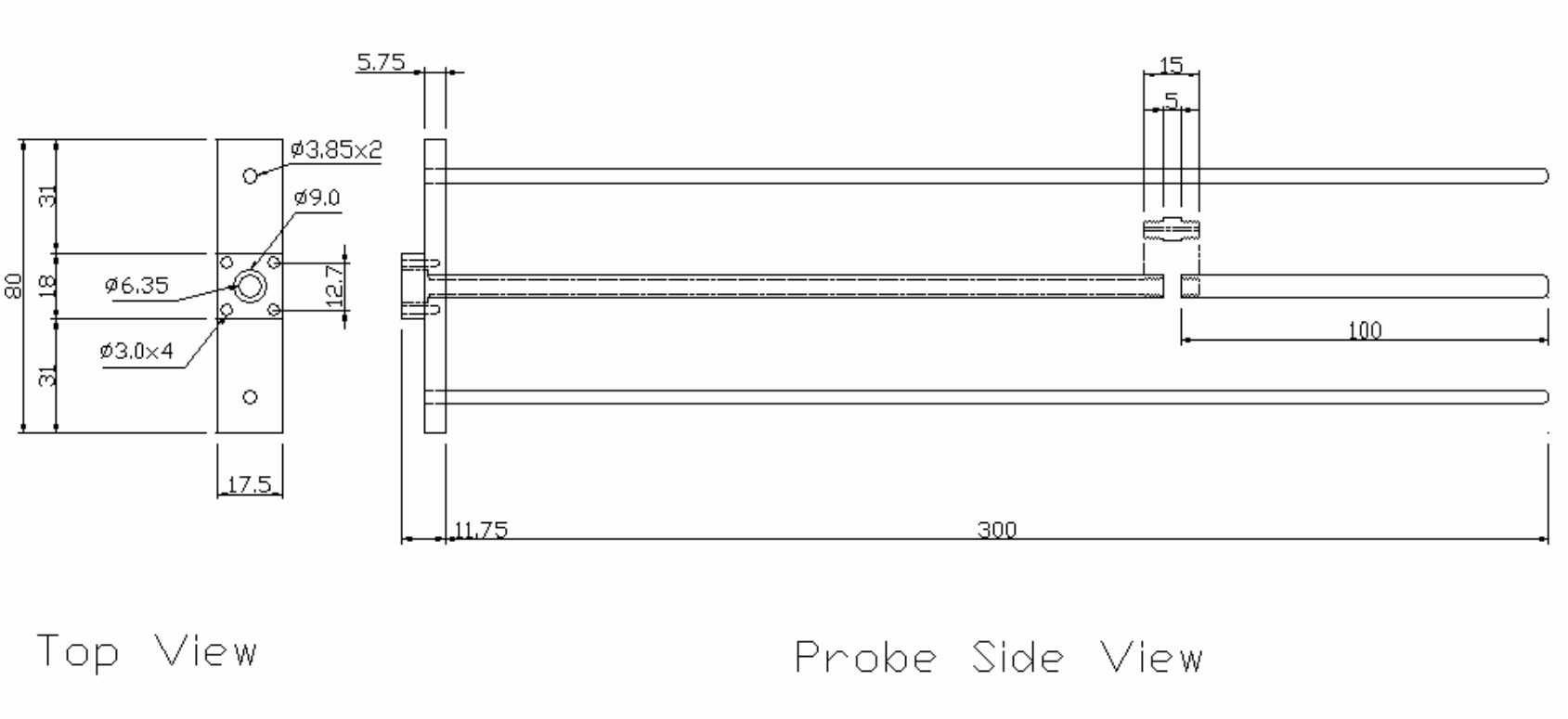

Figure D.5 *Engineering Drawings of Prototype Probe*

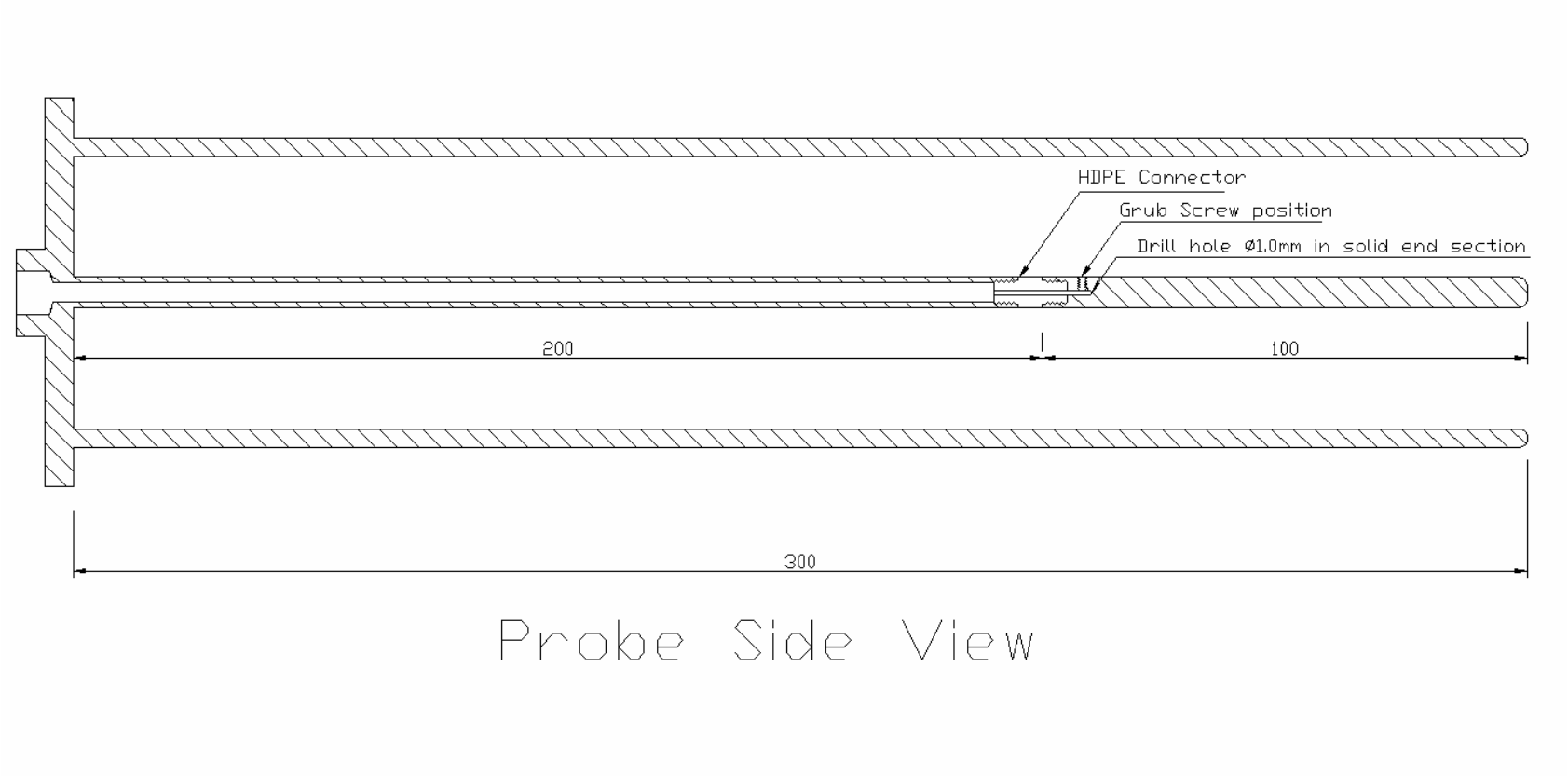

Figure D6 *Section View Drawings of Prototype Probe*

Appendix E: Laboratory Testing Results

Table E.1 *Measurement Results for All Probes*

TAG	Water Content (cc)	Soil Volume (cc)	Measured θv (%)		TRASE Measured Ka			TRASE Measured θv (%)			Wet Bulk Density (g/cc)
			Calculated	Sample	10cm Buriable	30cm Connector	New Probe	10cm Buriable	30cm Connector	New Probe	
DRY	0.0	19452.7	0.00	0.00	3.1	3.0	2.3	3.2	3.0	0.00	1.93
10WET	935.0	22393.3	4.18	3.93	7.3	4.3	2.7	13.8	6.3	0.00	1.56
6WET	1398.8	22619.5	6.18	5.63	7.9	4.8	3.2	15.3	7.4	1.49	1.54
WET10	1856.3	21714.7	8.55	8.00	7.7	6.3	3.8	14.9	11.0	4.79	1.63
WET12	2322.1	21488.5	10.80	10.96	8.0	6.9	5.1	15.4	12.5	9.32	1.67
WET16	2767.5	20809.9	13.30	13.35	12.9	8.8	6.5	25.1	17.4	12.92	1.74
WET18	3214.2	20131.3	15.97	17.30	9.4	11.0	9.0	18.6	21.9	18.03	1.82
WET21	3635.1	18548.0	19.60	20.60	12.0	13.5	11.9	23.7	25.8	22.91	1.99
WET24	4051.9	17190.8	23.57	23.39	16.0	16.0	14.1	28.5	28.5	26.19	2.13
WET27	4284.7	16738.4	25.60	26.05	17.7	17.8	15.2	30.4	30.6	27.73	2.11
WET30	4645.7	16512.2	28.13	28.68	19.7	19.8	17.6	33.1	33.1	30.93	2.11
WET35	4920.0	16512.2	29.80	30.90	21.7	20.8	21.6	35.5	34.5	35.86	2.07
Note: There is approx. a loss of 20-30ml of water each time the sample is mixed in the tub.											
This has been carefully measured and accounted for in the measurements shown											

Table E.2 *Summary Table of Stored TDR Waveforms for All Probes*

TAG	θv (%)	10cm Buriable Waveguide			30cm Connector Waveguide			New Probe	
		15-25ns	0-50ns	Auto Measure	15-25ns	0-50ns	Auto Measure	15-25ns	0-50ns
DRY	0.00	6	5	4	8	39	7	41	10
10WET	3.93	48	47	46	50	51	49	53	52
6WET	5.63	55	56	54	59	58	57	60	61
WET10	8.00	64	63	62	66	67	65	69	68
WET12	10.96	72	73	70,**71**	76	75	74	77	78
WET16	13.35	81	80	79	83	84	82	86	85
WET18	17.30	89	90	88	93	92	91	94	95
WET21	20.60	98	97	96	100	101	99	103	102
WET24	23.39	105	106	107	110	109	108	111	112
WET27	26.05	115	114	113	117	118	116	120	119
WET30	28.68	122	123	121	126	125	124	127	128
WET35	30.90	131	130	129	133	134	132	136	135

Note: Where multiple graphs are recorded, **bold** indicates the one selected for use.

A copy of all raw data files (stored as Microsoft® Excel Worksheets) are provided on the dissertation CD disk, under the directory: GaryDavidBolitho_appendices/. Each graph is stored in a separate file, as well as collated into appropriate summary Workbooks.

The summary Workbooks are separated according to type of probe being used, and under different capture window settings, for example:

- NewProbe_15-25ns.xls
- ConnectorProbe0-50ns.xls